Dissertations, Master's Theses and Master's Reports - Open

Dissertations, Master's Theses and Master's Reports

2010

Parametric combustion modeling for ethanol-gasoline fuelled spark ignition engines

Yeliana
Michigan Technological University

Follow this and additional works at: https://digitalcommons.mtu.edu/etds

Part of the Mechanical Engineering Commons

Recommended Citation

Follow this and additional works at: https://digitalcommons.mtu.edu/etds

Part of the Mechanical Engineering Commons

PARAMETRIC COMBUSTION MODELING FOR ETHANOL-GASOLINE

FUELLED SPARK IGNITION ENGINES

By:

Yeliana

A DISSERTATION

Submitted in partial fulfillment of the requirements for the degree of

DOCTOR OF PHILOSOPHY

Mechanical Engineering-Engineering Mechanics

MICHIGAN TECHNOLOGICAL UNIVERSITY

2010

This dissertation, "Parametric Combustion Modeling for Ethanol-Gasoline Fuelled Spark Ignition Engines," is here by approved in partial fulfillment of the requirements for the Degree of DOCTOR OF PHILOSOPHY IN MECHANICAL ENGINEERING-ENGINEERING MECHANICS.

DEPARTMENT OF MECHANICAL ENGINEERING-ENGINEERING MECHANICS

Signatures:

Dissertation Advisor _____

Jeffrey D. Naber

Department Chair _____

William W. Predebon

Date _____

In memory of my Father,

Mengenang Bapak,

I dedicate this dissertation to my Mother, Brothers and Sisters.

Saya persembahkan disertasi ini untuk Mamak, Saudara dan Saudariku.

TABLE OF CONTENTS

LIST OF FIGURES

ix

LIST OF TABLES

PREFACE

This dissertation contains reports and published and submitted articles related to development and integration of the GM-MTU parametric combustion model for spark ignition engines developed for General Motors.

In this dissertation, Chapter II and Section V.1 were published in the 2008 Journal of Kones, Powertrain & Transportation. Chapter III was presented in the 2008 SAE World congress. Chapter IV has been submitted to Combustion Science and Technology, Section V.2 has been submitted to Applied Thermal Engineering and Section V.3 is planned for submission in Applied Stochastic Models and Data Analysis. Chapter VI was a part of the documentation of GM-MTU Predictive Combustion Model delivered to General Motors in 2010. Chapter VII contains a report of GM-MTU Stochastic Parametric Combustion Model.

ACKNOWLEDGEMENTS

ABSTRACT

Ethanol-gasoline fuel blends are increasingly being used in spark ignition (SI) engines due to continued growth in renewable fuels as part of a growing renewable portfolio standard (RPS) [1]. This leads to the need for a simple and accurate ethanol-gasoline blends combustion model that is applicable to one-dimensional engine simulation.

A parametric combustion model has been developed, integrated into an engine simulation tool, and validated using SI engine experimental data. The parametric combustion model was built inside a user compound in GT-Power. In this model, selected burn durations were computed using correlations as functions of physically based non-dimensional groups that have been developed using the experimental engine database over a wide range of ethanol-gasoline blends, engine geometries, and operating conditions. A coefficient of variance (COV) of gross indicated mean effective pressure (IMEP) correlation was also added to the parametric combustion model. This correlation enables the cycle combustion variation modeling as a function of engine geometry and operating conditions. The computed burn durations were then used to fit single and double Wiebe functions. The single-Wiebe parametric combustion compound used the least squares method to compute the single-Wiebe parameters, while the double-Wiebe parametric combustion compound used an analytical solution to compute the double-Wiebe parameters. These compounds were then integrated into the engine model in GT-Power through the multi-Wiebe combustion template in which the values of Wiebe parameters (single-Wiebe or double-Wiebe) were sensed via RLT-dependence.

The parametric combustion models were validated by overlaying the simulated pressure trace from GT-Power on to experimentally measured pressure traces. A thermodynamic engine model was also developed to study the effect of fuel blends, engine geometries and operating conditions on both the burn durations and COV of gross IMEP simulation results.

I.   INTRODUCTION

I.1   BACKGROUND

An internal combustion (IC) engine is a heat engine in which chemical energy from fuel is combusted with the resulting high temperature and pressure gas trapped in the cylinder. The resulting expansion of the gases transfers the sensible energy of the working fluid to useful mechanical work. A spark ignition (SI) engine is an IC engine that uses a high voltage spark for ignition in the combustion chamber, controlling combustion phasing.

Combustion plays a major role in an SI engine because it provides the energy to do the work of the engine which depends on the fuel type and engine operating conditions. These contribute to the engine's efficiency, performance, and emissions [2, 3]. Current stringent emissions standards by Environmental Protection Agency (EPA) and Corporate Average Fuel Economy (CAFE) standards drive research in SI engines to not only focus on emissions but also on fuel consumption and efficiency. However, experimental study in engines is time consuming and expensive. Therefore the industry and academia have an incentive to find alternatives to experimental testing. One way that the cost of research and development can be decreased is to perform more computational simulations in place of empirical experiments. Furthermore, with the increase in computer capability, engine modeling becomes more attractive and continues to grow rapidly [4].

To model SI engines, one-dimensional engine simulation is widely used for design, development, calibration, and optimization because it is computationally efficient and enables the entire engine to be modeled [2, 3]. In general, the one-dimensional engine model consists of sub-models of selected processes that can be investigated using more detailed modeling approaches (quasi-dimensional or 3-dimensional models) to increase the accuracy of the overall engine simulation results.

Combustion modeling plays a critical part in the overall engine simulation. In one-dimensional engine simulations, the combustion model provides the burning rate that represents the heat release rate (HRR) in the combustion process for a given fuel blends, engine geometry, and set of operating conditions. The burning rate can be computed

empirically and or derived from physical, detailed coupled turbulent flames, or chemical kinetic correlations of combustion processes. Having a proper combustion model will enhance understanding of the physical phenomena, including the effects of valve phasing, type of fuel, compression ratio, exhaust gas recirculation (EGR), etc., and, thus, enable comprehensive design and optimization of the engine and its operation to meet the required objectives [2, 3].

Over the years, many researchers have developed combustion models based on mean or median cycle that are applicable to one-dimensional engine simulation by defining the burning rates of fuel-air mixtures based on the First Law of Thermodynamics [5-8]. The burning rates of the fuel air mixture can also be described as function of engine geometry and in-cylinder conditions, fuel air mixture properties and flame speed [9-12]. The burning rate is commonly expressed using the mass fraction burned (MFB), a normalized integral of burning rate, which has a characteristic S-shaped curve. The Wiebe function is the most common function used in SI one-dimensional engine modeling to describe the MFB as a function of engine position during the cycle (crank-angle) [2, 3]. The main difference in its application is in determining the Wiebe parameters ("m" and $\Delta\theta$) that define the burn combustion duration characteristics [3, 7, 13]. The Wiebe function parameters can be determined by fitting the Wiebe function to the MFB profile [14]. However, some references [15, 16] preferred to fit the HRR rather than fit the MFB, which is the normalized integrated HRR profile.

Cycle to cycle combustion variation in SI engines is also an important subject that has been widely studied because it limits the range of operation, especially under lean and highly diluted mixtures and combustion knock conditions [3, 17, 18]. Physical factors that lead to cycle to cycle combustion variation in SI engine are the imperfect mixing of fuel, air and residual, the location and phasing of spark, the size of the eddy discharged from the spark, and the mixture motion near the spark [19, 20]. By reducing the cycle variation, the dilution tolerance could be increased to the lean limit, or spark timing could be advanced further to achieve goals to reduce the emission and decrease the fuel consumption without encountering combustion knock [3]. There is a trade-off in cycle

variation and improved efficiency because of reducing heat transfer and pumping work. As a result, the best efficiency is typically achieved at the coefficient of variance (COV) of gross indicated mean effective pressure (IMEP) limit, not minimum COV [21].

The COV of IMEP is commonly used as a metric to quantify the cycle variation limits and trends. In the literature, Two correlations of COV of IMEP are found [22, 23]. In the first study, a linear regression of COV of IMEP was developed using 146 data point covering three different chamber geometries and varying the total exhaust gas recirculation (EGR), air-fuel ratio, spark timing, engine speed and fueling level using a single-cylinder 0.6 liter engine [22]. In the second study, a non-linear regression of a polynomial form for COV of IMEP was developed as a function of engine speed and load, equivalence ratio, residual fraction, burn duration of 0-10%, burn duration of 10-90% and location of 50% mass fraction burn (MFB) using 6000 operating conditions collected from 13 different engines from 1.6 to 4.6 liters in displacement [23]. Although this correlation was developed using a wider range of data as compare to the first study, this regression computed negative COVs of IMEP within the range of data used in the correlation. This is mainly caused by the nature of a polynomial functional form, which has a combination of positive and negative signs in the equation.

I.2   PROBLEM STATEMENT

Alcohol-based fuels have been used in many ways for over hundred years now, including as a fuel for IC engines replacing the existing gasoline fuel, as a fuel additive to boost the octane number replacing the existing petroleum-based and metallic additives, and as a fuel for direct conversion of chemical energy into electrical energy in a fuel cell [24]. Ethanol is the most common of alcohols that has been widely used as an alternative to gasoline, not only because ethanol is a renewable fuel, but also because ethanol is less toxic than other alcohol fuels [24].

In its recent application in SI engines, ethanol is blended with gasoline (10%-85%) to displace fossil fuels while at the same time increasing the octane number of the fuel blend

[25]. E10 (10% ethanol, 90% gasoline) has been used in the United States to oxygenate the fuel for cleaner combustion and lower carbon monoxide and hydrocarbon exhaust emissions. Recently, the Environmental Protection Agency granted the use of E15 for vehicle 2007 production and newer without necessary engine modifications [1]. However, E85 fuel (85% ethanol, 15% gasoline) requires modifications in the engine and or engine operating conditions.

Flexible Fuelled Vehicles (FFVs) provide a solution to the problem of requiring the engine to be modified in order to run efficiently with different fuel blends. FFVs have adaptable SI engines, which can operate efficiently using fuel blends containing 0 to 85% ethanol. These vehicles are designed to have variable fuel delivery system, injection duration, spark timing, and etc. to address the changes of engine operating conditions with ethanol-gasoline fuel blends. However, the optimal parameters for each of these operating conditions have not been determined for all ethanol gasoline blends, particularly for blends containing higher proportions of ethanol.

Fuel consumption is one of major concerns using ethanol blends in SI engine. The fuel consumption increases as the ethanol content increases in the fuel blends because ethanol has a lower energy content compared to gasoline. In addition, the ethanol is an oxygenated fuel which without careful property calculation will lead to enleanment in the air-fuel charge, thus lead to combustion stability problems. Engine cold start also dominates the ethanol blend fuels issues in the SI engines. However, regardless of these issues, ethanol decreases the amount of emissions, and generates less toxic emissions compared to petroleum–based fuels. Ethanol's high octane number reduces the tendency of knocking in the SI engines. This enables ethanol to be used in SI engines at a higher compression ratio, resulting in a higher thermal efficiency.

The concerns described above increases the need for a combustion model which incorporates the ethanol-gasoline blended fuel's properties and its combustion characteristics to optimize the tolerance of the SI engines to variety of ethanol blend fuels and maximize the efficiency and fuel consumption by optimizing the engine operating conditions for a wide range of ethanol blends. Integration of the ethanol-gasoline blends

combustion model into the one-dimensional engine modeling enables modeling of SI engine for design, development, calibration, and optimization purposes, specially for FFVs [3, 26].

This research will cover the development of a parametric combustion model for ethanol-gasoline blend SI engines, the integration of the parametric combustion model to the one dimensional engine model, and the validation by comparing the simulation results with the experimental data.

I.3   GOALS AND OBJECTIVES

Because engines have become more complex with additional degrees of freedom in design and operation, including variable valve timing (VVT), variable valve lift (VVL), variable compression ratio (VCR), fuel blends, and etc. Development and optimization of these engines have become complex multivariable problems. As a result, engine simulation has become critical to the engine design, development, calibration, and optimization because it reduces time and cost in comparison to experimental studies alone. The engine simulation is also used in preliminary studies to find which experiments need to be done or to find which variables need to be focused on. The effects of these variables on engine performance are often confounded by its complex interaction. Ideally the SI engine should produce emissions as low as possible, generate power as high as possible, and consume fuel as low as possible. At the same time it should be reliable, durable, and inexpensive.

The first goal of this research is to develop a physically based parametric combustion model for SI engines that includes the effects of ethanol-gasoline blends, engine geometries, and engine operating conditions, that is applicable for one-dimensional engine simulation tools for prediction of burn rates and cycle combustion variation. The second goal is to integrate the parametric combustion model into GT-Power, a one-dimensional engine simulation tool, to characterize the factors impacting combustion

5

rates and limits, thus, enabling the simulation to be used for improving the performance, and efficiency of SI engines.

The objectives to accomplish these goals are:

- Develop a method to compute ethanol-gasoline blends burned and unburned properties [Chapter II].

- Develop methods to analyze and quantify the mean value and stochastic nature of the combustion process in SI engines using the experimentally measured in-cylinder pressure trace [Chapter III].

- Develop a set of physically based parameters to characterize the combustion rates [Chapter IV].

- Develop methods to determine optimal non-dimensional groups of physically based parameters and to correlate them to the combustion metrics:

    o Combustion burn duration correlations [Chapter IV]

    o Cycle combustion variation correlation [Chapter VII]

- Develop methods to compute the Wiebe function parameters:

    o Single-Wiebe function parameters calculation using analytical solution and least squares methods [Section V.1]

    o Double-Wiebe function parameters calculation using least squares method [Section V.2]

    o Double-Wiebe function parameters calculation using analytical solution [Section V.3]

- Develop methods to validate the parametric combustion model:

    o Single-zone pressure model [Chapter V]

      o   Thermodynamic engine model [Chapter VII]

- Integrate the parametric combustion model into GT-Power [Chapter VI].

I.4   METHOD OF SOLUTION

Figure I-1 shows the process of developing a parametric combustion model for SI engines. The process starts from the **Development** block and continues to the **Validation** block. Both of these blocks are developed in MathWorks. The process then progresses to the **Integration** block which is developed in Gamma Technologies.

In the **Experimental** block, over 3700 test points were collected from Michigan Tech single cylinder - Cooperative Fuel Research (CFR) and Hydra engines, as well as General Motors multi cylinder Ecotec engines over a wide range of operating conditions. The detail specification of these engines can be found in Table IX-1 in Section IX.1 Appendices. Table IX-2 lists the range of operating conditions and number of test points for each of the four engines that were used in this research. These engine databases cover a wide range of compression ratios from 8:1 to 18.5:1, ethanol blends from 0 to 85%, external exhaust gas recirculation (EGR) from 0 to 30%, full sweep of intake and exhaust cam resulting variable of residual fraction trapped in the cylinder, full sweep of spark timings, engine speeds from 900 rpm to 6600 rpm, and multiple loads.

In the **Development** block, selection of methods to analyze and quantify the mean value and stochastic nature of the combustion profile using experimentally measured in-cylinder pressure trace were developed in Chapter III. A single-zone MFB method with two unknowns (temperature and mass fraction burn) and a two-zone MFB method with five unknowns (burned and unburned temperature, burned and unburned volume, and mass fraction burn) were developed based on the first law of thermodynamic and the ideal gas law. Both these methods were compared to the apparent heat release method which is also derived from the first law of thermodynamics and the ideal gas law. A composite fuel concept that was introduced in Chapter II, was incorporated in the

calculation in this section to accommodate the effect of fuel blend properties in the combustion profile analysis.

The method to determine the set of non-dimensional physically based Pi-groups and to correlate the combustion parameters was discussed in the **Development** block. A set of physically based parameters was selected from the literature using the coefficient correlation matrix and the principle component analysis methods. These physically based parameters were then grouped, resulting in the Pi-groups: $\dfrac{\overline{S}_p}{S_L}$, $\dfrac{S_L{}^2}{Q^*}$, $\dfrac{h}{B}$, and $\dfrac{h\,\overline{S}_p}{v}$.

These Pi-groups were then used to determine the combustion characteristics, including the burn durations and the coefficient of variation (COV) of gross indicated mean effective pressure (IMEP). Chapter IV focused on the development the burn durations correlations as a function of non-dimensional Pi-groups. While Chapter VII focused on the development of the COV of gross IMEP correlation. Appendices Section IX.3 presented the burn duration correlations for each of the four engines used in this research. Tables IX-3, IX-4, IX-5, IX-6, and IX-7 list the B0010, B1025, B1050, B1075, and B1090 correlations respectively, complete with the number of test points used in the correlation and the metrics to quantify the goodness of the fitted correlation including the R^2, root mean square error (RMSE), and Akaike's information criteria (AIC). Figures IX-1 and IX-2 show the B0010 and B1075 correlations for each engine used in this research. Each engine was found to have its own burn duration characteristics that correlate well with the physically based non-dimensional Pi-groups. Combination data taken from the GM multi-cylinder LAF engines, the GM multi-cylinder turbo-charged LNF engines, and the MTU single-cylinder Hydra engine was found to have a good correlation to the Pi-groups. The MTU single-cylinder CFR engine data, a representation of an older engine, was found to have different combustion characteristics in comparison to the rest of engine's data, used in this research, which represent the newer modern engines.

To reconstruct a MFB profile from burn durations (B0010, B1025, B1050, B1075, and B1090) in the **Validation** block, methods of calculating the Wiebe function parameters were developed, for both single-Wiebe and double-Wiebe functions. An analytical

solution, a least squares method, and a combination of both were used to compute the single-Wiebe function parameters which has two unknowns and the double-Wiebe function parameters which has five unknowns. Section V.1 focused on the single-Wiebe function, Section V.2 focused on the double-Wiebe function calculation using the least squares method, and Section V.3 focused on the double-Wiebe function calculation using the analytical solution. It was found that the double-Wiebe function matches the experimental MFB profile better than the single-Wiebe function.

To reconstruct a pressure trace from MFB profile in the **Validation** block, a single-zone pressure model was developed based on the first law of thermodynamics and the ideal gas law in Chapter V. This single-zone pressure model was also used in a thermodynamic engine model, developed in Chapter VII. In addition to the single-zone pressure model, the thermodynamic engine model also incorporates the single-Wiebe function parameter calculation and empirical correlations including the residual fraction correlation as a function of valve overlap factor, engine speed, equivalence ratio, intake, and exhaust pressure, the burn durations (B0010, B1025, B1050, B1075, and B1090) and COV of gross IMEP as a function of non-dimensional Pi-groups.

In the **Integration** block, a parametric combustion model was developed in the GT-Power interface. A user compound was developed to contain the burn durations and COV of gross IMEP correlations and the Wiebe function parameters calculation. Two parametric combustion models were developed including single-Wiebe and double-Wiebe parametric combustion models. Validation of the parametric combustion models was also performed in the GT-Power using multi-cylinder engine models. Chapter VI focused on the development and validation of parametric combustion model in GT-Power. Once the parametric combustion model is verified and validated, the parametric combustion model can be used in the **Application** block for engine design, engine calibration, and engine optimization.
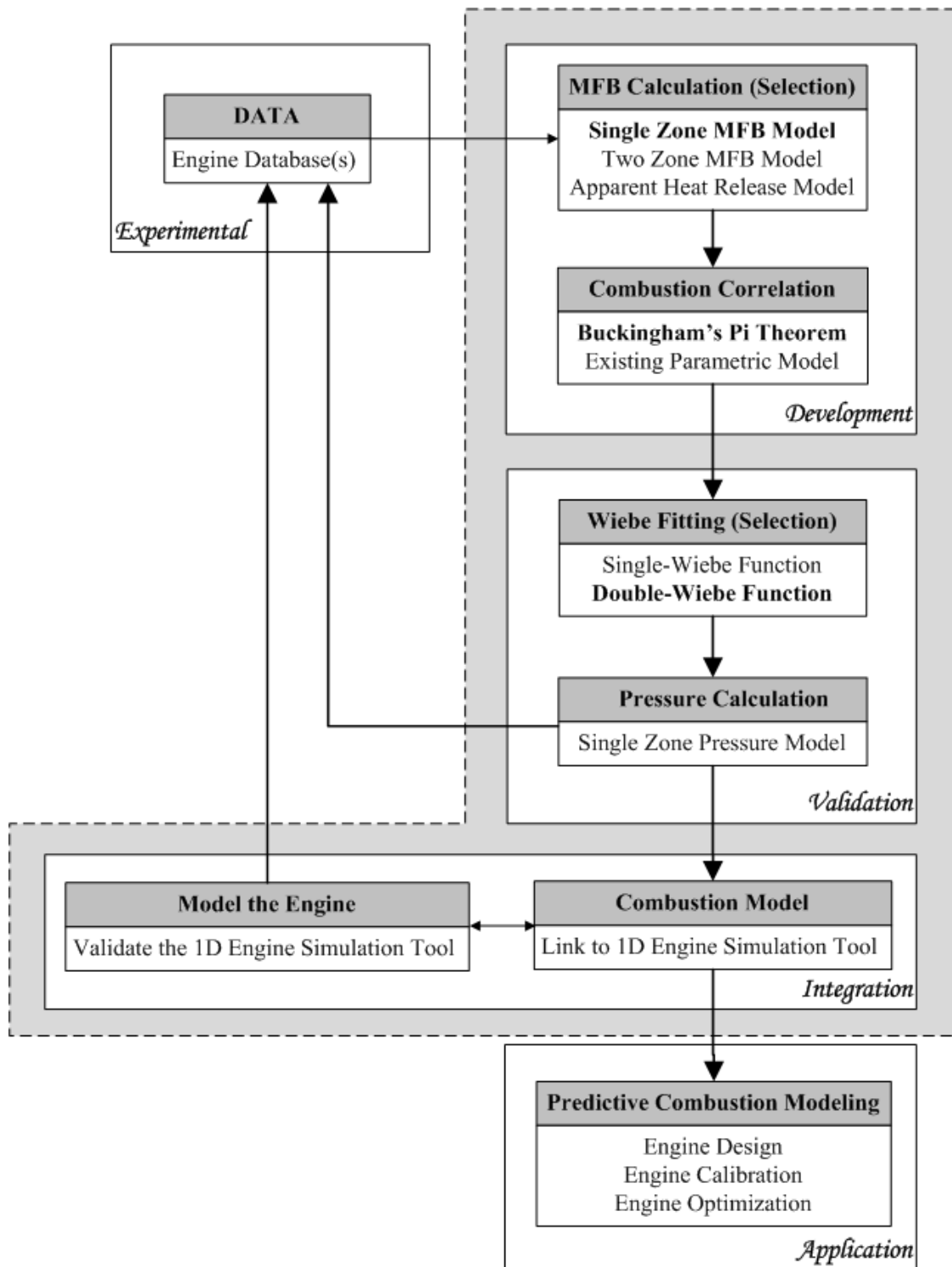
Figure I-1 Parametric combustion model development process

I.5   METHODS SUMMARY

Below is the summary of methods that were used in this dissertation. These methods were developed in the Matlab interface, unless mentioned otherwise.

- Composite fuel concept

    The composite fuel concept can be used to compute the burned and unburned fuel blends, not only for ethanol gasoline fuel blends but also for hydrocarbon, alcohol, and oxygenated hydrocarbon fuels. This concept is important in determining the air-fuel mixture properties to avoid enleanment in the air-fuel charge that may lead to cycle combustion variation.

- Single-zone and two-zone MFB analysis

    The single-zone and two-zone MFB including the effect of heat transfer and crevice volume can be used to quantify the combustion characteristics both mean value and cycle to cycle basis using the experimentally measured pressure trace. The single-zone MFB calculation is a robust data analysis in comparison to the two-zone MFB calculation. However for detailed combustion efficiency and in-cylinder temperature profile, the two-zone MFB calculation including the specific heat as a function of temperature, and the inclusion of heat transfer and crevice effects should be used since the thermodynamic properties of the burned and unburned mixture was more accurately quantified.

- Non-linear least square fitting method

    The non-linear least square fitting method can be used to correlate the combustion metrics (burn durations and COV of IMEP) to the physically based non-dimensional Pi-groups. This method also could be used to find correlation among experimental variables with many different functional forms, including sum-product, polynomial-product, and power-product functional forms. The power-

product functional form gives the clearest result of these functional forms because it allows significant variables to be identified by observing the correlation.

- Analytical solutions of single-Wiebe and double-Wiebe functions

The analytical solutions of single-Wiebe and double-Wiebe functions provide a simple straight forward formula to determine the single-Wiebe and double-Wiebe parameters which can be used in engine software that have limited computational capability.

- Least squares methods of the single-Wiebe and double-Wiebe functions

The least squares methods of the single-Wiebe and double-Wiebe functions provide more accurate result in determining the single-Wiebe and double-Wiebe parameters. Although the least squares method of single-Wiebe function is applicable for commonly used engine software, however the complexity of the computation in the least squares method applied to the double-Wiebe function limits its direct use in engine modeling software.

- Single-zone pressure model

The single-zone pressure model can be used to reconstruct pressure trace from a given or computed MFB profile. This model allows the combustion modeling result to be compared to the experimental pressure data, which enables analysis of engine performance, fuel consumption, and efficiency.

- Thermodynamic engine model

The thermodynamic engine model incorporates the methods for fitting the Wiebe function, reconstructing the pressure trace, and computing MFB, and the correlation of residual fraction, burn durations and COV of gross IMEP. The thermodynamic engine model can be used to exercise the engine response on performance, fuel consumption, and efficiency with multiple inputs of variables including engine geometries and operating conditions. This allows a faster

computational speed in comparison to commonly used engine software, GT-Power, which enables sensitivity studies of the variables with respect to the performance and efficiency of the engine. This also can be used to generate test data for further used in engine modeling including vehicle simulation and/or virtual test engines.

- GM-MTU single-Wiebe parametric combustion model developed in GT-Power interface

This combustion model can be integrated and used in any engine simulation in GT-Power which computes the single-Wiebe function parameters as a function of engine geometries and operating conditions through physically based parameters. Since the combustion model incorporates the empirical parameters, this allows the user to be confident in the single-Wiebe function parameters calculation for the range of engine geometries and operating conditions in which the combustion model was developed in comparison to arbitrary input of the single-Wiebe parameters in GT-Power.

- GM-MTU double-Wiebe parametric combustion model developed in GT-Power interface

This combustion model can be integrated and used in any engine simulation in GT-Power which computes the double-Wiebe function parameters as a function of engine geometries and operating conditions through physically based parameters. Similarly, since the combustion model incorporates the empirical parameters, this allows the user to be confident in the double-Wiebe function parameters calculation in the range of engine geometries and operating conditions in which the combustion model was developed in comparison to arbitrary input of the double-Wiebe parameters in GT-Power. The GM-MTU double-Wiebe parametric combustion model provides more accurate results, particularly for operating conditions that have a non-symmetrical burn profile. However, it also increases the computational complexity.

I.6   RESEARCH CONTRIBUTIONS AND SIGNIFICANT FINDINGS

Below are the main contributions of this research and the significant findings from this dissertation.

- Combustion modeling with predictive capability has been a fascinating subject for many years. The combustion model that is applicable to one-dimensional engine simulation is used to compute the burn rate which represents the in-cylinder pressure and temperature in the combustion chamber. Several empirical burn duration correlations, as a function of engine operating conditions, have been proposed. In the literature, the computed burn durations from measured pressure trace were correlated to the engine operating conditions using combination polynomial and product forms [27-29] and the product-power form [30-32].

  In general, the combination of polynomial and product functional forms found in the literature have a nested function of polynomial function of particular variable and its base condition that might vary for different engines. For example in literature [27], the burn duration was defined as a function of a fixed burn duration taken from base condition and product of laminar flame speed, spark timing, and speed correlations. Each of these correlations (laminar flame speed, spark timing, and engine speed correlations) has its own functional form, mainly a polynomial functional form. This nested function does not give a clear correlation between the variables by looking at the correlation. Additional variables involved in the correlation make the correlation more complex [27-29]. However, the combination of power and product functional forms found in the literature have simpler correlation which allows the correlation among the variables to be observed directly from the correlation and minimizes the potential for non-physical correlation [30-32].

  The burn duration was previously assumed to be a function of cylinder geometry and turbulent flame speed which are a function of engine speed and laminar flame speed only [11]. The burn duration was also correlated as a function of

compression ratio, engine speed, equivalence ratio, and the spark timing [28]. In addition to engine speed and the spark timing, the laminar flame speed was also included in the burn duration correlation [27]. Derived based on a turbulent combustion model for SI engines, the burn duration correlation was fitted to parameters including the height of combustion chamber (h), piston bore (B), mean piston speed ($\bar{S}_p$), laminar flame speed (S_L) and kinematic viscosity (v) [10, 30, 31].

The burn duration from 0 to 10% MFB (B0010) found in the literature [10, 31], known as the early flame development period, was derived from the turbulent flame propagation. B0010 was defined a function of $\left(\bar{S}_p \, v\right)$ to the power of 1/3, $\left(\dfrac{h}{S_L}\right)$ to the power of 2/3 and a constant that may change for different engines.

Similarly the burn duration from 10% to 90% MFB (B1090) found in the literature, known as the rapid burning period, was also derived from the turbulent flame propagation. B1090 was defined a function of $\left(\dfrac{B}{h*}\right)$, $\left(\bar{S}_p \, v*\right)$ to the power of 1/3, $\left(\dfrac{h}{S_L}\right)$ to the power of 2/3 and a constant that may change for different engines. The star symbol in this correlation indicates that the corresponding property was computed at the location of 50% MFB (CA50).

Based on this literature study and additional parameter investigations, six main parameters were selected and used in this dissertation. These physically based parameters include: engine bore (B) and height of the combustion chamber (h) to represent the engine dependence, mean piston speed (S_p) and laminar flame speed (S_L) to represent the flow dependence, and kinematic viscosity of the unburned mixture (v) and the specific internal energy ($Q* = (m_f/m) \, Q_{LHV}$) to represent the working gas property dependence. Additional parameters describe the engine parameters: mass fraction burn, residual fraction, spark timing, equivalence ratio,

15

engine speed, load, and valve timing [17, 30, 31]. A non-dimensional analysis using Buckingham's Pi Theorem [33] was performed using the parameters defined above, resulting in four Pi-groups $\dfrac{\bar{S}_p}{S_L}$, $\dfrac{S_L{}^2}{Q^*}$, $\dfrac{h}{B}$, and $\dfrac{h\,\bar{S}_p}{\nu}$. A non-linear least squares method was then used to correlate the burn durations with the Pi groups with a product-power form. The detailed process of developing the burn duration correlation can be found in Chapter IV that focuses on developing the burn duration correlation using data obtained from MTU-CFR engine using variable compression ratios from 8:1 to 16:1, a full sweep of spark timings and EGR from 0 to 30% using five different ethanol-gasoline blends.

Appendices Section IX.3 presents the burn duration correlations for each of the four engines used in this research. Tables IX-3 and IX-7 list the B0010 and B1075 correlations respectively complete with the number of test points used in the correlation and the metrics to quantify the goodness of the fitted correlation including the R^2 and the root mean square error (RMSE), and the Akaike's information criteria (AIC). The AIC not only quantifies the deviation of the fitted correlation from the data but also accounts for the number of parameters used in the correlation. The AIC is an important metric to avoid over-parameterization in the model fitting process. Figures IX-1 and IX-2 show the B0010 and B1075 correlations for each engine used in this research. Except for the GM-LAF, all the engine data was collected at stoichiometric mixture condition. As a result, the exponent for x5 in Table IX-3 was 0 for data collected from GM-LNF, MTU-Hydra, and MTU-CFR engines.

In general, the fuel related Pi-groups including $\dfrac{S_L{}^2}{Q^*}$ and $\dfrac{h\,\bar{S}_p}{\nu}$ have a weak effect on the B0010 correlation particularly with the newer engines used in this research (multi cylinder GM-LAF, multi cylinder turbo charged GM-LNF, single cylinder MTU-Hydra engines). However when the single cylinder MTU-CFR engine data was used, the correlation showed a significant impact of these fuel related Pi-

16

groups in B0010. This MTU-CFR engine represents an older engine design which has different combustion characteristics in comparison to the newer engine designs used in this research. Figure IX-1, rows 5 and 6 have fitted B0010 correlation plots using combine data obtained from all the engines and combine data obtained from all the newer engines respectively. It is confirmed that the MTU-CFR engine data has different characteristics in comparison to the newer engines data.

The following comparing the burn duration correlation developed in this dissertation to the existing burn duration correlation [30-32] using 2680 data point collected from GM-LAF and MTU-Hydra engines. The existing B0010 were obtained by fitting the data to Equation (I-1) to determine the coefficient C_1. The existing B1075 were obtained by fitting the data to Equation (I-2) to determine the coefficient C_2.

$$\Delta\theta_{0-10\%} = C_1 \quad (Sp \ v)^{1/3} \ (h/SL)^{2/3} \tag{I-1}$$

$$\Delta\theta_{10-75\%} = C_2 \ (B/h_{CA50}) \ (Sp \ v_{CA50})^{1/3} \ (h_{CA00}/SL_{CA50})^{2/3} \tag{I-2}$$

Figure I-2 shows the B0010 correlation as a function of Pi-groups developed in this dissertation. The R^2 is 0.91 and the RMSE is 2.28 ^{o}CA. Figure I-3 shows the existing B0010 correlation using the same data. The R^2 is -2.35 and the RMSE is 13.78 ^{o}CA. The negative value of R^2 indicates that the existing correlation is worse than a horizontal line that goes through the mean value of the B0010 [34]. It is clear to see that the two terms in the existing B0010 correlation are not enough to describe the B0010 taken from a wide range of geometries and operating conditions.

Figure I-4 shows the B1075 correlation as a function of Pi-groups developed in this dissertation. The R^2 is 0.89 and the RMSE is 1.40 ^{o}CA. Figure I-5 shows the existing B1075 correlation applied to the same data. The R^2 is -6.31 and the RMSE is 11.18 ^{o}CA. Similarly, the negative value of R^2 indicates that the existing

correlation is worse than a horizontal line that goes through the mean value of the B1075. This confirms that the existing B1075correlation with three terms is not sufficient to define the B1075 taken from engines with a wide range of geometries and operating conditions.

Figure I-2 B0010 correlation as a function of Pi-groups ($0 \leq E \leq 85$; $11 \leq CR \leq 15.5$; $1200 \leq N \leq 6600$; $257 \leq Net$ $IMEP \leq 1624$; $0.98 \leq \phi \leq 1.45$)

Figure I-3 Existing B0010 correlation ($0 \leq E \leq 85$; $11 \leq CR \leq 15.5$; $1200 \leq N$ ≤ 6600; $257 \leq Net\ IMEP \leq 1624$; 0.98 $\leq \phi \leq 1.45$)

Figure I-4 B0010 correlation as a function of Pi-groups ($0 \leq E \leq 85$; $11 \leq$ $CR \leq 15.5$; $1200 \leq N \leq 6600$; $257 \leq Net$ $IMEP \leq 1624$; $0.98 \leq \phi \leq 1.45$)

Figure I-5 Existing B0010 correlation ($0 \leq E \leq 85$; $11 \leq CR \leq 15.5$; $1200 \leq N$ ≤ 6600; $257 \leq Net\ IMEP \leq 1624$; 0.98 $\leq \phi \leq 1.45$)

18

- The coefficient of variation (COV) of indicated mean effective pressure (IMEP) is commonly used to describe cycle variations. Although the maximum pressure, the location of maximum pressure, the maximum rate of pressure rise, the location of the maximum pressure rise, the in-cylinder pressure trace over a certain range of crank angle, and the burn durations of 0-1%, 0-10%, 0-50% and 0-90% are also found in the literature as metrics to quantify the cycle variation limits and trends [3].

Two correlations of COV of IMEP are found in the literature [22, 23]. In the first study, a linear regression of COV of IMEP was developed using 146 data points obtained from three different chamber geometries, varying the total exhaust gas recirculation (EGR), air-fuel ratio, spark timing, engine speed and fueling level using a single-cylinder 0.6 liter displacement engine [22]. Using a wide range of engine geometries and operating conditions, The COV of IMEP was found to have a non-linear correlation to the engine geometry and operating conditions [23].

In the second study, a non-linear regression of a polynomial form for COV of IMEP was developed as a function of engine speed and load, equivalence ratio, residual fraction, burn duration of 0-10%, burn duration of 10-90% and location of 50% mass fraction burn (MFB) using 6000 conditions collected from 13 different engines from 1.6 to 4.6 liters in displacement [23]. Although this correlation was developed using a wider range of data compared to the first study, this regression computed negative COVs of IMEP within the range of data used in the correlation. This was mainly caused by the nature of the polynomial functional form, which has a combination of positive and negative signs in the equation.

In this dissertation, the COV of gross IMEP is correlated using data taken from two engine families over nearly 2900 operating conditions using a product-power functional form. The engines data vary from 1200 rpm to 6600 rpm with net indicated mean effective pressures ranging from 230 kPa to 1500 kPa,

19

compression ratios ranging from 11:1 to 15.5:1, and equivalence ratios ranging from 0.9 to 1.45, using seven different ethanol-gasoline blends. A correlation coefficient matrix was used to observe the non-linear power correlation between the COV of gross IMEP and the potential informative variables, including the burn durations, the COV of burn durations, and non-dimensional Pi-groups that was used in the burn duration correlation.

In comparison to the standard deviation (SD) of gross IMEP, the COV of gross IMEP was found to correlate well with the variables. The COV of gross IMEP was also found to highly correlate with B1075. Therefore it enables the COV of gross IMEP to be estimated only using the B1075. This allows safe operating conditions to be determined for engine experimental testing preventing potential damage to the engine. This will also allow more effective selection of conditions for experimental testing. The detailed process of developing the COV of gross IMEP correlation can be found in Chapter VII that focuses on developing the COV of gross IMEP correlation using data obtained from GM-LAF and MTU-Hydra engines on variable of compression ratios, full sweep of spark timing and cam phasing, a wide range of engine speeds and loads, and using seven different ethanol-gasoline blends.

The following compares the COV of gross IMEP correlation developed in this dissertation to the existing COV of gross IMEP correlation [23] using 2680 data points collected from GM-LAF and MTU-Hydra engines. The existing COV of gross IMEP were obtained using Equation (I-3) [23].

$$COV\ of\ IMEP = 18.5 + 1.41725\ RMF\ RPM^2$$
$$+0.00406\ B0010\ RPM^2 - 0.00328\ CA50^2$$
$$-0.00375\ CA50\ RPM^2 - 0.7326\ RPM\ \phi^2$$
$$-0.0011\ RPM\ IMEP\ CA50$$
$$+0.02809\ RPM\ IMEP + 0.00777\ B1090\ CA50$$
$$-0.00124\ RPM\ B0010^2 - 0.00015\ RPM\ B1090^2$$
$$+0.000888\ RPM\ CA50^2 - 19.57882\ \phi^3$$
$$+126.70806\ \phi^2\ RMF + 0.2419\ RMF\ B0010$$
$$+0.04414\ \phi^2\ CA50 + 50.73515\ \phi^2$$
$$-1.05318\ \phi\ RMF\ B0010$$
$$-238.75107\ \phi\ RMF - 0.27622\ \phi\ B1090 - 44.85289\ \phi$$
$$+199.32368\ RMF^3 - 0.02918\ RMF\ B1090\ CA50$$
$$+0.99062\ RMF\ B1090 + 0.05177\ RMF\ CA50^2$$
$$-0.7169\ RMF\ CA50 + 106.26606\ RMF$$
$$-0.19389\ B0010 + 0.00109\ B1090^2$$
$$-0.00007\ B1090\ CA50^2 + 0.00555\ B0010^2$$

(I-3)

Where:

RPM	engine speed (revolution per minute / 1000)
IMEP	engine load (bar)
ϕ	equivalence ratio
RMF	residual gas fraction
B0010	burn duration 0-10% MFB
B1090	burn duration 10% to 90% MFB
CA50	location of 50% MFB

Figure I-6 shows the COV of gross IMEP correlation as a function of Pi-groups developed in this dissertation. The R^2 is 0.63 and the RMSE is 0.88%. Figure I-7 shows the existing COV of gross IMEP correlation using the same data. The R^2 is -13.56 and the RMSE is 5.49%. Again, the negative value of R^2 indicates that the

existing correlation is worse than a horizontal line that goes through the mean value of the COV of gross IMEP. It is clear that the COV of gross IMEP as a function of Pi-groups has better correlation in comparison to the existing COV of gross IMEP correlation. Negative values are also observed in the existing COV of gross IMEP.

COV of gross IMEP in this dissertation was also developed as a function of burn durations. It was found that the COV of gross IMEP is highly correlated with B1075. Figure VII-2a in Chapter VII shows a correlation of COV of gross IMEP as a function of B1075. The R^2 is 0.7 and the RMSE is 0.79%.
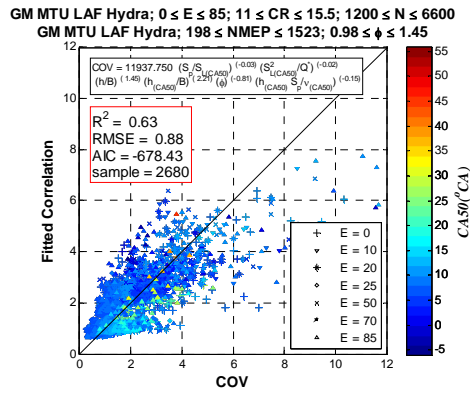
Figure I-6 COV of gross IMEP correlation as a function of Pi-groups (0 ≤ E ≤ 85; 11 ≤ CR ≤ 15.5; 1200 ≤ N ≤ 6600; 257 ≤ Net IMEP ≤ 1624; 0.98 ≤ φ ≤ 1.45)
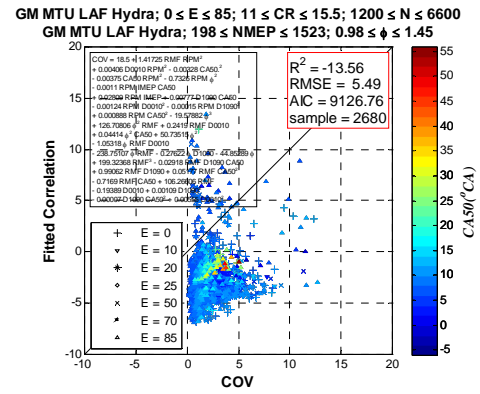
Figure I-7 Existing COV of gross IMEP correlation (0 ≤ E ≤ 85; 11 ≤ CR ≤ 15.5; 1200 ≤ N ≤ 6600; 257 ≤ Net IMEP ≤ 1624; 0.98 ≤ φ ≤ 1.45)

I.7   DISSERTATION OUTLINE

This dissertation is presented based on a number of publications including reports, published manuscripts, and manuscripts submitted at the time of writing this dissertation.

Each chapter focuses on a different subject and has its own introduction, discussion, and conclusion. The first page of each chapter contains summary of that chapter.

The motivation statement in the introduction in some chapters is similar in some cases. For example: Chapter V contains three articles about the Wiebe function parameters calculations. The first article focuses on the single-Wiebe function parameters calculation using the analytical solution and the least squares method approaches. The second article focuses on the double-Wiebe function parameters calculation using the least squares method. The last article focuses on the double-Wiebe function parameters calculation using the analytical solution which has a simple and straight forward calculation that is applicable to the engine simulation tool, GT-Power, which has a limited computational capability.

The chapters in this dissertation are outlined as follow:

CHAPTER II FUEL BLENDS PROPERTY CALCULATION

Properties of the fuel-air and combusted gas mixtures play an important role in the mass fraction burn and heat release analysis. A composite fuel was introduced to represent fuel-blend, including hydrocarbon, alcohol, and oxygenated hydrocarbon fuels. This method is robust in calculating fuel blends properties, thus, in calculating the properties of burned and unburned mixture application to IC engines, including the air fuel ratio, molecular weight, specific heat, viscosity, and lower heating value.

CHAPTER III MASS FRACTION BURN ANALYSIS

Mass fraction burn (MFB) calculation tools, including estimation of the heat transfer and crevice volume effects, have been developed to analyze the mean value and stochastic nature of combustion process using experimentally measured pressure traces. Single-zone MFB with two unknowns (temperature and mass fraction burn) and two-zone MFB with five unknowns (burned and unburned temperature, burned and unburned volume, and mass fraction burn) analyses have been exercised to calculate the MFB and have been compared to the apparent heat release method. The single-zone, two-zone and apparent

heat release methods can be used to study the MFB profile, however the two-zone model should be used if the detail in-cylinder temperature data an or the accurate combustion efficiency were needed.

CHAPTER IV BURN DURATION CORRELATIONS

A set of physically based parameters has been selected based on the literature study. Buckingham's Pi theorem was used to group these parameters into non-dimensional Pi-groups. A non-linear least squares method was developed and used to correlate the burn duration as a function of the physically based non-dimensional Pi-group parameters using a power-product functional form. Using these burn duration correlations, the effect of engine geometry variables and operating conditions can be observed.

CHAPTER V WIEBE FUNCTION PARAMETER ESTIMATION

Methods to determine the both single-Wiebe and double-Wiebe functions parameters have been developed by fitting the Wiebe function to the MFB profile. An analytical solution, a least squares method, and a combination of both were used to estimate the single-Wiebe function parameters which has two unknowns and the double-Wiebe function parameters which has five unknowns. Section V.1 focused on the single-Wiebe function parameters estimation using both analytical solution and the least squares method. To improve the fit to the experimental MFB profiles, Section V.2 focused on the double-Wiebe function parameters estimation using the least squares method. Section V.3 focused on the analytical solution for the double-Wiebe function parameters using a limited burn durations information (B0010, B1025, B1050, B1075, and B1090).

To measure the fit of the estimated Wiebe function, a single-zone pressure model was developed to reconstruct the pressure trace from a given MFB profile. The reconstructed pressure trace from the estimated Wiebe function was then compared with the experimentally measured pressure trace using metrics including the RMSE, the difference in Net IMEP, and the maximum difference in pressure trace. The double-Wiebe function fits better to the experimental MFB profile thus its reconstructed pressure trace matches

better to the experimentally measured pressure trace in comparison to the single-Wiebe function.

CHAPTER VI COMBUSTION MODEL INTEGRATION

A user compound was developed in GT-Power to contain the parametric combustion model. The user compound was chosen because of its flexibility in GT-Power interface, including sharing the compound with other GT-Power users and further modifications in the compound. An RLT-dependence was used to connect the predictive combustion compound with the multi-Wiebe combustion template in the main engine model. The RLT-dependence was chosen because there were no signal ports available in the multi-Wiebe combustion template at the time this parametric combustion compound being built. Even though this parametric combustion compound was built in GT-Suite V6 built-12, this parametric combustion compound was ready for the GT-Suite V7 which has open ports in the multi-Wiebe combustion template, thus enables the direct connection in and out the multi-Wiebe template.

CHAPTER VII CYCLE COMBUSTION VARIATION

Coefficient of variance (COV) of gross indicated mean effective pressure (IMEP) is commonly used to characterize the combustion duration and phasing variation in SI engines. A parametric model to predict the COV of gross IMEP in SI engines has been developed and integrated into the engine simulation tool GT-Power. A thermodynamic engine model has been developed to study the sensitivity of independent variables in the correlations, including burn durations and cycle combustion variation correlations. This thermodynamic engine model employed a residual fraction correlation as a function of overlap factor, engine speed, map and exhaust pressure, compression ratio, and equivalence ratio, burn duration and COV of gross IMEP correlations as a function of physically based non-dimensional groups.

CHAPTER VIII SUMMARY

A comparison between the single-Wiebe and double-Wiebe parametric combustion model were discussed. This chapter also discusses several ways to improve the parametric combustion modeling in the future.

CHAPTER IX APPENDICES

The appendices contain a compilation of short reports related to the development of the parametric combustion model including the engine databases specifications, range of operating conditions, comparison of burn duration correlations for each engine datasets, and copyright permissions to reprint the published papers.

I.8   PUBLICATIONS

Publications included in this document:

1.   Yeliana, C.Cooney, J.Worm, J.Naber, *Calculation of Mass Fraction Burn Rates of Ethanol-Gasoline Blended Fuels Using Single and Two-Zone Models.* SAE 2008-01-0320, 2008.

2.   Yeliana, J. Worm, D. Michalek, J. Naber, *Property Determination for Ethanol-Gasoline Blends with Application to Mass Fraction Burn Analysis in a Spark Ignition Engine.* Journal of Kones, Powertrain & Transportation, 2008. 15, No. 2: p. 553-561.

3.   Yeliana, C. Cooney, J. Worm, D. Michalek, J. Naber, *Wiebe Function Parameter Determination for Mass Fraction Burn Calculation in an Ethanol-Gasoline Fuelled SI Engine.* Journal of Kones, Powertrain & Transportation, 2008. 15, No. 3: p. 567-574.

4.   Yeliana, Y., C. Cooney, J. Worm, D. Michalek, J. Naber, *Estimation of Double-Wiebe Function Parameters for Burn Durations of Ethanol-*

Gasoline Blends in a SI Engine over Variable Compression Ratios and EGR levels. Submitted to Applied Thermal Engineering, 2010.

5.   Yeliana, Y., D. Loveland, C. Cooney, J. Worm, D. Michalek, J. Naber, *Parametric Study of Burn Durations of Ethanol-Gasoline Blends in a SI Engine over Variable Compression Ratios and EGR Levels.* Submitted to Combustion Science & Technology, 2010.

6.   Yeliana, J.Worm, D. Michalek, J. Naber, *Analytical Solution of Double-Wiebe Function Parameters Estimation for SI Engines.* TBD, 2010.

7.   Yeliana, *GM-MTU Predictive Combustion Model*, Report, 2010

Related publications not included in this dissertation:

8.   Cooney, C.P., **Yeliana**, J.Worm, J.Naber, *Combustion Characterization in an Internal Combustion Engine with Ethanol- Gasoline Blended Fuels Varying Compression Ratios and Ignition Timing.* Energy & Fuels, 2009. 23: p. 2319-2324.

9.   Syed, I. Z., **Yeliana**, Mukherjee, A., Naber, J., Michalek, D., *Numerical Investigation of Laminar Flame Speed of Gasoline-Ethanol/Air Mixtures with Varying Pressure, Temperature and Dilution.* SAE Int. J. Engines 3(1): 517-528, 2010.

II.   FUEL BLENDS PROPERTY CALCULATION

Properties of the fuel-air and combusted gas mixtures play an important role in the mass fraction burn and heat release analysis. A composite fuel was introduced to represent a certain fuel blend by assuming an ideal and non-reacting state throughout the mixing process. This method is robust in calculating fuel blends properties, including hydrocarbon, alcohol, and oxygenated hydrocarbon fuels. Once the fuel mixture properties were known, the properties of burned and unburned mixture properties were determined for a combustion reaction based on mole fraction and returned results on a mass basis for application to IC engine calculations.

Since the manuscript was written on a mole fraction basis, the following equations can be used to exchange the units back and forth between mole fraction, volume fraction and mass fraction. Considering two components of fuels, the mole fraction and mass fraction of the ethanol in the ethanol-gasoline blends is defined as follow:

$$\% \, Mole \, Ethanol = \frac{\% \, Vol \, Ethanol \, {}^{\rho_E}\!/\!_{MW_E}}{\left({}^{\rho_E}\!/\!_{MW_E} \, \% \, Vol \, Ethanol + {}^{\rho_G}\!/\!_{MW_G} \left(1 - \% \, Vol \, Ethanol\right) \right)} \quad \text{(II-1)}$$

$$\% \, Mass \, Ethanol = \frac{\% \, Vol \, Ethanol \, \rho_E}{\left(\rho_E \, \% \, Vol \, Ethanol + \rho_G \left(1 - \% \, Vol \, Ethanol\right) \right)} \quad \text{(II-2)}$$

Where:

% Vol Ethanol	Fraction volume of ethanol in the ethanol-gasoline blends
% Mole Ethanol	Fraction mole of ethanol in the ethanol-gasoline blends
% Mass Ethanol	Fraction mass of ethanol in the ethanol-gasoline blends
ρ	Density of species (Kg/m^3)
MW	Molecular Weight of species (kg/kmol)
Subscript E	Ethanol
Subscript G	Gasoline

PROPERTY DETERMINATION FOR ETHANOL-GASOLINE BLENDS WITH APPLICATION TO MASS FRACTION BURN ANALYSIS IN A SPARK IGNITION ENGINE[1]

Yeliana, J. Worm, D. Michalek, J. Naber

Michigan Technological University

Mechanical Engineering-Engineering Mechanics

1400 Townsend Drive, Houghton, Michigan, USA 49931-1295

Phone: +1 906 487-2551, fax: +1 906 487-2822

E-mail: yyeliana@mtu.edu, jjworm@mtu.edu, donna@mtu.edu, jnaber@mtu.edu

www.me.mtu.edu/reseachAreas/aice/

Abstract

The Mass Fraction Burn (MFB) and Heat Release Rate (HRR) reflect the amount of fuel burned, and the rate of burning throughout the combustion process in an internal combustion engine. These parameters play a crucial role in research and development endeavors focused on engine efficiency, emissions, and overall operating performance. They are computed by analyzing measured pressure data and applying thermodynamic principals to determine the energy released during the combustion process. Thus, the properties of the fuel-air and combusted gas mixtures play an important role in the analysis.

Engine pressure data were taken from a Spark-Ignition Cooperative Fuels Research (CFR) engine operating at a constant load of 330 kPa Net Indicated Mean Effective Pressure (Net IMEP) and using five ethanol-gasoline fuel blends: E0 (gasoline), E20, E40, E60, and E84. The fuels were assumed to be in a non-reacting state throughout the mixing process. Once the fuel mixture properties were known, the fuel-air and burned mixture properties were determined using the fuel-air mass ratio. The analysis presented within this paper details the process by which the fuel, fuel-air, and burned mixture properties can be determined. The MFB of five different fuel blends at a chosen operating condition was also presented along with the pressure trace, the temperature, and the gamma profile at the end of this paper.

Keywords: ethanol-gasoline blend, mass fraction burn, heat release, IC engine, fuel-air mixture properties

Introduction

Properties of species that are involved in engine combustion as a function of temperature can be found in JANAF thermochemical data tables [35]. However, the property of the mixture of particular species is not readily available. Newhall and Starkman [36]

developed the thermodynamic properties charts of burned and unburned mixtures of octane and air. Later, Olikara and Borman [37] developed a computer program to calculate the properties of products based on equilibrium combustion. Both of these works started the calculation based on mole fraction and returned results on a mass basis for application to IC engine calculations. Investigation of the thermodynamic properties of ethanol and gasoline blends in this research started from the concept of blending the fuels and then moved to the concept of mixing between the air, fuels and the products of the combustion. This included the calculation of gamma. Gamma is the ratio of the constant pressure specific heat to the constant volume specific heat which depends on the fuel and air mixture conditions and plays an important role in further analysis of the combustion process in IC engines.

Mass fraction burned as a function of crank angle represents the percentage of fuel consumed versus crank angle during the combustion process in an engine cycle. It shows that the rate at which the fuel-air mixture burns increases after the spark discharge to a maximum about halfway through the burning process and then decreases to zero as the combustion process ends. The mass fraction burned curve, which has a characteristic S-shape, is commonly used to characterize and develop the combustion process. A single-zone model has been developed and compared with a two-zone model using ethanol-gasoline fuel blends in a CFR engine [38]. Derived from the energy balance and the ideal gas equations, the single-zone model, with two unknowns (temperature and mass fraction burn), is proven to correlate well with the two-zone model, particularly in regards to combustion phasing. In this work, the mass fraction burn is calculated from experimental data using the single-zone model.

Experimental Setup

A single cylinder CFR engine, (manufactured by the Waukesha Motor Company), was used to generate the data used in this research. Several modifications have been incorporated to meet the criteria for this research. The experiments were conducted by

sweeping ethanol concentration, spark timing and compression ratio at constant engine speed and a constant indicated load of 330 kPa Net IMEP. The cylinder pressure data was obtained with an AVL GH12D piezoelectric pressure transducer. Data acquisition, including the measurement of cylinder pressure and various other critical pressures and temperatures, was accomplished using a combination of National Instruments (NI) hardware and software. A control system for this CFR engine had been previously developed by Naber, et al., [39], with Mototron's Motohawk rapid engine control development environment. Mototron's Mototune was used as the calibration tool and ECU interface. The calibration tool was also used to record engine control parameters such as intake manifold pressure, air flow rate, spark timing, fuel injection pressure, injection duration, commanded equivalence ratio, etc.

Composite Fuel

Assuming an ideal, non-reacting mixing process, the formation of one mole of total fuel blend is expressed as:

$$\left(1-\overline{E}\right)\left(CH_{\beta}O_z\right)_{\alpha}\Big|_{gasoline} + \overline{E}\left(CH_{\beta}O_z\right)_{\alpha}\Big|_{ethanol} = \left(CH_{\beta*}O_{z*}\right)_{\alpha*} \tag{II-3}$$

The indexes of the composite fuel can be obtained as follow:

$$\alpha* = \left(1-\overline{E}\right)\cdot\alpha_{gasoline} + \left(\overline{E}\right)\cdot\alpha_{ethanol} \tag{II-4}$$

$$\beta* = \frac{\left(1-\overline{E}\right)\cdot\beta_{gasoline}\cdot\alpha_{gasoline} + \left(\overline{E}\right)\cdot\beta_{ethanol}\cdot\alpha_{ethanol}}{\left(1-\overline{E}\right)\cdot\alpha_{gasoline} + \left(\overline{E}\right)\cdot\alpha_{ethanol}} \tag{II-5}$$

$$z* = \frac{\left(1-\overline{E}\right)\cdot z_{gasoline}\cdot\alpha_{gasoline} + \left(\overline{E}\right)\cdot z_{ethanol}\cdot\alpha_{ethanol}}{\left(1-\overline{E}\right)\cdot\alpha_{gasoline} + \left(\overline{E}\right)\cdot\alpha_{ethanol}} \tag{II-6}$$

Since gasoline is a refined petroleum product which consists of many hydrocarbons, given the molecular weight of 105 and the hydrogen to carbon ratio of 1.87, the averaged number of carbon atoms (equal to 7.56) can be calculated. Table II-1 shows the composition of gasoline-ethanol mixtures in the $(CH_{\beta}O_z)_{\alpha}$ form. The α, β, and z for

gasoline and ethanol data are taken from Heywood [3], while the α, β, and z for gasoline ethanol blends are calculated using the composite fuel concept using the given base fuel composition.

Table II-1 Composition of gasoline-ethanol blends in the $(CH_\beta O_z)_\alpha$ form

	Gasoline	$_E 20$	$_E 40$	$_E 60$	$_E 85$	Ethanol
α	7.56	6.44	5.33	4.22	2.83	2.00
β	1.87	1.94	2.04	2.19	2.55	3.00
z	0.00	0.03	0.07	0.14	0.30	0.50

Combustion Reaction

Considering complete combustion, the reaction of a single mole of an oxygenated-hydrocarbon fuel can be expressed as follows:

$$\left(CH_\beta O_z\right)_\alpha + \alpha\frac{A_s - z/2}{\phi}\left(O_2 + \psi N_2\right) = n_{CO_2}CO_2 + n_{H_2O}H_2O + n_{N_2}N_2 + n_{O_2}O_2 + n_{CO}CO + n_{H_2}H_2 \quad \text{(II-7)}$$

$$\alpha = \frac{MW_f}{12.011 + 1.008 \cdot \beta + 16.00 \cdot z} \quad \text{(II-8)}$$

$$A_s = 1 + \frac{\beta}{4} \quad \text{(II-9)}$$

The reactant and product compositions of one mole of oxygenated-hydrocarbon fuel reacted with air is summarized in Table II-5 (appendix). For a fuel-rich mixture, the water gas shift reaction constant is assumed to be a function of temperature, and there is no oxygen in the products. For a fuel-lean mixture, carbon monoxide and hydrogen are assumed not present in the products [3]. The ratio of the number of moles of products to

33

reactants does not vary significantly with respect to the ethanol concentration, as shown in Figure II-1. However, the total number of moles of reactants and products decreases significantly with higher ethanol content, particularly in the lean condition, as shown in Figure II-2. The inflection point that marks the stoichiometric reaction is caused by the difference in the rich and lean composition assumptions.
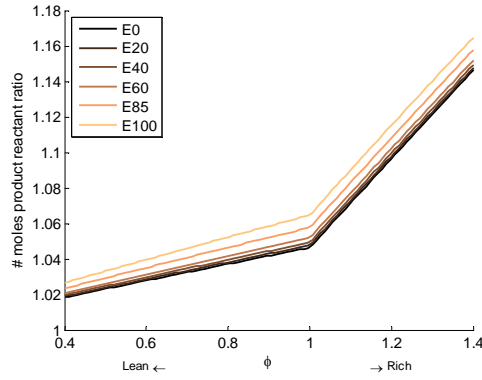
Figure II-1 Ratio of number of moles of products to reactants of gasoline-ethanol blends as function of equivalence ratio based one mole of fuel
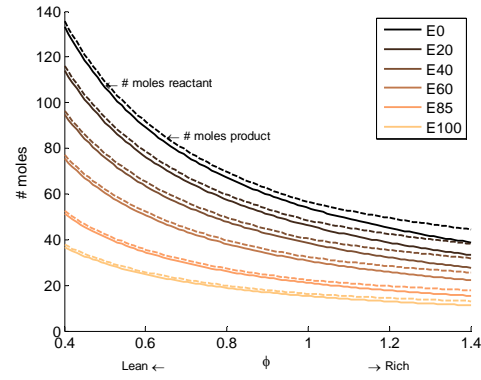
Figure II-2 Number of moles of products and reactants of gasoline-ethanol blends as function of equivalence ratio based one mole of fuel

The number of moles of reactant and product for stoichiometric combustion can be expressed:

$$\frac{\#\, moles\, products}{\#\, moles\, reac\tan s} = \frac{\alpha + \alpha\, \beta/2 + \alpha\psi\left(1 + \beta/4 - z/2\right)}{1 + \alpha\left(1 + \beta/4 - z/2\right)(1+\psi)} \tag{II-10}$$

Table II-2 shows the number of moles of reactant and product for stoichiometric combustion of the blended fuel in this research.

Table II-2 Ratio of number of moles of products to reactants of gasoline-ethanol blends
at stoichiometric condition

	Gasoline	$_E 20$	$_E 40$	$_E 60$	$_E 85$	Ethanol
#moles products	56.46	48.43	40.39	32.36	22.32	16.29
#moles reactants	53.93	46.20	38.47	30.75	21.09	15.30
#moles products/#moles reactants	1.05	1.05	1.05	1.05	1.06	1.07

Lower Heating Value

Using the fuel compositions provided in Table II-1, the molecular weight of the composite fuel is:

$$MW_f = \alpha(12.011 + 1.008 \cdot \beta + 16.00 \cdot z) \qquad \text{(II-11)}$$

The lower heating value of the blended fuel mixture on a molar basis is expressed as:

$$\overline{LHV}_f = (1 - \overline{E}) \cdot \overline{LHV}_{gasoline} + (\overline{E}) \cdot \overline{LHV}_{ethanol} \qquad \text{(II-12)}$$

The lower heating value of the blended fuel mixture on a mass basis is expressed as:

$$LHV_f = \frac{\overline{LHV}_f}{MW_f} \qquad \text{(II-13)}$$

Air Fuel Ratio

The air fuel ratio to completely burn the blended fuel can be calculated from equation below, where the number of moles of oxygen and nitrogen are given in Table II-5:

$$AFR = \frac{n_{O_2} \cdot MW_{O_2} + n_{N_2} \cdot MW_{N_2}}{n_f \cdot MW_f} \qquad \text{(II-14)}$$

Table II-3 shows the molecular weight, lower heating value and the stoichiometric air fuel ratio of the blended fuels in this research.

Table II-3 Molecular weight, the lower heating value and the stoichiometric air fuel ratio of gasoline-ethanol mixture using composite fuel calculation

	Gasoline	$\bar{E}20$	$\bar{E}40$	$\bar{E}60$	$\bar{E}85$	Ethanol
MW$_f$	105.00	93.20	81.40	69.60	54.85	46.00
LHV (MJ/kg)	43.46	41.83	39.72	36.90	31.66	26.90
AFR	14.54	13.99	13.28	12.33	10.56	8.96

Molecular Weight - Reactants and Products

Based on the composite fuel and combustion reaction calculation given in Table II-1 and Table II-5, the molecular weight of an oxygenated-hydrocarbon-air reactant mixture is calculated as:

$$MW_u = \frac{n_f \cdot MW_f + n_{o_2} \cdot MW_{o_2} + n_{N_2} \cdot MW_{N_2}}{n_u} \qquad \text{(II-15)}$$

And the molecular weight of the combustion products mixture is calculated as:

$$MW_b = \frac{n_{CO_2} \cdot MW_{CO_2} + n_{CO} \cdot MW_{CO} + n_{H_2O} \cdot MW_{H_2O} + n_{O_2} \cdot MW_{O_2} + n_{N_2} \cdot MW_{N_2} + n_{H_2} \cdot MW_{H_2}}{n_b} \qquad \text{(II-16)}$$

Figure II-3 shows the unburned molecular weight of gasoline-ethanol blends in mixture with air and the burned molecular weight of gasoline-ethanol blends after complete combustion. Due to the different assumption for products for rich and lean mixture, the molecular weight of the burned mixture has an inflection point at an equivalence ratio

equal to one. The effect of ethanol concentration is more pronounced in the burned portion than in the unburned portion. Table II-4 shows the unburned and burned molecular weight corresponding to the fuel blends used in this work for a stoichiometric reaction.
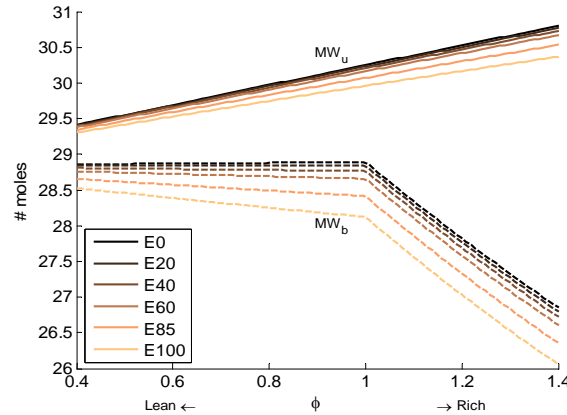
Figure II-3 Molecular weight of unburned and burned of gasoline-ethanol blends – air mixture as function of equivalence ratio

Table II-4 Stoichiometric unburned and burned molecular weight of a gasoline-ethanol air reaction

	Gasoline	$_E 20$	$_E 40$	$_E 60$	$_E 85$	Ethanol
MW_u	30.25	30.23	30.20	30.16	30.07	29.96
MW_b	28.89	28.84	28.77	28.66	28.41	28.12

Gamma (Specific Heat Ratio)

The gamma of the fuel mixture can be derived from the constant pressure heat capacity data that is widely available for ethanol and gasoline [3]. Similarly, for the unburned and burned mixtures, gamma is calculated based on each species. The constant pressure heat

capacity of those species can be found in Heywood [3]. The constant pressure specific heat capacity for the blended fuel mixture expressed on a molar basis is given by:

$$\overline{Cp}_f = (1 - \overline{E}) \cdot \overline{Cp}_{gasoline} + (\overline{E}) \cdot \overline{Cp}_{ethanol} \qquad \text{(II-17)}$$

The constant pressure specific heat capacity of an oxygenated-hydrocarbon-air reactant mixture that represents the unburned composition will be:

$$\overline{Cp}_u = \frac{n_f \cdot \overline{Cp}_f + n_{O_2} \cdot \overline{Cp}_{O_2} + n_{N_2} \cdot \overline{Cp}_{N_2}}{n_u} \qquad \text{(II-18)}$$

Similarly, the constant pressure specific heat capacity of the combustion products will be:

$$\overline{Cp}_b = \frac{n_{CO_2} \cdot \overline{Cp}_{CO_2} + n_{CO} \cdot \overline{Cp}_{CO} + n_{H_2O} \cdot \overline{Cp}_{H_2O} + n_{O_2} \cdot \overline{Cp}_{O_2} + n_{N_2} \cdot \overline{Cp}_{N_2} + n_{H_2} \cdot \overline{Cp}_{H_2}}{n_b} \qquad \text{(II-19)}$$

Gamma can be calculated equal to $(C_p / (C_p - R))$. Figure II-4 shows the unburned gamma of a gasoline-ethanol blend − air mixture as a function of temperature, and Figure II-5 shows the burned gamma assuming ideal combustion. Overall, the gamma decreases as the ethanol concentration increases, and as the temperature increases.
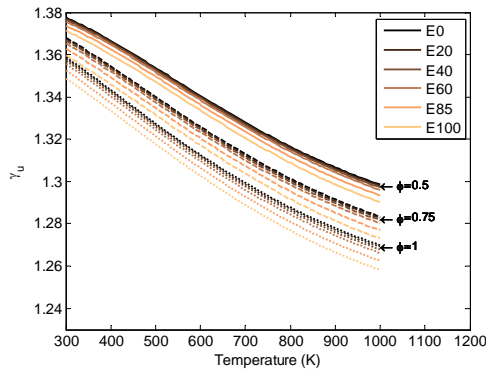
Figure II-4 Gamma unburned of gasoline-ethanol blend – air mixture as a function of temperature
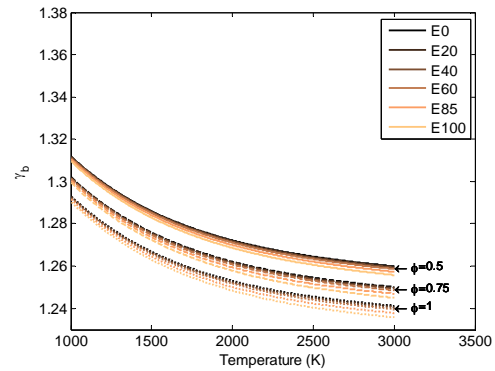
Figure II-5 Gamma burned of gasoline-ethanol blend – air mixture as a function of temperature

38

Alternatively, the gamma of the burned mixture as a function of burned temperature and can be expressed by the following equation that covers stoichiometric combustion for all the fuel blends from E0 – E84 that have been used in this research with an error less than 0.18%. Using this equation simplifies subsequent fraction burned calculations.

$$\gamma_b = -0.0130\left(\frac{T_b}{1000}\right)^3 + 0.0880\left(\frac{T_b}{1000}\right)^2 - 0.2144\left(\frac{T_b}{1000}\right) + 1.4329 \qquad \text{(II-20)}$$

Mass Fraction Burn Analysis

Figure II-6a shows the in-cylinder pressure trace in a CFR engine operating at a constant load and spark timing, for five different gasoline-ethanol fuel blends. Figure II-6b shows the mass fraction burn estimation using a single zone model, with the in-cylinder temperature profile and gamma as a function of temperature as inputs to the calculation. It is clearly shown that the mass fraction burn curve is a function of the pressure trace. The higher the ethanol content in the fuel blend, the higher the heat release rate, and thus the shorter the combustion duration. Figure II-6c shows the temperature profile, and Figure II-6d shows the gamma profiles starting from the point of ignition. The gamma decreases as the temperature increases. This trend, as well as the rank ordering of the different ethanol concentrations is consistent with the results shown in Figure II-5.

a.   Pressure trace   *b.   Mass fraction burn*

c.   *Temperature profile*   d.   *Gamma profile*
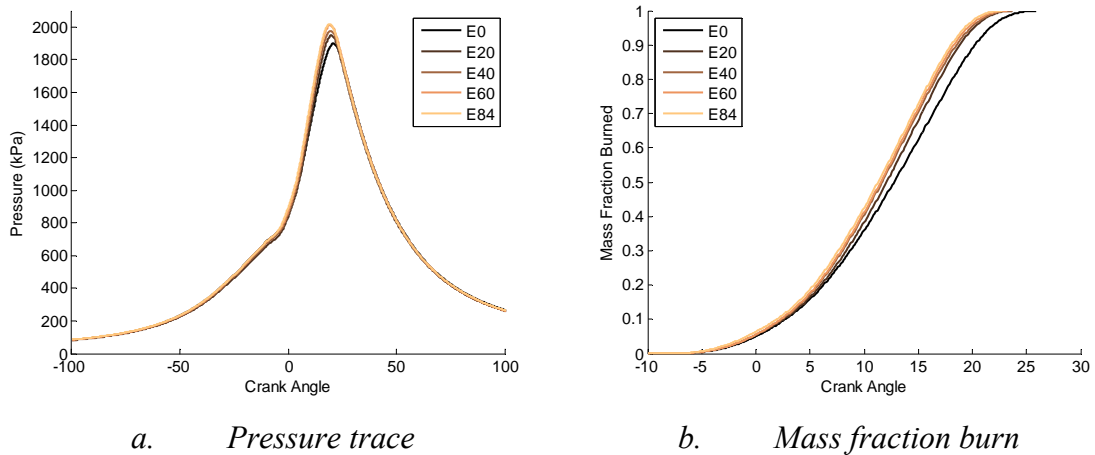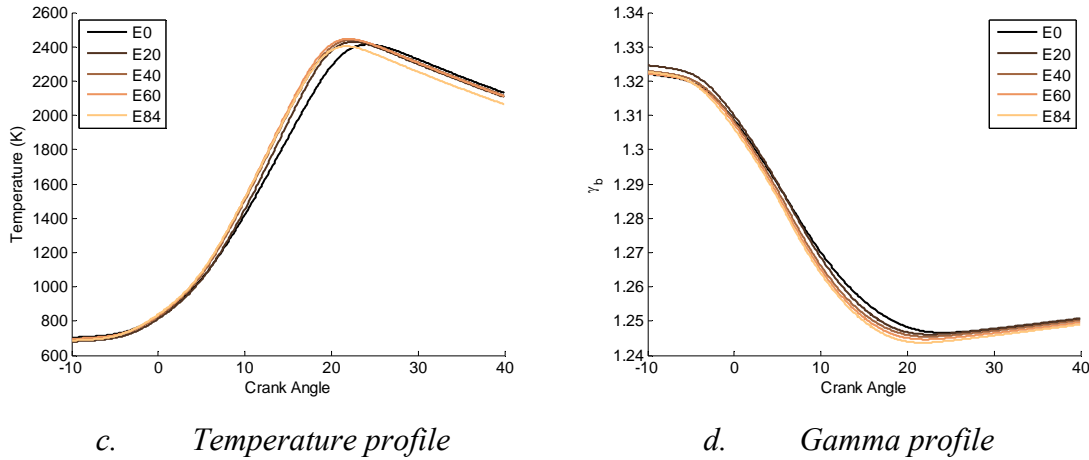
Figure II-6 Five different gasoline-ethanol blends using single zone mass fraction burn model (CFR engine, CR = 8.0:1, spark advanced = 10° BTDC, speed = 900 RPM, load = 330 kPa Net IMEP)

Conclusions

Several equations have been reviewed and introduced that can be used to calculate various thermodynamic properties of blends of different fuels, fuel and air mixtures, and products of combustion. Throughout this paper, these equations have been applied to the gasoline – ethanol blend ratios used in this research, and the results presented. Following are several conclusions that can be drawn from this work:

- The composite fuel concept that has been discussed in this paper is a simple and robust method for calculating various thermodynamic properties of fuel and fuel-air blends, as well as products of combustion.
- The number of moles of products and reactants is a function of both fuel composition as well as equivalence ratio.
- The Molecular Weight of the burned mixture is affected by ethanol concentration much more significantly than the molecular weight of the unburned mixture.
- The Molecular Weight of the burned mixture is a weak function of equivalence ratio for mixtures lean of stoichiometric, while it is a strong function of equivalence ratio for mixtures rich of stoichiometric.

40

- The gamma of both the unburned and burned mixtures is affected by variables such as ethanol concentration, equivalence ratio, and temperature. Except in the burned mixture, rich of stoichiometric, gamma tends to decrease with increasing ethanol concentration, and equivalence ratio. For burned mixtures rich of stoichiometric, gamma increases with increasing equivalence ratio.

- The properties of all species will affect the in-cylinder temperature profile calculation.

Nomenclature

$\overline{E}$	mole fraction of ethanol in the ethanol - gasoline mixture.
α	number of carbon atoms in the fuel
β	hydrogen to carbon ratio of the fuel
z	oxygen to carbon ratio of the fuel
A_s	stoichiometric moles of oxygen for hydrocarbon combustion
ψ	nitrogen to oxygen ratio of the air
ϕ	equivalence ratio
MW_f	molecular weight of the fuel
n	number of moles
AFR	air fuel ratio
LHV	lower heating value

Subscripts

b	burned
e	ethanol
f	fuel
g	gasoline
u	unburned
s	stochiometric reaction

Acknowledgments

Appendix

Table II-5 Gas composition of 1 mole of oxygenated-hydrocarbon fuel combusted with air

Unburned Composition	Burned Composition	
	$\phi \leq 1$ (lean and stoic mixtures) CO and H_2 can be neglected	$\phi \geq 1$ (rich mixtures) O_2 can be neglected
$n_f = 1$	$n_{CO_2} = \alpha$	$n_{CO_2} = \alpha(1-n)$
$n_{O_2} = \alpha \dfrac{A_s - z/2}{\phi}$	$n_{H_2O} = 2\,\alpha(A_s - 1)$	$n_{H_2O} = \alpha(-d + 2(A_s - 1) + n)$
$n_{N_2} = \alpha \dfrac{A_s - z/2}{\phi}\psi$	$n_{N_2} = \alpha \dfrac{\psi\,A_s}{\phi}\left(1 - \dfrac{z}{2\,A_s}\right)$	$n_{N_2} = \alpha \dfrac{\psi\,A_s}{\phi}\left(1 - \dfrac{z}{2\,A_s}\right)$
	$n_{O_2} = \alpha\,A_s\left(\dfrac{1}{\xi\phi} - 1\right)$	$n_{O_2} = 0$
	$n_{H_2} = 0$	$n_{H_2} = \alpha(d - n)$
	$n_{CO} = 0$	$n_{CO} = \alpha\,n$
	$\xi = \dfrac{2}{\left(2 - \dfrac{z}{A_s}(1-\phi)\right)}$	$n = \dfrac{-b \pm \sqrt{b^2 - 4\,ac}}{2\,a}$
		$a = 1 - \kappa$
		$b = 2\,(A_s - 1) + \kappa - d(1 - \kappa)$
		$c = -\,d\,\kappa$
		$d = 2\,A_s\left(1 - \dfrac{1}{\xi\phi}\right)$
		$\kappa = \dfrac{n_{H_2O}\,n_{CO}}{n_{CO_2}\,n_{H_2}}$
$n_u = n_f + n_{O_2} + n_{N_2}$	$n_b = n_{CO_2} + n_{H_2O} + n_{N_2} + n_{O_2} + n_{H_2} + n_{CO}$	

III. MASS FRACTION BURN ANALYSIS

Mass fraction burn (MFB) calculation tools have been developed to analyze the stochastic nature of the combustion process using measured pressure trace from engines for various ethanol-gasoline blend, over different engine geometries and operating conditions. One-dimensional single-zone MFB with two unknowns (temperature and mass fraction burn) and two-zone with five unknowns (burned and unburned temperature, burned and unburned volume, and mass fraction burn) analyses have been exercised to calculate the mass fraction burned in an engine operating on ethanol/gasoline-blended fuels using the cylinder pressure and volume data. Heat transfer and crevice volume effects were included in the both single-zone and two-zone MFB analysis methods. A comparison between the two methods was performed starting from the derivation of conservation of energy and the method to solve the mass fraction burned rates through the results including detailed explanation of the observed differences and trends. The apparent heat release method was used as a point of reference in the comparison process.

It is concluded that if the objective of a heat release analysis is simply to study the shape and / or locations on the mass fraction burned curves, then any of the three models can be used with reasonable success. However, if the objective includes accurate calculations of combustion efficiency, or the need for detailed in-cylinder temperature data (such as when doing further kinetic type modeling), the two zone model, with gamma as a function of temperature and gas composition, and with the effects of heat transfer and crevices should be employed.

THE CALCULATION OF MASS FRACTION BURN OF ETHANOL-GASOLINE BLENDED FUELS USING SINGLE AND TWO-ZONE MODELS[2]

Yeliana, Christopher Cooney, Jeremy Worm, and Jeffrey D. Naber

Michigan Technological University

Abstract

One-dimensional single-zone and two-zone analyses have been exercised to calculate the mass fraction burned in an engine operating on ethanol/gasoline-blended fuels using the cylinder pressure and volume data. The analyses include heat transfer and crevice volume effects on the calculated mass fraction burned. A comparison between the two methods is performed starting from the derivation of conservation of energy and the method to solve the mass fraction burned rates through the results including detailed explanation of the observed differences and trends. The apparent heat release method is used as a point of reference in the comparison process. Both models are solved using the LU matrix factorization and first-order Euler integration.

Experiments were conducted with a Cooperative Fuels Research (CFR) engine holding Net Indicated Mean Effective Pressure (Net IMEP) constant at 330 kPa and fueling at the respective stoichiometric condition for the air flow and ethanol fuel blend being tested. This study included four ethanol-gasoline fuel blends: E20, E40, E60, E84, and gasoline (E0) as a baseline. The results show that all three models consistently produce similar mass fraction burned profiles for the five different fuels tested. Furthermore, utilizing the gasoline case with gamma as a function of temperature shows that the two-zone model indicated 3% higher combustion efficiency compared to the single-zone model and 17%

---

higher than the apparent heat release method. However, the location of the 10%, 50%, and 90% mass fraction burn points calculated between the methods are within 1° of each other when combustion phasing is near maximum brake torque (MBT). For both the single and two-zone models, the effect of crevice and heat transfer effects appears near the end of the combustion process. Without the crevice model, the computed combustion efficiency of the single-zone model decreases by 8%. Without both crevice and heat transfer models the combustion efficiency decreases by 15% compared to the result of the single-zone full model. The combustion efficiency as calculated with the two-zone model decrease by 5% without crevice effects and 11% without both crevice and heat transfer effects.

Introduction

An experimental project is in process to characterize the interactions between ethanol concentration in ethanol / gasoline fuel mixtures, compression ratio, combustion phasing, and dilution. A critical step in a study such as this is to perform detailed heat release analysis to better understand the combustion process. However, before embarking on this task, the authors felt it best to fully investigate the commonly known analytical methods, including their ability to indicate changes due to ethanol concentration, as well as their sensitivity to the ratio of specific heat capacity of the gases (gamma), and the impact of heat transfer and crevice volume effects. As such, this paper will provide an explanation and comparison of select heat release methods, while presenting the resultant effects of ethanol concentration, gamma variation, and heat transfer and crevice volume dependencies.

The rate of heat release of the combustion process is strongly influenced by parameters such as the engine design, operating conditions, and fuel type. The heat release rate then has a significant impact on engine performance, not only in terms of specific output, but also in terms of efficiency and emissions. The integrated rate of heat release is often represented by the mass fraction burned (MFB). The mass fraction burn as a function of

crank angle has a characteristic S-shaped curve which represents the percentage of fuel consumed versus crank angle during the combustion portion of an engine cycle. The varying slope of this curve shows that the rate at which the fuel-air mixture burns, increases after the spark discharge to maximum level approximately halfway through the burning process and then decreases to zero as the combustion process ends. The MFB curve is commonly used to study and characterize the spark ignition combustion process.

By analyzing the pressure in the cylinder of the engine (typically measured with a piezo-electric pressure transducer), it is possible to compute the heat release rate as the fuel burns. Due to the combustion of fuel, the pressure inside the cylinder exceeds that which would have resulted from closed volume polytropic compression and expansion (i.e. the motored pressure trace). The pressure rise over a given crank angle interval is proportional to the mass of fuel burned over that same interval. This method, commonly known as the apparent heat release method, was developed by Rassweiler and Withrow in the 1930's [5].

Krieger and Borman [6] developed a method to include both the effects of heat transfer and the dissociation of the products of combustion in the calculation of the apparent heat release. This method was also used by Heywood et al. [7] with application to SI engine simulation. In fact, due to its simplicity, this method has been widely used by many engine researchers since its initial development.

Gatowski et al. [8] developed a single-zone heat release model, and later, Chun and Heywood [40] improved upon this single-zone model by introducing an accurate way to model the ratio of specific heats (gamma). The method averages the gamma computed from two separate zones. The same field of study in finding the correct gamma is done by Klein and Eriksson [41]. Later Cheung and Heywood [42] concluded that the single-zone heat release model is remarkably robust, and any error is most likely from the measured pressure and mass flow rate data.

The development and application of a two-zone heat release model by separating the charge into two regions (a burned and unburned region) had been previously discussed by

Krieger and Borman [6] and Heywood et al. [7]. As computational resources increased, Guezennec and Hamama [43] developed a two-zone model for SI engines that included heat transfer effects in the heat release analysis.

The research discussed within this paper is focused on examining the single-zone and two-zone models discussed in [5-8, 40-43] and comparing the results of these two models along with the results of the apparent heat release method. The analyses will cover the effects of gamma, heat transfer, and crevice volume on the calculated mass fraction burned.

Experimental Setup

A single cylinder CFR engine manufactured by the Waukesha Motor Company was used to collect the data used in this research. Table III-1 displays the CFR engine specifications. Several modifications have been incorporated. The piston is modified such that the engine could be operated over a wider range of compression ratios. Other changes include a relocation of the spark plug to top of the combustion chamber, and full electronic control of the spark, fueling rate, and throttle. The cylinder pressure data was obtained with an AVL GH12D piezoelectric transducer utilizing a PH01 flame arrestor mounted in a 2.0 mm diameter X 6.0 mm long passage. Data acquisition, including cylinder pressure and various other critical pressures and temperatures, is accomplished using a combination of National Instruments (NI) hardware and software. A control system for this CFR engine had been previously developed with Mototron's Motohawk rapid engine control development environment (Naber, et al., [39]). Mototron's Mototune was used as the calibration tool and ECU interface. The calibration tool was also used to record engine control parameters such as intake manifold pressure, air flow rate, spark timing, fuel injection pressure, injection duration, equivalence ratio, etc.

Table III-1 CFR engine specifications

Compression Ratio	4.5-17.5
Bore (cm)	8.26
Stroke (cm)	11.43
Displacement Volume (cm^3)	611.2
Intake Valve Opening (IVO)	10° ATDC
Intake Valve Closing (IVC)	34° ABDC
Exhaust Valve Opening (EVO)	40° BBDC
Exhaust Valve Closing (EVC)	15° ATDC
Maximum Speed (rpm)	900

The experiments were conducted by sweeping combustion phasing, ethanol concentration, and compression ratio at constant engine speed and indicated load. At each value of ethanol concentration and compression ratio, combustion phasing (via spark timing) was swept in 2° increments from a 50% mass fraction burned location (CA50) of ~30° ATDC to the point of heavy audible knock, or until the combustion phasing was clearly advanced beyond MBT, whichever came first. During this sweep, the point of borderline audible knock (if applicable) was noted in the data. At each set point the throttle was adjusted to maintain 330 kPa NET IMEP, the fueling was adjusted to achieve a stoichiometric equivalence ratio and 300 consecutive engine cycles were recorded. Averaging the pressure of each engine cycle was done based on the fact that statistically,

the average of N measurements is more reliable, and the engine itself responds to mean values of air and fuel flow (Lancaster, et al. [44]).

Calculation Methodology

Apparent Heat Release Method

As previously stated, the Apparent Heat Release Method relies upon the fact that the pressure rise above that due to compression and expansion over a given crank angle interval is proportional to the mass of fuel burned over that same interval. By assuming an ideal gas, the energy balance can be simplified to calculate the heat release from the system. This equation as a function of gamma is known as the apparent heat release, as expressed Equation (III-1). Gamma is the ratio of the constant pressure specific heat to the constant volume specific heat.

$$dQ_{Apparent} = \frac{\gamma}{\gamma - 1} p \, dV + \frac{1}{\gamma - 1} V \, dp \qquad \text{(III-1)}$$

Single-Zone Heat Release Model

Within the context of this paper, the single-zone model has the following initial conditions and assumptions:

1. Derivation is done based on thermodynamic principles of conservation of mass and energy.

2. The Woshni formulation [3] is used for the heat transfer coefficient.

3. A single aggregate volume is used to approximate the crevice volume.

4. The averaged pressure trace is taken from experimental data.

5. Thermodynamic properties and constants of the burned and unburned mixture are the same for both models.

6. Temperature is assumed to be uniform for all exposed cylinder surfaces.

7. Initial conditions are taken from the cylinder conditions at the time of spark.

8. Geometrical data corresponds to the modified CFR engine (see Table III-1).

The single-zone model that has been examined in this study is nearly the same as the apparent heat release model, except for the method of solving the equations. The apparent heat release calculation is derived by substituting the temperature from the ideal gas equation into the energy equation, calculating the heat release rate, and integrating to get the mass fraction burned. However, the single-zone mass fraction burned calculation solves both equations simultaneously to get the mass fraction burned profile and the in-cylinder temperature profile. The energy balance for the single-zone model is given as follows:

$$\left(\frac{Q_{LHV} \, m_c}{\left(A/F + 1 \right)} \right) dx_b - m_c \, Cv \, dT = p \, dV + A \, \bar{h} \left(T - T_w \right) + \frac{h \, V_{cr}}{\bar{R}/M \, T_w} \, dp \qquad \text{(III-2)}$$

Two-Zone Heat Release Model

The initial conditions and assumptions for the two-zone model are the same as those listed for the single-zone model, except that the initial temperature of burned fraction is equal to the adiabatic flame temperature of the fuel. However, while the single-zone model has two unknowns which requires 2 equations (x_b, T), the two-zone model requires 5 equations to solve for its five unknowns (x_b, T_u, T_b, V_u, V_b) simultaneously. In terms of the thermodynamic analysis of spark ignition engine combustion, it is commonly assumed that the more equations involved, the more accurate the analysis will be (Chun and Heywood [40]). However, more equations mean more complex calculations and

50

more computational time is required. The energy balance for the two-zone model is given as follows:

$$\left(\frac{Q_{LHV}\, m_c}{\left(A/F + 1\right)} + m_c\, Cv_u\, T_u - m_c\, Cv_b\, T_b\right) dx_b - m_c\left(1 - x_b\right) Cv_u\, dT_u - m_c\, x_b\, Cv_b\, dT_b$$

$$- p\, dV_u - p\, dV_b = A_u\, \bar{h}_u\left(T_u - T_w\right) + A_b\, \bar{h}_b\left(T_b - T_w\right) + \frac{h_u\, V_{cr}}{\bar{R}_u / M_u\, T_w}\, dp \tag{III-3}$$

It should also be mentioned that throughout the remainder of this paper, for all of the analysis models, it is assumed the combustion process follows the description given by Heywood [3]. A brief summary of that description follows.

- The first stage, known as the early flame development period, starts with spark discharge which initiates the combustion process and continues to the point where 10% of the charge has burned.

- The second stage is the rapid burning period. In this stage, the major portion of the charge burns as the flame propagates to the combustion chamber walls and the cylinder pressure steadily rises above the value it would have been in the absence of combustion. This period, corresponding to 10-90% mass fraction burned, represents the bulk of the combustion process, thus, is sometimes referred to as the bulk burn period.

- The final stage is the flame termination period, where the flame extinguishes on the combustion chamber surfaces. This period mostly reflects the heat transfer losses to the combustion chamber walls. The pressure decreases as the cylinder expands during this period.

Once the heat release data has been computed (regardless of which model is being used), the combustion efficiency can be calculated. The combustion efficiency is often used to determine the completeness of the combustion process. Combustion efficiency is the ratio

of the total heat release in the combustion chamber to the energy available from the fuel. The combustion efficiency was calculated from the following equation:

$$\eta_{comb} = \frac{Q}{\left(\dfrac{m_c}{\left(A/F + 1\right)}\right) Q_{LHV}}$$

(III-4)

Combustion efficiency is often determined by exhaust gas analysis [3]. However, emissions were not measured in this study. The comparison of the combustion efficiencies based upon the different models will provide insight to the effects of the investigated parameters have.

Results & Discussions

Effect of Ethanol Concentration

Since the experimental portion of this work included a sweep of ethanol concentration, one of the first variables to be examined was the effect of ethanol concentration on the indicated heat release results. This was done to determine the different models sensitivity and impact on the combustion rates and MFB profiles as the ethanol fuel concentration was changed.   The three different models, the apparent heat release (Equation III-1), single-zone (Equation III-2), and two-zone (Equation III-3) were used to investigate the effect of various ethanol-gasoline blends on the mass fraction burned profiles. Holding gamma constant and equal to 1.3, with no heat transfer or crevice effects, the three models produced similar mass fraction burned profiles. Figure III-1 shows both the mass fraction burned profile and the rates of the mass fraction burned of the various fuel blends with the three different models with constant gamma.

Although not apparent in Figure III-1 (a) and (b), the results of the three models are plotted for each fuel. The results are so closely matched that they are nearly overlaid. This can be seen in Figure III-1 (c) where the axis limits have been adjusted to see the

mass fraction burn rates for gasoline (E0) around its peak rate at 15°. Table III-2 summarizes three important combustion metrics from the MFB curves: (i) 0-10% MFB, (ii) location of 50% MFB and (iii) 10-90% MFB for the three models for each of the ethanol fuel blends. The maximum difference of the combustion phasing among the three models observation was 0.1°. Figure III-1 and Table III-2 show that the MFB results are very similar for all three methods. In addition, the observed effects and trends of the ethanol concentration in the fuel were not affected by the model.
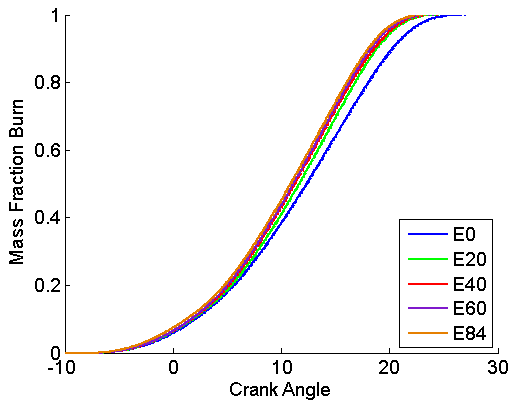
(a). Mass Fraction Burn Profiles
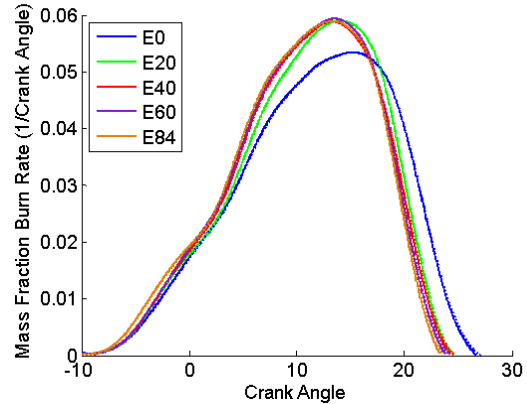
(b). Mass Fraction Burn Rate Profiles
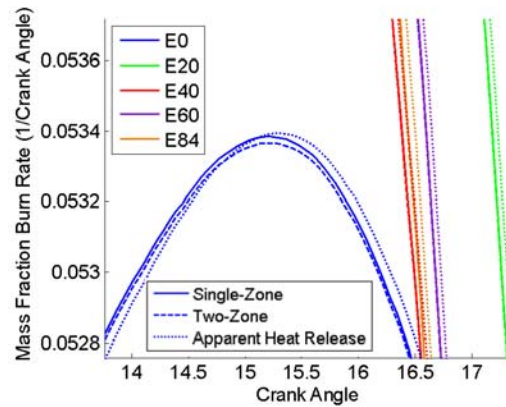
(c). Mass Fraction Burn Rate Profiles

Figure III-1 Combustion phasing profiles calculated with the 3 models with constant gamma (CR = 8.0:1, spark advanced = 10° BTDC, speed = 900 RPM, load = 330 kPa Net IMEP)

Table III-2 The combustion phasing of different ethanol concentration fuels calculated
with the 3 models with constant gamma (CR = 8.0:1, spark advanced = 10° BTDC, speed
= 900 RPM, load = 330 kPa Net IMEP)

		Single-Zone Model (γ=1.3)	Two - Zone Model (γ=1.3)	Apparent Heat Release (γ=1.3)
Duration of 0-10% MFB (° CA)	E0	12.1	12.2	12.3
	E20	11.8	11.8	11.9
	E40	11.7	11.7	11.8
	E60	11.6	11.6	11.7
	E84	11.2	11.2	11.3
Location of 50% MFB (° CA)	E0	12.4	12.4	12.5
	E20	11.6	11.6	11.7
	E40	11.2	11.2	11.3
	E60	11.1	11.1	11.2
	E84	10.9	10.9	10.9
Duration of 10-90% MFB (° CA)	E0	18.1	18.1	18.0
	E20	17.0	17.0	17.0
	E40	16.8	16.9	16.8
	E60	16.7	16.7	16.7
	E84	16.9	16.9	16.8

Effect of Gamma

Given the result above that each of the three models is equally capable of identifying changes in combustion due to ethanol concentrations, the discussion of the impact of gamma and heat transfer and crevice volume models on the MFB curves will be based on gasoline data.

When performing a heat release analysis, finding the appropriate gamma becomes an important factor. In the early development of heat release analysis, many researchers studied a method to define an appropriate gamma that accurately represented the combustion process. The motivation was to avoid the complications of the two-zone model, and thus enable high levels of accuracy with the single-zone model. Chun and Heywood [40] used the average of the gamma calculated from the burned and unburned zone. Gatowski et al. [8] formulated a gamma with a linear function of cylinder

temperature. Heywood [3] then provided gamma as a function of the temperature of the combusted gases.

In this part of the study, gamma is computed as a function of temperature and gas composition during the combustion process (see appendix C). Figure III-2 shows the gamma profiles of the gasoline-air mixture and combustion products that have been used in the calculations presented afterward. As expected, gamma decreases as the combustion progresses as a result of increases in temperature. Using the single-zone model, the single curve of gamma decreases until it reaches a minimum at approximately 20° after which the increasing volume reduces the temperature as the piston travel down to the BDC. The two separated curves of gamma when using the two-zone model are also shown in Figure III-2. The burned gamma increases initially (black circle) as the temperature in the burned gases adjust from the initial assumed temperature of the adiabatic constant pressure temperature above the unburned gas temperature. Then as the burned and unburned gases are compressed from the continuing combustion processes the gammas decrease until expansion begins to reduce the gas temperatures similar to the single zone model.
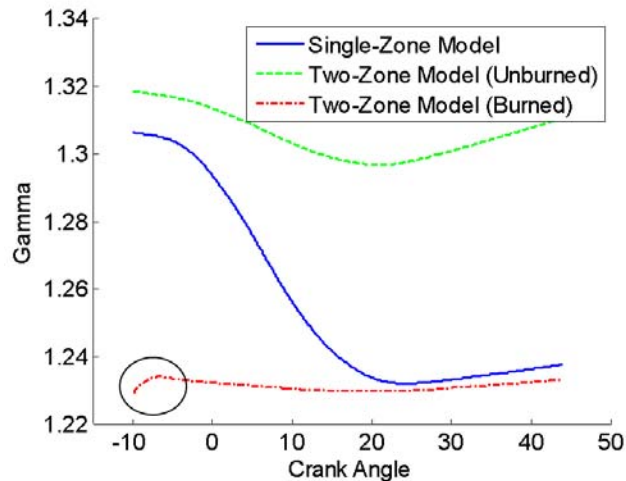
Figure III-2 A comparison of the gamma profile of gasoline (CR = 8.0:1, spark advanced = 10° BTDC, speed = 900 RPM, load = 330 kPa Net IMEP)

55

Figure III-3 presents the mass fraction burned profile and the mass fraction burned rates calculated with the three different methods. The first two methods, utilize the single-zone and the two-zone model with gamma calculated as a function of the temperature and composition of the exhaust gas. In this case, the exhaust composition is based on the stoichiometric reaction assuming ideal and complete reaction products. The third method is the apparent heat release method utilizing a constant gamma of 1.3. As shown in Figure III-3, each model has a similar trend which indicates that each model predicts similar combustion phasing.

Table III-3 summarizes the combustion phasing, combustion durations, and computed combustion efficiencies of gasoline calculated using the three models. The combustion efficiency resulting from both the single and two-zone models computed when using gamma as a function of gas temperatures is higher than that predicted using a constant gamma of 1.3 in each of the models respectively. The combustion efficiency of the two-zone model is 8% higher than the single-zone model under non MBT conditions (advanced or retarded). On average, over the range of compression ratios, spark advance and ethanol concentrations tested the two-zone model results in a computed combustion efficiency that is 3% higher than the single-zone model, and 17% higher than the apparent heat release model. It is important to recall, however, that although gamma has a significant effect on the combustion efficiency as computed with the various analysis models, the combustion phasing of each model did not varied more than 1°.
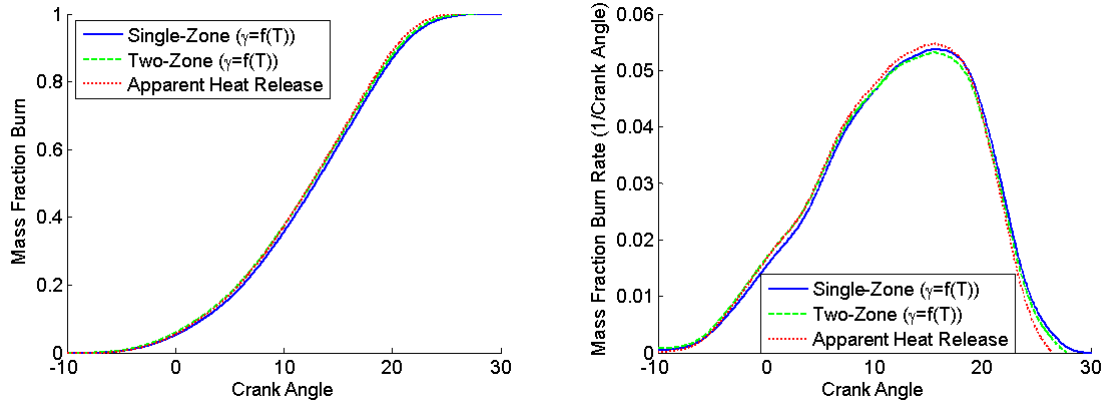
(a). Mass fraction burn profiles

(b). Mass fraction burn rate profiles

Figure III-3 Combustion phasing for gasoline calculated with the 3 models (CR = 8.0:1, spark advanced = 10° BTDC, speed = 900 RPM, load = 330 kPa Net IMEP)

Table III-3 Combustion phasing of gasoline calculated with the 3 models (CR = 8.0:1, spark advanced = 10° BTDC, speed = 900 RPM, load = 330 kPa Net IMEP)

	Single-Zone Model (γ=f(T))	Two - Zone Model (γ=f(T))	Apparent Heat Release (γ=1.3)
0-10% MFB (° CA)	13.1	12.3	12.3
50% MFB (° CA)	13.4	12.7	12.5
10-90% MFB (° CA)	17.8	18.4	18.0
Comb. Efficiency (%)	90.8	94.3	78.5

Effect of Heat Transfer And Crevice Volume

The same set of data is post processed by considering that some part of the heat is transferred to the cylinder wall and some part of mass is trapped and escapes combustion in the crevice volume. Figure III-4 shows the MFB and the MFB rate profiles of the single-zone model with and without the crevice and heat transfer effects included. The combustion phasing for this case is shown in
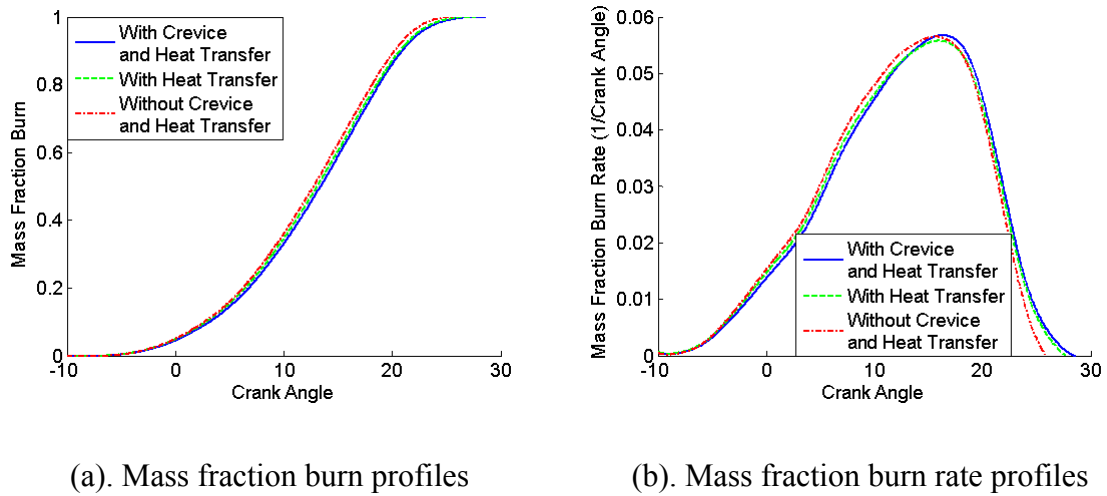
(a). Mass fraction burn profiles   (b). Mass fraction burn rate profiles

Figure III-4 A comparison of the single-zone mass fraction burned calculated with and without the crevice and heat transfer effects (CR = 8.0:1, spark advanced = 10° BTDC, speed = 900 RPM, load = 330 kPa Net IMEP)

Table III-4. Similarly, Figure III-5 shows the mass fraction burned and the mass fraction burned rate profile of the two-zone model with and without the crevice and heat transfer effects. Table III-5 summarizes the effect of crevice and heat transfer on the combustion phasing parameters of two-zone model.

Without crevice and heat transfer effects in the model, the useful energy will be lower and combustion efficiency will be significantly decreased. Using the single-zone model as shown in
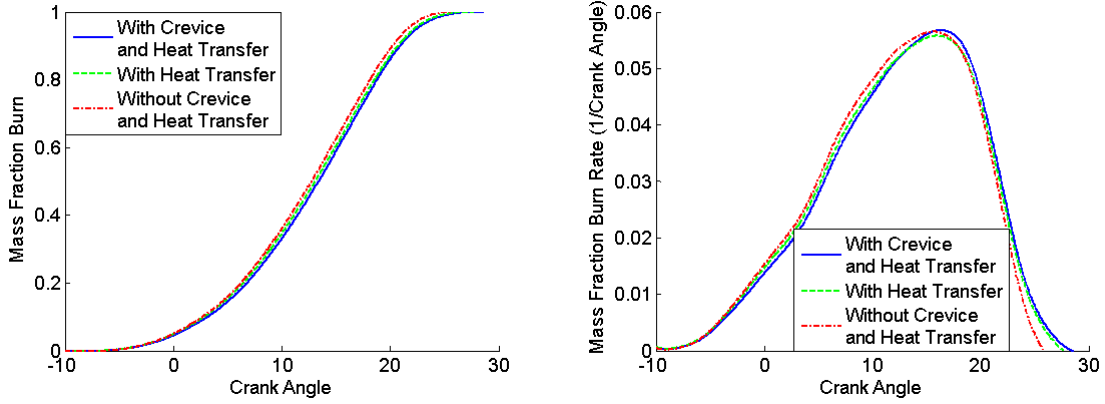
(a). Mass fraction burn profiles   (b). Mass fraction burn rate profiles

Figure III-4 A comparison of the single-zone mass fraction burned calculated with and without the crevice and heat transfer effects (CR = 8.0:1, spark advanced = 10° BTDC, speed = 900 RPM, load = 330 kPa Net IMEP)

Table III-4, without the crevice model the combustion efficiency decreases 8% and 15% without both the crevice and heat transfer in the models. For the two-zone model, as shown in Table III-5, without the crevice model only, the combustion efficiency decreases by 5%, and without both the crevice and heat transfer models the combustion efficiency decreases by 11% from the two-zone full model calculation.

In both the single-zone and two-zone models, the burn rate is faster during the first half of the combustion event because of not including the crevice and heat transfer effect. This is mainly the effect of shorter combustion duration and lower heat release from the combustion process. Although the inclusion of crevice and heat transfer models have large impacts on the computed combustion efficiency, the combustion phasing and duration is impacted by less than 1° crank angle.
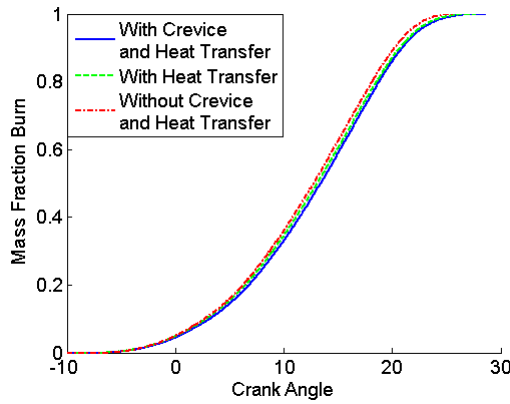
(a). Mass fraction burn profiles   (b). Mass fraction burn rate profiles
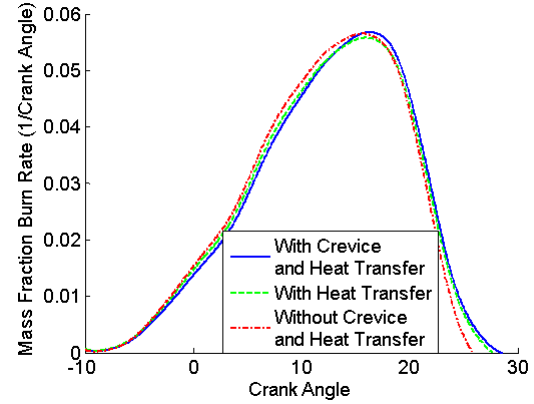
Figure III-4 A comparison of the single-zone mass fraction burned calculated with and without the crevice and heat transfer effects (CR = 8.0:1, spark advanced = 10° BTDC, speed = 900 RPM, load = 330 kPa Net IMEP)

Table III-4 A comparison of the single-zone mass fraction burned calculated with and without the crevice and heat transfer effect (CR = 8.0:1, spark advanced = 10° BTDC, speed = 900 RPM, load = 330 kPa Net IMEP)

	With Crevice and Heat Transfer Effect	With only Heat Transfer Effect	Without Crevice and Heat Transfer Effect
0-10% MFB (° CA)	13.1	12.8	12.6
50% MFB (° CA)	13.4	13.0	12.7
10-90% MFB (° CA)	17.8	17.9	17.5
Comb. Efficiency (%)	90.8	81.2	75.9
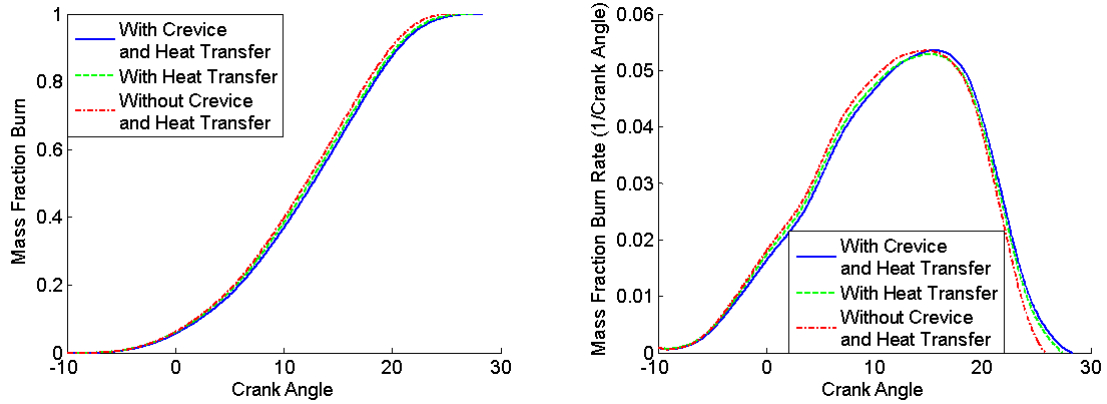
(a). Mass fraction burn profiles   (b). Mass fraction burn rate profiles

Figure III-5 A comparison of the two-zone mass fraction burned calculated with and without the crevice and heat transfer effects (CR = 8.0:1, spark advanced = 10° BTDC, speed = 900 RPM, load = 330 kPa Net IMEP)

Table III-5 A comparison of the two-zone mass fraction burned calculated with or without the crevice and heat transfer effect (CR = 8.0:1, spark advanced = 10° BTDC, speed = 900 RPM, load = 330 kPa Net IMEP)

	With Crevice and Heat Transfer Effect	With only Heat Transfer Effect	Without Crevice and Heat Transfer Effect
0-10% MFB (° CA)	12.3	11.9	11.8
50% MFB (° CA)	12.7	12.3	12.0
10-90% MFB (° CA)	18.4	18.4	18.1
Comb. Efficiency (%)	94.3	85.5	80.6

<u>Effect of Individual Cycle Calculations</u>

In order to show the cycle to cycle variation and for comparison of the average pressure-based mass fraction burn result to the individual cycle results, the mass fraction burn calculation is computed on an individual cycle basis. For this, the single-zone model with gamma constant and equal to 1.3 with the models for heat transfer and crevice volume turned off is used. The results for the individual cycle are then fit to a normal distribution and the probability distributions (PDFs) determined. Figure III-6 shows the PDFs of the resulting normal distributions for the 0-10% MFB, the 50% MFB location and the 10-90% MFB for various ethanol fuel blends for a spark advance of 0° BTDC. This data is similar to that provided in Table III-2 except that for Table III-2 the data is at a spark advance of 10° BTDC. Also shown for each distribution in Figure III-6 is a circle which is placed at the crank angle location of the mass fraction burn parameter as calculated based upon the averaged pressure signal using the same model.

First examining these figures for the effect of ethanol concentration, it is seen that as the ethanol concentration is increased, the 0-10% mass fraction burn reduces, the CA50 location advances, and the 10-90% mass fraction burn duration decreases. These results are again similar to those observed for the 10° spark advance. One other factor that can be observed in these plots is that the distributions for the gasoline (E0) data are wider with lower peaks, indicating more cycle to cycle variation.

Next, if we compare the peaks of the distributions from the cycle to cycle data we see they are well aligned with the circles from the pressure averaged data. This comparison is made in Table III-6. In the Table the mean and the median of the individual cycle data is given along with the result from the average pressure data for the three combustion metrics. Comparing the mean and the median of the data, it is seen that they are in close agreement with some cases with 0.1 to 0.2° higher means than medians. This would indicate a very small positive skewness of the distributions.

Finally comparing the mean of the individual cycle to the average pressure data, it is seen that the combustion metrics are within 0.2° of each other. This is in agreement with the

recommendation given by given by Lancaster, et al. [44] with respect to using the cycle averaged cylinder pressure for analysis.
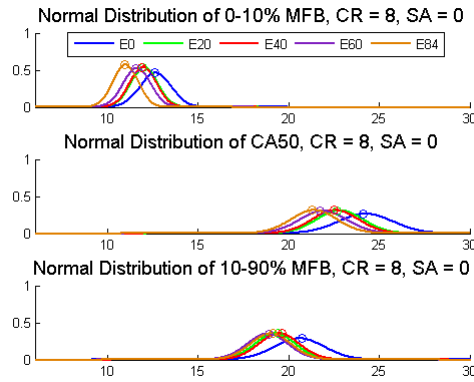
Figure III-6 Normal distribution of the combustion phasing calculated using the single-zone mass fraction burned with constant gamma of 1.3 (spark timing at TDC, speed = 900 RPM, load = 330 kPa Net IMEP)

Table III-6 The combustion phasing of different ethanol concentration fuels calculated with the single-zone model with constant gamma (CR = 8.0:1, spark advanced at TDC, speed = 900 RPM, load = 330 kPa Net IMEP)

		Mean of Individual Cycle	Median of Individual Cycle	Averaged Pressure Trace
Duration of 0-10% MFB (° CA)	E0	12.7	12.6	12.6
	E20	12.0	12.0	11.9
	E40	12.0	11.9	11.9
	E60	11.6	11.6	11.5
	E84	11.0	11.0	10.9
Location of 50% MFB (° CA)	E0	24.3	24.2	24.1
	E20	22.8	22.7	22.7
	E40	22.6	22.4	22.5
	E60	21.9	21.7	21.7
	E84	21.4	21.4	21.3
Duration of 10-90% MFB (° CA)	E0	20.6	20.7	20.7
	E20	19.3	19.3	19.4
	E40	19.5	19.4	19.6
	E60	18.9	18.8	18.9
	E84	19.0	19.0	19.1

Summary & Conclusions

Comparisons have been made between single-zone, two-zone, and apparent heat release methods of calculating the mass fraction burned using the cylinder pressure and volume data. The models are examined with respect to ethanol concentration in the fuel, the sensitivity of the results with respect to gamma, and the heat transfer and crevice volume effects. As a result, the following conclusions are made:

1. The results of the single-zone, two-zone, and apparent heat release combustion analysis models are all equally affected by changes in the ethanol concentration in the fuel.

2. Combustion metrics such as specific burn locations and durations are relatively insensitive to the type of model used, and model inputs including gamma, and the inclusion of heat transfer and crevice effects.

3. Combustion efficiency is significantly affected by the type of model used, and model inputs including gamma, and the inclusion of heat transfer and crevice models.

4. The change in computed results with the inclusion of heat transfer and crevice volume effects is approximately the same for both the single-zone and two-zone models.

5. Differences between the cycle to cycle means and the cycle averaged pressure result for the combustion metrics examined were small. This is likely a result of the fact that the cycle to cycle data examined in this study are not highly skewed. If individual cycle results showed non-normal distribution characteristics including skewness, further investigations are recommended.

Based on these points, it is concluded that if the objective of a heat release analysis is simply to study the shape and / or locations on the mass fraction burned curves, then any of the three models can be used with reasonable success. However, if the objective includes accurate calculations of combustion efficiency, or the need for detailed in-cylinder temperature data (such as when doing further kinetic type modeling), the two

zone model, with gamma a function of temperature and gas composition, and with the effects of heat transfer and crevices should be employed.

Nomenclature

A	combustion chamber surface area
B	piston bore
Cv	specific heat at constant volume
E	ethanol percentage
h	enthalpy
$\bar{h}$	average heat transfer coefficient
L	stroke
M	molecular weight
m	mass of the charge
N	engine speed
p	pressure
Q	heat
R	ratio of connecting rod to crank radius
$\bar{R}$	universal gas constant
T	temperature
V	volume
x	mass fraction
y	mole fraction
A/F	air fuel ratio
α	molar air
β	molar H/C ratio
γ	gamma or ratio of specific heat
ϕ	fuel air equivalence ratio
θ	crank angle

ρ density

ψ molar N/O ratio

Subscripts

a   air

b   burned

c   charge

ch   chemical

cr   crevice

d   displacement

e   ethanol

f   fuel

g   gasoline

ht   heat transfer

u   unburned

LHV   lower heating value

m   motored condition

r   reference state

s   stochiometric reaction

w   wall

Contacts

Yeliana   : yyeliana@mtu.edu

Christopher Cooney : cpcooney@mtu.edu

Jeremy Worm   : jjworm@mtu.edu

Jeffrey D. Naber : jnaber@mtu.edu

MEEM Department

Michigan Technological University

1400 Townsend Drive

Houghton, MI USA 49931-1295

Phone : (906) 487-2551

Fax : (906) 487-2822

Engine laboratories at MTU:

www.me.mtu.edu/researchAreas/aice/

Appendices

A) SINGLE-ZONE MODEL

The single-zone mass fraction burned model applies only one zone for all the mixture in the cylinder. The single-zone calculations are based upon the following assumptions:

1. Closed system analysis is employed within the limits from intake valve closing to exhaust valve opening.

2. The cylinder pressure at a given crank angle is uniform throughout the entire combustion chamber.

3. Instantaneous burning of fuel in heat addition calculations.

4. All mixtures are homogeneous, both air and fuel in the unburned mixture and combustion products in the burned mixture.

5. The initial conditions of temperature are calculated based on the ideal gas law from the measured pressure trace, volume and mass that was trapped in the combustion chamber. The mass of air is measured using an LFE (Laminar Flow Element), the mass of fuel is calculated using the measured air-fuel ratio, and the residual mass is assumed to be 10% of the total mass trapped in the combustion chamber based on discussion in Fox, et al. [45]

6. The heat transfer coefficient between the charge and the wall is predicted using the Woshni equation. The heat transfer contact area is assumed to be equal to the total surface area of combustion chamber.

7. The crevice volume is assumed to be 2% of the clearance volume and has a temperature equal to the wall temperature and a pressure the same as the cylinder pressure.

8. The wall temperature is 400K and constant for the combustion process.

The mass conservation in the cylinder during the combustion process is:

$$m = m_c + m_{cr} \tag{III-5}$$

Assuming that crevice mass is very small compared to the cylinder mass, the crevice mass is constant with respect to crank angle.

$$dm = dm_c = 0 \tag{III-6}$$

During the combustion process, the charge mass is modeled in two regions. The unburned mass is the mass of unburned charge, which is reduced during the combustion process while the burned mass increases.

$$m_c = m_b + m_u \tag{III-7}$$

The mass fraction burned is defined as a ratio of the burned mass to the charge mass in cylinder. The derivative of burned and unburned mass is given as, respectively:

68

$$dm_b \;=\; m_c\,dx_b \tag{III-8}$$

$$dm_u \;=\; -m_c\,dx_b \tag{III-9}$$

Assuming the cylinder pressure of the unburned and burned zone are the same, and the working fluid as an ideal gas, the equation of state is then defined as:

$$pV \;=\; m\,\frac{\overline{R}}{M}\,T \tag{III-10}$$

In derivative form, assuming constant molecular weight, the equation of state of the unburned and burned zone is expressed as:

$$m_c\,\frac{\overline{R}}{M}\,dT = V\,dp + p\,dV \tag{III-11}$$

Considering a closed system as shown in Figure III-7, the energy release from combustion is equal to the change in internal energy, the work that acts upon the piston, the crevice effects and the heat transfer loss to the walls of the combustion chamber. The energy conservation is:

$$\delta Q = dU + \delta W + \sum dm_{cr}\,h_{cr} \tag{III-12}$$
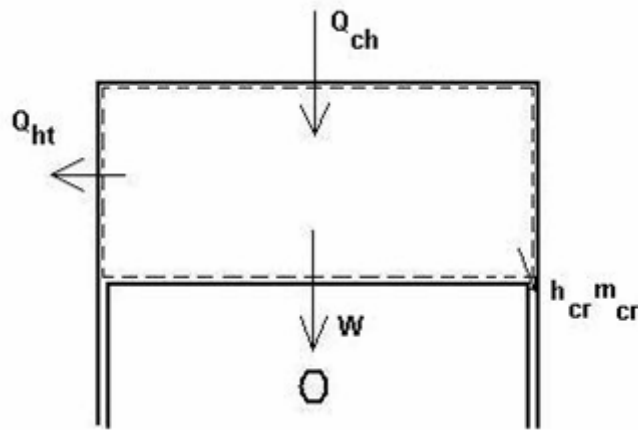
Figure III-7 Schematic system in cylinder

The internal energy can be express as:

$$dU = m_c \, Cv \, dT \tag{III-13}$$

The work is defined as:

$$\delta W = p \, dV \tag{III-14}$$

The heat transfer to the system consists of the heat release from combustion of the fuel and heat lost to the surrounding wall.

$$\delta Q = \delta Q_{ch} - \delta Q_{ht} \tag{III-15}$$

The energy release from combustion is calculated from:

$$dQ_{ch} = Q_{LHV} \left(\frac{m_c}{\left(A/F + 1 \right)} dx_b \right) \tag{III-16}$$

The heat transfer is modeled only between the working fluid to the cylinder walls in a convection manner. The heat transfer formulation is given by:

$$dQ_{ht} = A \, \bar{h} \, (T - T_w) \tag{III-17}$$

The heat transfer coefficient using the Woschni formulation (Heywood, [3]) is:

$$\bar{h} = 3.26 \, B^{-0.2} \, p^{0.8} \, T^{-0.55} \left(4.56 \, L \, N + 0.00324 \frac{V_d \, T_r}{p_r \, V_r} (p - p_m) \right)^{0.8} \tag{III-18}$$

The combustion chamber surface area is simulated from the total surface area.

$$A = A_{pistonhead} + A_{cylhead} + \frac{\pi \, B \, L}{2} \left(R + 1 - \cos(\theta) - \left(R^2 - \sin^2(\theta) \right)^{1/2} \right) \tag{III-19}$$

The crevice volume in the engine includes the gap above the top ring between the cylinder and piston, the area around the spark plug, the small gap between the cylinder

block and the head, etc. In order to simplify the equation, the crevice volume is assumed to be a single aggregate volume where the gas inside has the same pressure as the cylinder pressure, and the gas temperature in the crevice is assumed to be the same as the wall temperature since the crevice walls are colder than the combustion chamber. Gatowski et al. [8] notes that normally the crevice volume is 1-2% of the clearance volume. The crevice effect is modeled using the formulation below:

$$m_{cr} = \frac{p\,V_{cr}}{\frac{R}{M}\,T_w} \tag{III-20}$$

The energy conservation can be express as:

$$\left(\frac{Q_{LHV}\,m_c}{\left(\frac{A}{F}+1\right)}\right)dx_b - m_c\,Cv\,dT = p\,dV + A\,\bar{h}\left(T - T_w\right) + \frac{h\,V_{cr}}{\frac{R}{M}\,T_w}\,dp \tag{III-21}$$

The mass fraction burned of single-zone model is a result of solving Equations III-11 and III-21 simultaneously.

B) TWO-ZONE MODEL

The basis of the two-zone model is to set apart the combustion chamber into two regions, a burned and unburned portion based on the mass fraction burned scale. Both regions are separated by a thin layer of flame front. The same assumptions as the single-zone are taken for the two-zone mass fraction burned analysis, with addition of the following:

1. No heat transfer occurs across the flame front

2. Each zone has a separate heat transfer coefficient which is predicted using the Woshni equation and has a separate contact area which is calculated based on the instantaneous mass fraction burned

The derivative of burned and unburned mass is given previously in the single-zone model derivation.

Similarly, the volume in cylinder during the combustion process consists of burned volume, unburned volume and crevice volume. The crevice volume is constant with respect to crank angle, while the burned and unburned volume is changing during the combustion process.

Determining the volume of burned gases and the shape of the flame front surrounding the burned volume are the most difficult challenges of the two-zone model, and were discussed by Krieger and Borman [6]. Assuming a round shape for the flame front solves the calculation of the contact heat transfer area from both the burned and unburned region to the walls. Furthermore, the nature of premixed flame propagation in SI engines allows the effect of heat transfer over the flame front to be ignored. In these models, the burned and unburned volume is taken as separate variables.

$$dV_u + dV_b = dV \tag{III-22}$$

Assuming the working fluid is an ideal gas, the cylinder pressure of the unburned and burned zone are the same, and the unburned and burned molecular weight is constant, the equation of state for the unburned and burned zone in derivative form is:

$$-m_c \frac{\overline{R}_u}{M_u} T_u \, dx_b + (1 - x_b) m_c \frac{\overline{R}_u}{M_u} dT_u - p \, dV_u = V_u \, dp \tag{III-23}$$

$$m_c \frac{\overline{R}_b}{M_b} T_b \, dx_b + x_b \, m_c \frac{\overline{R}_b}{M_b} dT_b - p \, dV_b = V_b \, dp \tag{III-24}$$

Considering a closed system, the derivation of energy conservation is given during the previous single-zone model discussion. The energy conservation can be express as:

$$\left(\frac{Q_{LHV}\ m_c}{\left(A/F + 1\right)} + m_c\ Cv_u\ T_u - m_c\ Cv_b\ T_b\right)dx_b - m_c\left(1-x_b\right)Cv_u\ dT_u - m_c\ x_b\ Cv_b\ dT_b$$

$$- p\ dV_u - p\ dV_b = A_u\ \bar{h}_u\left(T_u - T_w\right) + A_b\ \bar{h}_b\left(T_b - T_w\right) + \frac{h_u\ V_{cr}}{\bar{R}_u / M_u\ T_w}\ dp \tag{III-25}$$

Similarly, as shown in Figure III-8, the energy conservation for the unburned zone can be express as:

$$- m_c\ \bar{R}_u / M_u\ T_u\ dx_b - m_c\left(1-x_b\right)Cv_u\ dT_u - p\ dV_u = A_u\ \bar{h}_u\left(T_u - T_w\right) \tag{III-26}$$
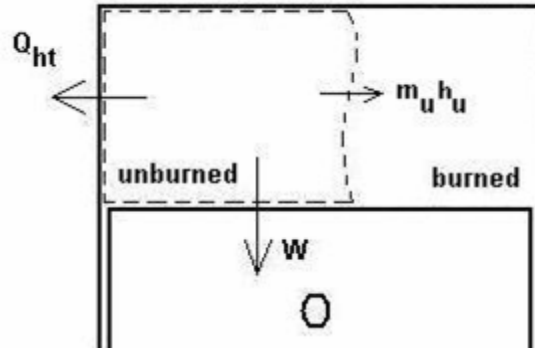
Figure III-8 Schematic system of the unburned zone

The mass fraction burned of two-zone model is a result of solving Equations III-22, III-23, III-24, III-25 and III-26 simultaneously.

C) COMBUSTION STOICHIOMETRY

The following derivation is done in order to calculate the gamma as a function of the burned gas temperature and composition.

It is sufficiently accurate to regard the mole fraction of oxygen and the mole fraction of nitrogen in dry atmospheric air as 0.2095 and 0.7905, respectively. Considering only six

species (CO_2, H_2O, N_2, O_2, CO, H_2) in the combustion products, the chemical reaction for burning one mole of hydrocarbon fuel can be written as:

$$CH_\beta + \frac{\alpha_s}{\phi}\left(O_2 + \psi\, N_2\right) = n_{CO_2}CO_2 + n_{H_2O}H_2O + n_{N_2}N_2 + n_{O_2}O_2 + n_{CO}CO + n_{H_2}H_2 \quad \text{(III-27)}$$

$$\alpha_s = 1 + \frac{\beta}{4} \quad \text{(III-28)}$$

For $\phi \leq 1$ (lean and stoichiometric mixtures), CO and H_2 at the exhaust can be neglected.

$$n_{CO_2} = 1$$

$$n_{H_2O} = 2\left(\alpha_s - 1\right)$$

$$n_{O_2} = \alpha_s \left(\frac{1}{\phi} - 1\right)$$

$$n_{N_2} = \frac{\psi\, \alpha_s}{\phi}$$

For alcohol or alcohol-hydrocarbon blends, the reactant mixture is:

$$CH_\beta O_z + \frac{\alpha_s - {}^z\!/_2}{\phi}\left(O_2 + \psi\, N_2\right) \quad \text{(III-29)}$$

Rearranging the reactant per mole of hydrocarbon:

$$CH_\beta + \left(\frac{\alpha_s - {}^z\!/_2}{\phi} + \frac{z}{2}\right)O_2 + \left(\frac{\alpha_s - {}^z\!/_2}{\phi}\psi\right)N_2 \quad \text{(III-30)}$$

The alcohol-hydrocarbon fuel combustion products calculation is the same as the hydrocarbon fuel calculations as follows:

$$\phi^* = \xi \, \phi \qquad \text{(III-31)}$$

$$\psi^* = \xi \left(1 - \frac{z}{2\,\alpha_s}\right)\psi \qquad \text{(III-32)}$$

$$\xi = \frac{2}{\left(2 - \dfrac{z}{\alpha_s}(1 - \phi)\right)} \qquad \text{(III-33)}$$

Based on the stoichiometric reaction, the specific heat of each species in the product can be predicted. The specific heat as a function of temperature for each species is given in Heywood [3]. The following Table III-7 summarizes the coefficients that being used in this current research.

D) THERMODYNAMIC PROPERTIES

Ethanol and gasoline are mixed based on percent volume. Assuming the gasoline is C_8H_{18} and the ethanol is C_2H_5OH, the amount of carbon, hydrogen and oxygen atoms in the fuel mixtures, respectively are: $(2\,\rho_e - 8\,\rho_g)E + 8\,\rho_g$, $(6\,\rho_e - 18\,\rho_g)E + 18\,\rho_g$, and $(\rho_e)E$. The molecular weight of the fuel blend is:

$$M_f = \left((2\,\rho_e - 8\,\rho_g)E + 8\,\rho_g\right)12.01 + \left((6\,\rho_e - 18\,\rho_g)E + 18\,\rho_g\right)1.008 + (\rho_e E)16 \qquad \text{(III-34)}$$

The molecular weight of the unburned gas is given by:

$$M_u = y_a\,M_a + y_f\,M_f \qquad \text{(III-35)}$$

Where:

$$y_f = \frac{1}{1 + \dfrac{4.773\,\alpha_s}{\phi}} \qquad \text{(III-36)}$$

$$y_a = 1 - y_f \qquad \text{(III-37)}$$

Finally, the molecular weight of the burned gas is expressed by:

$$M_b = y_{CO_2} M_{CO_2} + y_{H_2O} M_{H_2O} + y_{N_2} M_{N_2} + y_{O_2} M_{O_2} + y_{CO} M_{CO} + y_{H_2} M_{H_2} \qquad \text{(III-38)}$$

The following Table lists the physical properties of ethanol and gasoline.

Table III-7 Specific heat coefficients [3]

T = 300-1000K

$Cp\_CO_2=(0.44608E1+0.30982E-2*T-0.12393E-5*T^2+0.22741E-9*T^3-0.15526E-13*T^4)$

$Cp\_H_2O=(0.27168E1+0.29451E-2*T-0.80224E-6*T^2+0.10227E-9*T^3-0.48472E-14*T^4)$

$Cp\_CO=(0.29841E1+0.14891E-2*T-0.57900E-6*T^2+0.10365E-9*T^3-0.69354E-14*T^4)$

$Cp\_H_2=(0.31002E1+0.51119E-3*T+0.52644E-7*T^2-0.34910E-10*T^3+0.36945E-14*T^4)$

$Cp\_N_2=(0.28963E1+0.15155E-2*T-0.57235E-6*T^2+0.99807E-10*T^3-0.65224E-14*T^4)$

$Cp\_O_2=(0.36220E1+0.73618E-3*T-0.19652E-6*T^2+0.36202E-10*T^3-0.28946E-14*T^4)$

T = 1000-5000K

$Cp\_CO_2=(0.24008E1+0.87351E-2*T-0.66071E-5*T^2+0.20022E-8*T^3+0.63274E-15*T^4)$

$Cp\_H_2O=(0.40701E1-0.11084E-2*T+0.41521E-5*T^2-0.29637E-8*T^3+0.80702E-12*T^4)$

$Cp\_CO=(0.37101E1-0.16191E-2*T+0.36924E-5*T^2-0.20320E-8*T^3+0.23953E-12*T^4)$

$Cp\_H_2=(0.30574E1+0.26765E-2*T-0.58099E-5*T^2+0.55210E-8*T^3-0.18123E-11*T^4)$

$Cp\_N_2=(0.36748E1-0.12082E-2*T+0.23240E-5*T^2-0.63218E-9*T^3-0.22577E-12*T^4)$

$Cp\_O_2=(0.36256E1-0.18782E-3*T+0.70555E-5*T^2-0.67635E-8*T^3+0.21556E-11*T^4)$

Fuels

$Cp(gasoline)=(-22.501+227.99*(T/1000)-177.26*(T/1000)^2+56.048*(T/1000)^3+0.4845/((T/1000)^2))$

$Cp(ethanol)=(6.990+39.741*(T/1000)-11.926*(T/1000)^2)$

Table III-8 Physical properties of ethanol and gasoline (Bromberg, et al. [25])

	Gasoline	Ethanol
Density (kg/m^3)	720	790
C_p (J/kg.K)	2420	2470
Thermal Conductivity (W/m.K)	0.147	0.182
Viscosity (kg/m.s)	0.00054	0.0012
Molecular Weight (kg/kmol)	~97	41
Latent Heat (kJ/kg)	306	855
Boiling Temperature (K)	339	351
Lower Heating Value (MJ/kg)	44	26.9
Octane Number (ON)	87-95	115

IV.   BURN DURATION CORRELATIONS

Based on the existing literature, several parameters that correlate to the combustion process have been proposed. Dimensional analysis was used to group these physically based parameters into non-dimensional groups. Burn duration correlations were then developed using these non-dimensional groups. A non-linear least squares method was used to correlate the burn duration with the physically based parameters. In this paper, the experimental data taken from cooperative fuel research (CFR) engine covers various compression ratios, spark timings, and exhaust gas recirculation levels using five different gasoline-ethanol blends.

It is concluded that the burn duration correlations were in a good agreement with the burn duration computed from experimental data, which within 1° crank angle for both early burn and bulk burn correlations. Furthermore, these correlations can be use to observe the effect of engine geometry variables and operating conditions, thus reduce the experimental cost.

PARAMETRIC STUDY OF BURN DURATIONS OF ETHANOL-GASOLINE BLENDS IN A SI ENGINE OVER VARIABLE COMPRESSION RATIOS AND EGR LEVELS

Authors: Yeliana[a], D Loveland[b], C Cooney[a], J Worm[a], D J Michalek[a], J D Naber[a]

(yyeliana@mtu.edu, dustin.loveland@gm.com, cpcooney@mtu.edu, jjworm@mtu.edu, donna@mtu.edu, jnaber@mtu.edu)

Affiliations: [a] Department of Mechanical Engineering - Engineering Mechanics, College of Engineering, 1400 Townsend Drive, Houghton, MI USA 49931-1295, Phone 906.487.2551, Fax 906.487.2822

[b] GM Powertrain- Advanced Powertrain Engineering, Building C-895 Joslyn Road Pontiac, MI 48340, Phone 586.709.3424

Corresponding Author: yyeliana@mtu.edu

Abstract

Ethanol-gasoline fuel blends are increasingly being used in spark ignition engines due to continued growth in renewable fuels. This leads to the need for a simple and accurate combustion model for ethanol-gasoline blends that is applicable to zero-dimensional engine modeling for design, simulation, and optimization purposes. In this research, experiments with various compression ratios, spark timings, and exhaust gas recirculation levels using five different gasoline-ethanol blends were conducted on a cooperative fuel research engine operating at a constant load of 330 kPa net mean effective pressure and at a constant speed of 900 RPM. A single zone mass fraction burn model was used to analyze burn durations determined from the experimentally measured in-cylinder pressure.

Based on the existing literature, several parameters that correlate to the combustion process have been proposed. With these as guidelines, dimensional analysis was used to group these physically based parameters into non-dimensional groups. Burn duration correlations were then developed using these non-dimensional groups. A non-linear least squares method was used to correlate the burn duration with the physically based parameters. The coefficient of correlation and the root mean square error of burn duration were used as metrics to quantify the error of the correlations for burn durations in comparison to those computed from the experimental measurements.

Keywords: Spark Ignition Engine, Ethanol, Combustion Modeling, Burn Durations, Parametric Study

Introduction

Ethanol has been used as an alternative to petroleum for quite some time [24]. However, in its recent application, ethanol is blended with gasoline to displace fossil fuels while at the same time its increases the fuel blends resistance to engine knock [25]. Since the ethanol contains less energy per unit mass and volume than gasoline, the challenge is to design an engine that takes advantage of the high octane number of ethanol and reduces the fuel consumption penalty. This leads to the need for a simple and accurate combustion model for ethanol-gasoline blended fuels that is applicable to one-dimensional engine modeling for design, simulation, and optimization purposes [2, 3, 26].

One-dimensional engine modeling is widely used for design, development, calibration, and optimization of spark ignition (SI) engines because it is computationally efficient and enables modeling of the engine as a system including the dynamics of the flows [3]. In general, the one-dimensional model consists of sub-models of selected processes that can be analyzed using more detailed modeling approaches, e.g. quasi-dimensional or 3-dimensional models to increase the accuracy of the overall modeling results. Specifically, modeling combustion plays a critical role in the overall engine simulation. This combustion sub-model provides the burning rate that represents the heat release rate in the combustion process for a given geometry and engine operating condition. The burning rate can be determined empirically or derived from physical and chemical kinetic correlations of the combustion process. Having a proper combustion model will enhance understanding of the physical phenomena including the effects of valve phasing, type of fuel, compression ratio, exhaust gas recirculation (EGR), etc [2, 3].

This paper will focus on parametric study of burn duration including analysis of the burn durations and development of the burn duration correlations using experimentally measured pressure trace of Cooperative Fuel Research (CFR) engine over the range of ethanol blends from E0-E84 and combustion phasing sweeps with variable compression ratios and EGR percentages.

Experimental Design

The cylinder pressure data presented in this paper were obtained from a single cylinder CFR engine, which has been modified to meet the criteria for this research [38, 46]. A custom piston was used which allows the engine to be operated over a higher range of compression ratios from 4.5:1 to 17.5:1. The location of the spark plug on the top of the combustion chamber improved flame propagation and better emulated the modern SI engine combustion chamber geometry. An AVL GH12D piezoelectric pressure transducer and an AVL PH01 flame arrestor used to sense the in-cylinder pressure. Cylinder pressure data acquisition and preliminary analysis (such as for data quality checks) was performed with a DSP ACAP system [47]. Other high speed and low speed data, including fuel and airflow rates and various other critical pressures and temperatures, were measured and acquired using a combination of National Instruments (NI) hardware and software. A fully electronic control system for this CFR engine has been developed with Mototron's Motohawk rapid prototyping engine control development environment [39]. A full electronic control system including spark, fuel injection, and throttle was added. Mototron's Mototune was used as the calibration tool interfaced to the engine control unit (ECU). The calibration tool was also used to record engine control parameters including intake manifold pressure, throttle position, air flow rate, commanded spark timing, fuel injection pressure, commanded injection duration, equivalence ratio, and EGR level.

The experiments were conducted by sweeping combustion phasing via spark timing, ethanol concentration, EGR rate, and compression ratio at a constant engine speed of 900 rpm and a constant load of 330 kPa NMEP[3] while maintaining a stoichiometric equivalence ratio. Combustion phasing was swept in 2° increments from a highly retarded location of 50% MFB (CA50) of approximately 4° after top dead center (TDC) to the point of heavy audible knock or until the combustion phasing was clearly advanced beyond maximum brake torque (MBT). During this sweep, the point of borderline audible knock (if applicable) was noted in the data. Three hundred consecutive engine

---

[3] The Net Mean Effective Pressure refers to the IMEP computed over the 720° operating cycle (high pressure loop plus pumping loop).

cycles were recorded at each test set-point and the cycle averaged data was used to compute MFB profile [38].

Experimental Results

The mass fraction burn represents the percentage of fuel consumed versus crank-angle during the combustion portion of an engine cycle and is obtained by analyzing the in-cylinder pressure. The MFB curve is commonly used to study and characterize the spark-ignition combustion process. This curve is strongly influenced by a number of parameters including the engine design, operating conditions, and fuel type and has a significant impact on engine performance including efficiency and emissions.

An apparent heat release analysis method is one of many techniques used to calculate the MFB from in-cylinder pressure data [5, 6]. A comparison among the single-zone [8, 40-42], two-zone [6, 7, 43], and the apparent heat release models was performed, and it showed that the apparent heat release method was found to be in good agreement with the single-zone and two-zone models, particularly with respect to combustion phasing [38]. The apparent heat release method is derived from the balance of energy in the combustion chamber by assuming the products and reactants behave as an ideal gas, the mass is constant, and both the products and reactants have a constant molecular weight during the combustion process. The energy balance is given below:

$$\left(\frac{Q_{LHV} \, m_c \, (1 - x_{dil})}{\left(1 + \frac{AFR_s}{\phi}\right)} \right) dx_b = \frac{\gamma}{\gamma - 1} \, p \, dV + \frac{1}{\gamma - 1} \, V \, dp \qquad \text{(IV-1)}$$

where, Q_{LHV} is the heat release, m_c is mass of charge, x_{dil} is residual fraction, AFR_s is stoichiometric air fuel ratio, ϕ is equivalence ratio, γ is the ratio of the constant pressure specific heat to the constant volume specific heat, p is the in-cylinder pressure, and V is the volume of combustion chamber.

Figure IV-1a shows the 0-10% MFB duration and Figure IV-1b shows the 10-75% MFB duration of five different fuel blends at a compression ratio of 8:1, speed of 900 RPM, and load of 330 kPa NMEP as a function of spark timing. All the data presented in this paper is in the range of normal combustion, which was quantified using a Coefficient of Variance (COV) of IMEP from 0-5%, and a 95 percentile peak knock pressure (PP95) [18] from 0-50 kPa. Figure IV-1a and Figure IV-1b show that the higher the ethanol concentration the faster the combustion process. This is indicated by the shorter early flame development period and the bulk burn duration. The early development period has a minimum duration at a spark timing of top dead center (TDC), which corresponds to the maximum compression height of the combustion chamber, and thus a higher temperature and laminar flame speed. Generally, the early development period increases as the spark is advanced. However, the bulk burn duration decreases as the spark is advanced toward TDC. These trends result from the in-cylinder temperature during the different phases of the combustion process. When the spark occurs near TDC, the in-cylinder temperature is high due to the compression heating, which in turn increases the reaction rates and decreases the 0-10% burn duration. Advancing the spark beyond TDC results in a 0-10% burn event that occurs at lower temperatures, and thus takes longer, however, in this advanced case, the bulk burn occurs nearer the high temperature TDC phase, and thus has higher reaction rates and a faster burn. If the spark would have been advanced even farther, the bulk burn would have shown a reversing trend as well. In fact, it is possible to see in Figure IV-1b a slight increase starting in the bulk burn duration at the most advanced spark timings. In these experiments spark could not be advanced any farther due to auto-ignition (knock) limitations.

The knock limit of gasoline with respect to spark advance increases as the ethanol concentration increases. At a compression ratio of 8:1, the Knock Limited Spark Advance (KLSA) using gasoline is limited at 18°BTDC (indicated by the arrow in Figure IV-1a and Figure IV-1b). However, the KLSA is increased to 30°BTDC as the ethanol concentration increased to 84% by volume.

(a)   (b)
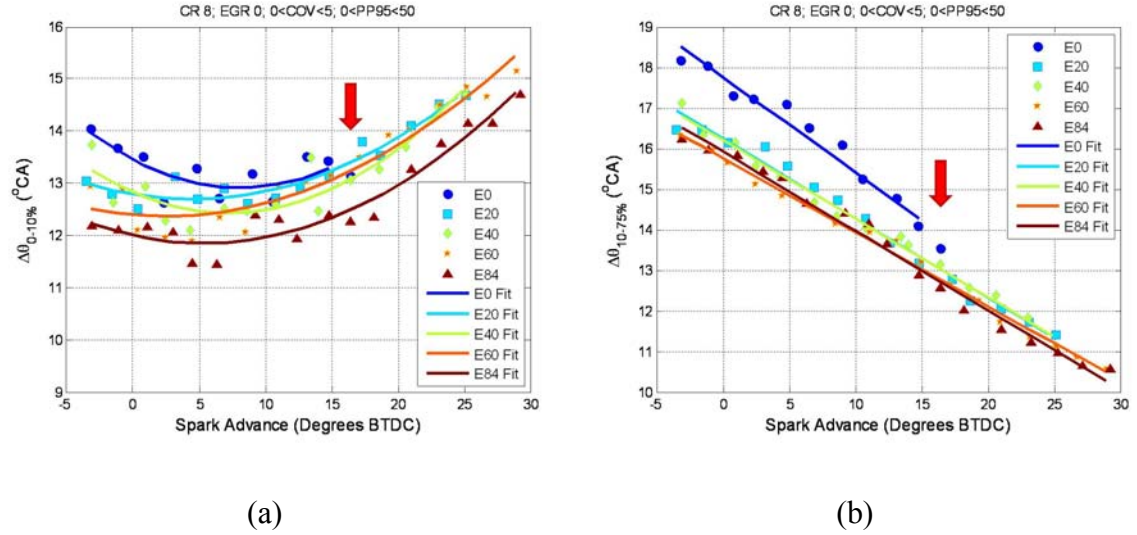
Figure IV-1 Effect of spark timing on the early development and bulk burn period
(CR=8:1; EGR=0; Speed=900 RPM; Load=330kPa NMEP)

Figure IV-2a shows the 0-10% MFB duration and Figure IV-2b shows the 10-75% MFB duration of five different fuels for spark timing around TDC, a constant speed of 900 RPM, and a constant load of 330 kPa NMEP as a function of compression ratio. The burn duration becomes shorter as the compression ratio increases. The reason for this trend is the same as the effect of combustion phasing discussed above. The higher compression ratios caused a higher density of charge and higher temperatures and pressure during the combustion process and thus higher reaction rates and faster burns.

Also in Figure IV-2a and Figure IV-2b, the effect of ethanol concentration is clearly shown at low compression ratios (CR = 8:1 and CR = 10:1) where it was possible to collect data on all fuel blends without auto-ignition. Once again it is clear that the higher the ethanol content the faster the combustion process. The Knock Limited Compression Ratio (KLCR) is also evident in Figure IV-2a and Figure IV-2b. Here it is shown that at these operating conditions, the KLCR of gasoline is 10:1 (as marked by the arrow in Figure IV-2a and Figure IV-2b), whereas fuels with an ethanol concentration greater than E40 can reach at least a compression ratio of 16:1. Data were not collected at compression ratios greater than 16:1 for this research.
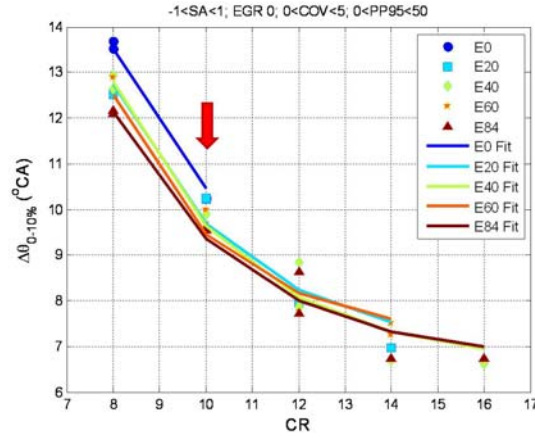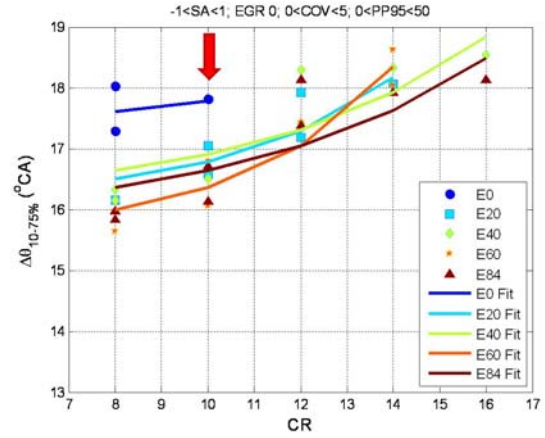
(a)	(b)

Figure IV-2 Effect of compression ratio on the early development and bulk burn period (-1<SA<1; EGR=0; Speed=900 RPM; Load=330kPa NMEP)

The effect of EGR on the 0-10% MFB and 10-75% MFB durations at near MBT spark timing for E84% is presented in Figure IV-3a and Figure IV-3b. As the EGR increases, the burn duration increases and therefore the spark timing to achieve MBT advances. The solid line in Figure IV-3 represents the trend line of the MBT timing at a compression ratio of 8:1 and the dashed line represents the MBT timing at a compression ratio of 10:1. As discussed previously, by increasing the compression ratio, the temperature in the combustion chamber increases resulting in a shorter burn duration. This trend is also shown in Figure IV-3a when comparing the solid and dashed trendlines.

Another trend that is evident in Figure IV-3a and Figure IV-3b is the effect of increased dilution on burn duration. Here it is shown that as the EGR rate is increased, both early and bulk burn durations increase. This is a result of the diluent absorbing the heat of combustion and slowing down the reaction rates. Thus enables to operate a lean and stable combustion at higher compression ratio to achieve higher thermal efficiency.

(a)	(b)
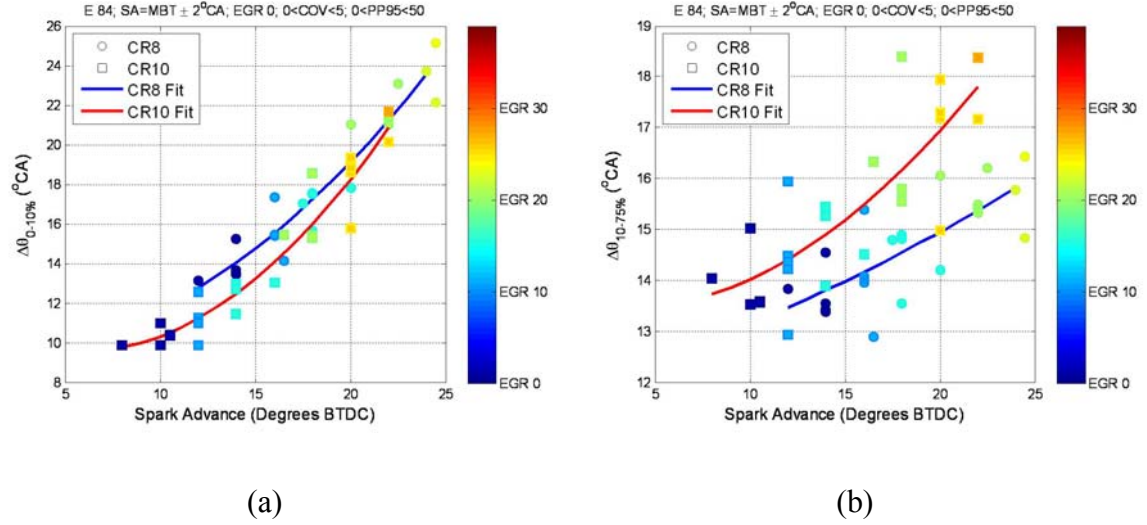
Figure IV-3 Effect of EGR on the early flame development and bulk burn period (SA=3 Spark Timing ± 2° MBT; Speed=900 RPM; Load=330kPa NMEP)

Parametric Study

Combustion model with predictive capability has been a fascinating subject for many years. The combustion model is used to compute the burn rate which represents the in-cylinder pressure and temperature in the combustion chamber. Several empirical burn duration correlations as a function of engine operating condition have been proposed. The computed burn duration from measured pressure trace were correlated to the engine operating conditions in forms including polynomial [11], combination polynomial and product form [27-29], product-power form [30-32], etc.

Burn duration was assumed as function of cylinder geometry and turbulent flame speed which solely as a function of engine speed and laminar flame speed [11]. Burn duration was also observed as a function of compression ratio, engine speed, equivalence ratio, and the spark timing [28]. In addition to engine speed and the spark timing, the laminar flame speed was included in the burn duration correlation [27]. Derived based on a turbulent combustion model for SI engines the burn duration correlation was fitted to

parameter including the height of combustion chamber, piston bore, mean piston speed, laminar flame speed and kinematic viscosity [10, 30, 31].

In this paper, there are six main parameters have been selected including: engine bore (B), height of the combustion chamber (h), mean piston speed (S_p), laminar flame speed (S_L), specific internal energy ($Q^* = (m_f /m) Q_{LHV}$), and kinematic viscosity of the unburned mixture (ν). Additional parameters describe the engine parameters: mass fraction burn, residual fraction, spark timing, equivalence ratio, engine speed, load, and valve timing [17, 30, 31]. Among those physically based parameters, bore, equivalence ratio and mean piston speed were constant in this research, but height of combustion chamber, laminar flame speed, specific internal energy and kinematic viscosity varied as a result of varying the compression ratio, spark timing and fuel properties in the testing.

A non-dimensional analysis using Buckingham's Pi Theorem [33] was performed using the parameters defined above to represent the burn duration. The five non-dimensional groups resulting from the seven variables are expressed in functional relationship in Equation (IV-2). A non-linear least squares method is then used to correlate the burn duration with the Pi groups with given product-power form. The Pi groups are:

$$\frac{\Delta\theta \, S_L}{h} = f\left(\frac{\bar{S}_p}{S_L}, \ \frac{h \, S_L}{\nu}, \ \frac{h}{B}, \ \frac{Q^*}{S_L^2} \right) \qquad \text{(IV-2)}$$

Laminar Flame Speed Calculation

Numerous empirical models have been developed to predict the laminar flame speed of a given fuel in the combustion chamber as a function of pressure, unburned gas temperature, fuel-air equivalence ratio, and residual fraction. Annand [12] summarized and compared the empirical laminar flame speed correlations and recommended the correlation developed by Metgalchi and Keck [48], which was developed for propane-air mixtures without dilution. The same relation was used by Gulder [49, 50] to correlate

measurements of laminar flame speed of alternative fuels, including ethanol and ethanol-gasoline blends. The laminar flame speed estimation used in this work is given as:

$$S_L = S_{lo} \left[\frac{T}{T_o} \right]^\alpha \left[\frac{p}{p_o} \right]^\beta \left(1 - 2.3\, x_{dil} \right) \qquad \text{(IV-3)}$$

$$S_{lo} = \left(1 + 0.07\, E^{0.35} \right) 0.4658\, \phi^{-0.326} \exp\!\left(-4.48 (\phi - 1.075)^2 \right) \qquad \text{(IV-4)}$$

where S_{lo} is laminar flame speed at the reference conditions, T_o is the reference temperature of 298K, p_o is reference pressure of 1 bar, and α, β, Z, W, η, ξ are constant values.

Table IV-1 shows the constants for the laminar flame speed calculation for ethanol-gasoline blended fuels taken from by Gulder [49, 51].

Table IV-1 Values of α and β for isooctane-ethanol blends [49, 51]

α	β	
	$\phi \leq 1$	$\phi \geq 1$
$\alpha = 1.56 + 0.23\, E^{0.46}$	$\beta = -0.22(1-E) - 0.17\, E / \sqrt{\phi}$	$\beta = -0.22(1-E) - 0.17\, E \sqrt{\phi}$

Kinematic Viscosity Calculation

The kinematic viscosity of the unburned mixture at the ignition point is calculated by dividing the dynamic viscosity by the density of the unburned mixture. Dynamic viscosity (μ) of ethanol, gasoline, and air are given by Turns [52]. The dynamic viscosity

of the gas mixture is then calculated based on the constituent viscosities using the formula of Wilke [53]:

$$\mu_u = \sum_i \left[\frac{x_i \cdot \mu_i}{\sum_j x_j \cdot \phi_{ij}} \right] \qquad \text{(IV-5)}$$

$$\phi_{ij} = \frac{\left[1 + \left(\mu_i / \mu_j \right)^{1/2} \left(MW_j / MW_i \right)^{1/4} \right]^2}{2\sqrt{2} \left(1 + MW_i / MW_j \right)^{1/2}} \qquad \text{(IV-6)}$$

where MW is the molecular weight, x is the mass fraction, and subscript i and j represent the species.

Height of Combustion Chamber Calculation

The height of the combustion chamber (h) at the ignition point is the height of the clearance volume plus the distance (s) of the piston from the head at TDC. Considering the wrist pin offset (X), the distance between the crank axis and the piston pin axis is given as:

$$s = \sqrt{(l+a)^2 - X^2} - a \cos\theta - \sqrt{l^2 - X^2 - a^2 \sin^2\theta - 2\,a\,X \sin\theta} \qquad \text{(IV-7)}$$

where l is the connecting rod length, a is the crank radius, and X is the wrist pin offset.

Burn Duration Correlation

As previously noted, the experimental matrix used in this research included sweeps of compression ratio, ethanol concentration, spark timing, and dilution level. Collectively, these variables account for the effect of the laminar flame speed, the kinematic viscosity,

and the depth of the combustion chamber on the early burned duration. Figure IV-4 shows the results of the experimental data points plotted with an x-axis of 0-10% MFB duration determined from the measured cylinder pressure and a y-axis of 0-10% MFB duration computed from Equation (IV-8) below. The COV of NMEP of the data used in the correlation is varied from 0 to 5 and the PP95 from 0 to 50 kPa. The marker type represents the fuel type and the color code represents the percentage of EGR. The average error of the model compared to the engine data is less than 1° crank angle.

$$\Delta\theta_{0-10\%} = 1.3 \left(\frac{Sp}{SL}\right)^{-3.2} \left(\frac{SL^2}{Q^*}\right)^{-1.7} \left(\frac{h_{CA00}}{B}\right)^{0.9} \left(\frac{h}{B}\right)^{0.1} \left(\frac{h\,Sp}{v}\right)^{0.8} \qquad \text{(IV-8)}$$
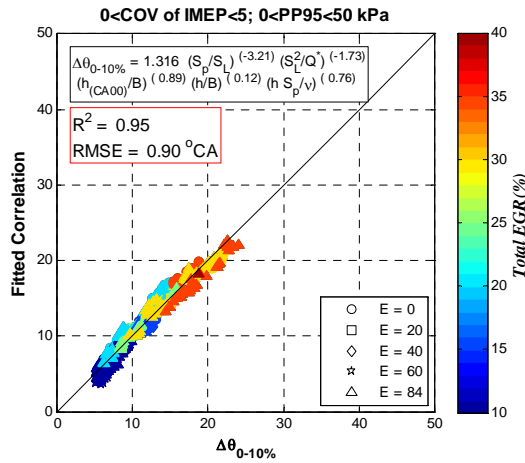
Figure IV-4 Burn duration 0-10% MFB correlation of CFR engine data over wide range variable compression ratio, spark timing sweep, and EGR sweep using five different ethanol blends at a constant load of 330 kPa NMEP and constant engine speed of 900 RPM
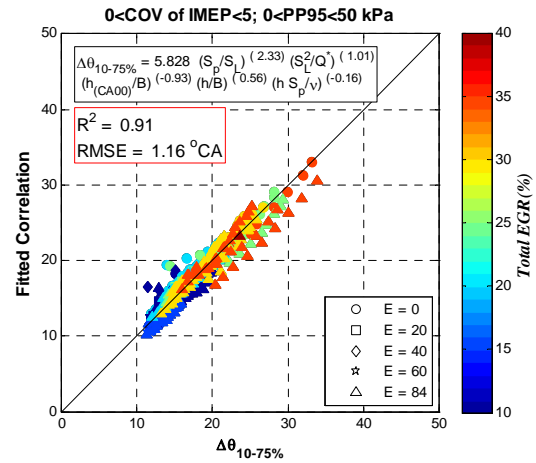
Figure IV-5 Burn duration 10-75% MFB correlation of CFR engine data over wide range variable compression ratio, spark timing sweep, and EGR sweep using five different ethanol blends at a constant load of 330 kPa NMEP and constant engine speed of 900 RPM

Figure IV-5 shows the bulk burn duration correlation for 10-75% MFB. Similarly the x-axis is the computed 10-75% MFB duration from the measured cylinder pressure and the y-axis is computed from Equation (IV-9) below. The average error compared to the engine data is less than 1° crank angle.

$$\Delta\theta_{10-75\%} = 5.8 \left(\frac{Sp}{SL}\right)^{2.3} \left(\frac{SL^2}{Q^*}\right)^{1.0} \left(\frac{h_{CA00}}{B}\right)^{-0.9} \left(\frac{h}{B}\right)^{0.6} \left(\frac{h\,Sp}{v}\right)^{-0.2} \tag{IV-9}$$

Validation of Burn Duration Correlations

An estimated response surfaces as a result of modeling exercise can be generated using the correlations in Equation (IV-8) and Equation (IV-9) over the range of ethanol concentration from 0-100, compression ratio from 8-16, spark advance from 0-30, and EGR rate from 0-30. This effort filled the gap between the experimental testing points.

Figure IV-6 and Figure IV-7 show the surface plot and projection of the early burn period and bulk burn respectively, as functions of ethanol concentration and EGR rate at a compression ratio of 10:1 and CA50 from 8-11°CA near MBT. The black crosses represent the experiment data points. The early burn period increases approximately 173% as the EGR rate increases from 0 to 30% and approximately 8% as the ethanol concentration decreases from E85 to E0. The bulk burn period increases approximately 37% as the EGR rate increases and approximately 4% as the ethanol concentration decreases. It is also shown that the experiment data agree well with the data calculated from the burn duration correlations. The subplot shows the error between the model and the experiment data. The maximum errors are 1.9°CA and 0.9°CA for B0010 and B1075, respectively, which use E84 at 25% EGR.

Figure IV-8 and Figure IV-9 show the surface plot and its projection to the x-y plane of the early burn and bulk burn period as a function of compression ratio and ethanol concentration generated from the burn duration correlations on Equations (IV-8) and Equation (IV-9). The early burn duration increases 54% as the compression ratio

decreases from 16:1 to 8:1 and approximately 9% as the ethanol concentration decreases from E85 to E0. However, the bulk burn duration increases approximately 30% as the compression ratio increases and 5% as ethanol concentration decreases. The maximum error for B0010 is $0.8^{\circ}CA$ and is $1.9^{\circ}CA$ for B1075.

The effects of compression ratio and EGR rate on the early burn and bulk burn duration are shown in the Figure IV-10 and Figure IV-11, respectively. A simulation for E84 within range of CA50 from $8-11^{\circ}CA$ shows that on average the early burn duration increases approximately 56% as the compression ratio decreases from 16:1 to 8:1 and approximately 150% as the EGR increases from 0 to 30%. It also shows that the bulk burn duration increases approximately 25% as the compression ratio increases and 33% as the EGR rate increases. These results agreed with the results shown in Figure IV-3b. The maximum error for B0010 is $1.9^{\circ}CA$ and is $1.9^{\circ}CA$ for B1075.
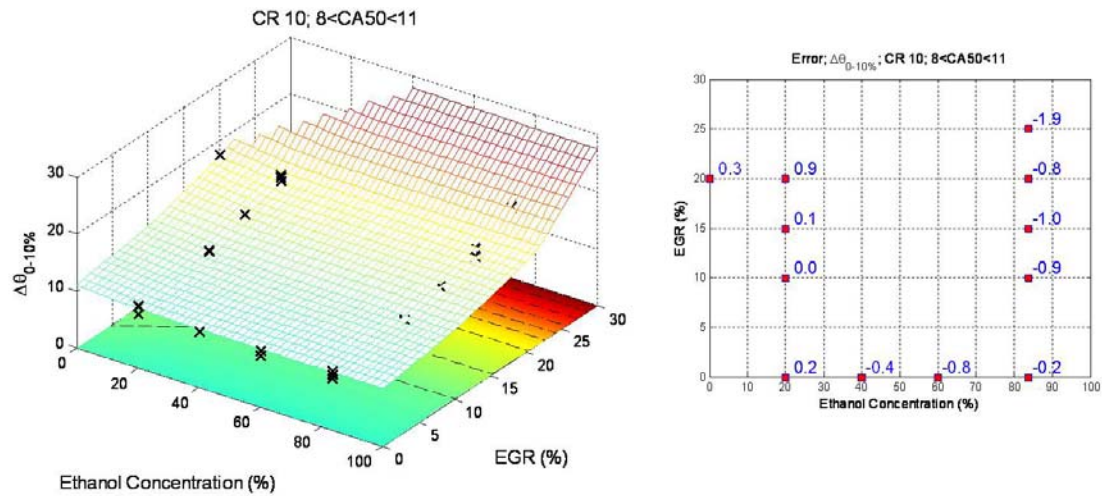
Figure IV-6 Surface plot and projection to the x-y plane of early burn period at compression ratio 10 within range of CA50 from 8-11 as function of ethanol concentration and EGR rate
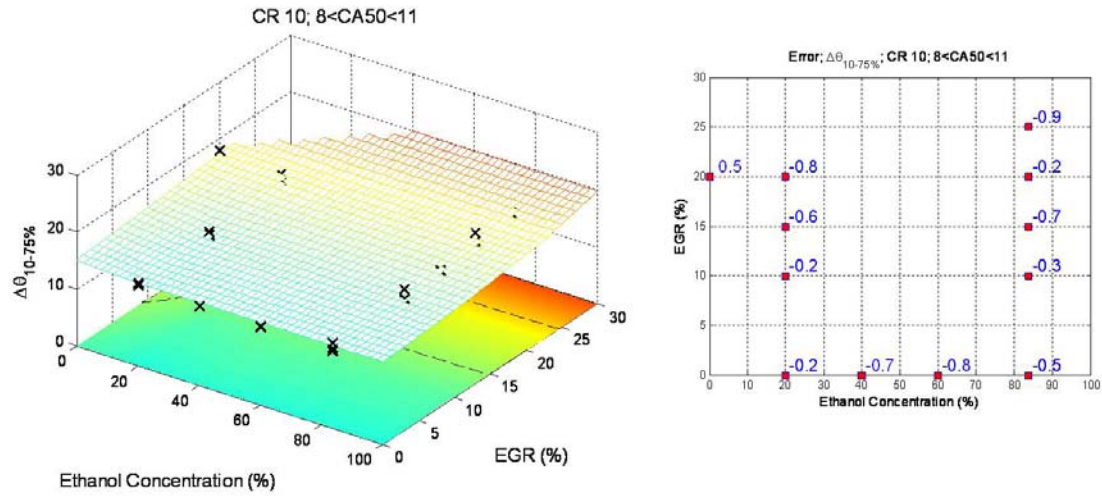
Figure IV-7 Surface plot and projection to the x-y plane of early burn period at compression ratio 10 within range of CA50 from 8-11 as function of ethanol concentration and EGR rate
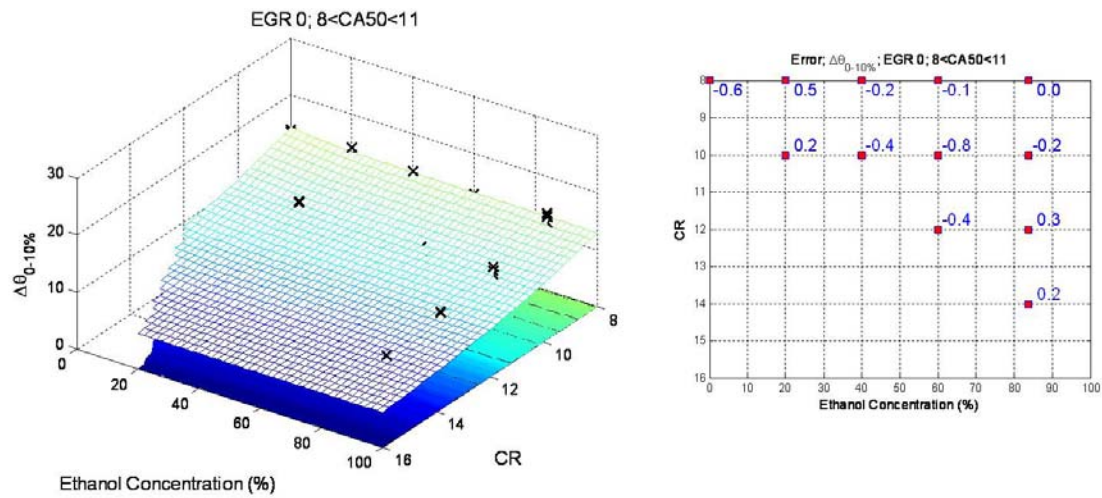
Figure IV-8 Surface plot and projection to the x-y plane of early burn period at EGR rate of 0 within range of CA50 from 8-11 as function of ethanol concentration and compression ratio
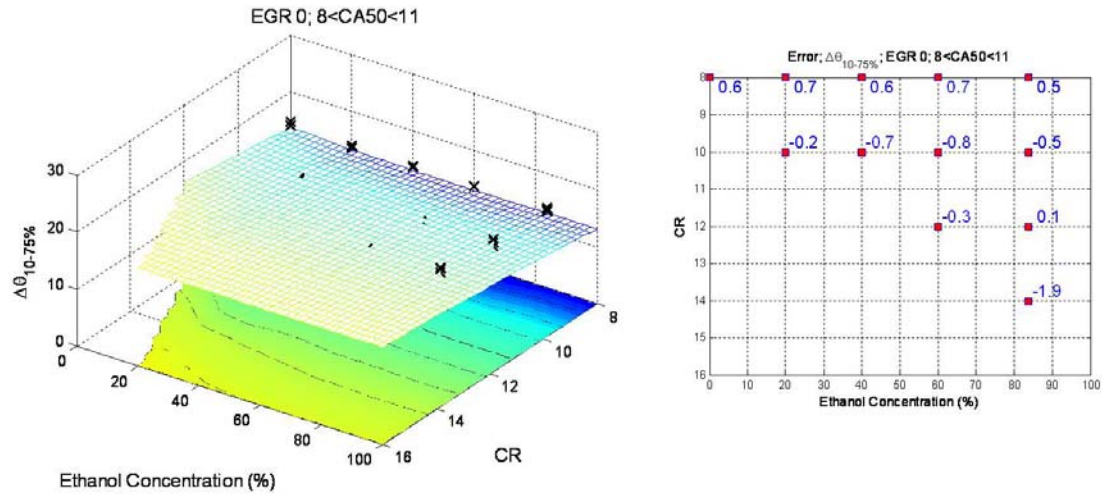
Figure IV-9 Surface plot and projection to the x-y plane of early burn period at EGR rate of 0 within range of CA50 from 8-11 as function of ethanol concentration and compression ratio
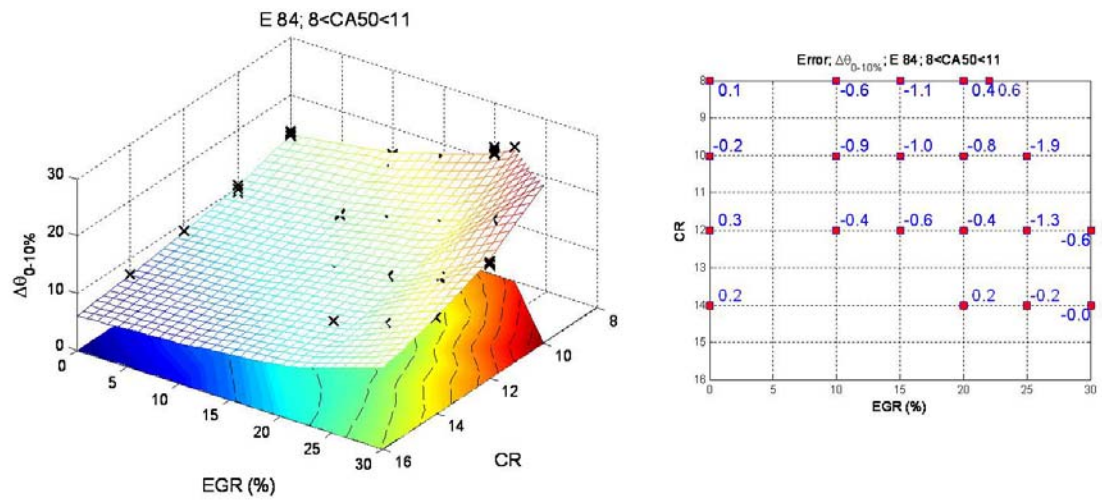
Figure IV-10 Surface plot and projection to the x-y plane of early burn period of E84 within range of CA50 from 8-11 as function of EGR rate and compression ratio
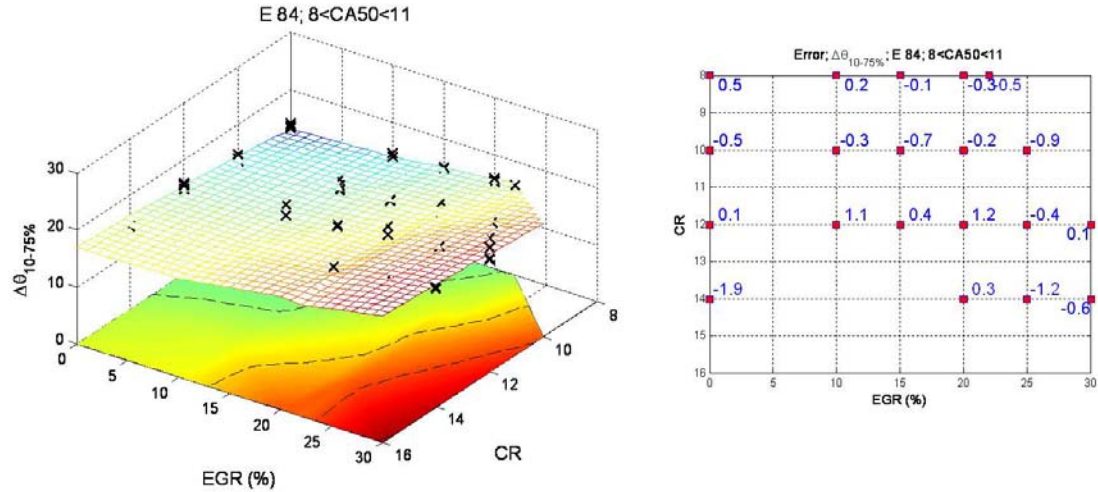
Figure IV-11 Surface plot and projection to the x-y plane of early burn period of E84 within range of CA50 from 8-11 as function of EGR rate and compression ratio

Summary and Conclusions

Expression for burn durations were developed using non-dimensional analysis of four Pi-groups and the least squares fitting method. These correlations cover fuels including gasoline, ethanol and ethanol-gasoline blends, and combustion phasing by sweeping the spark timing, compression ratio, and charge dilution via percentage of EGR for CFR engine.

Several conclusions can be drawn. First, when compared to the burn duration computed from the experimental data, the RMSE of those correlations are within 1° crank angle for both early burn and bulk burn correlations. Second, using the correlations (Equations IV-8 and IV-9), the effect of engine geometry variables and operating conditions can be observed, thus reduce the experimental cost. In order to have burn duration correlations for wider speed and load range, similar procedure should be repeated using wider range of speed and load experimental data. Burn duration correlations were developed by authors using proprietary dataset under a much wider conditions including engine speeds from 1000 RPM to 6000 RPM, NMEP range from 220 kPa to 1500 kPa, and equivalence

ratios from 0.8 to 1.45. It is confirmed that the physically based non-dimensional pi-groups were highly correlated to the burn duration.

Furthermore using this burn duration correlations, the mass fraction burn profile can also be reconstructed using a standard Wiebe function, and thus the pressure trace can be estimated to validate these burn duration correlations. This work will be discussed in the second paper which will enclose the combustion modeling for flex-fuel vehicles.

Nomenclature

a	Crank radius
AFR	Air Fuel Ratio
B	Bore
C,α,β	Constant
cr	Compression ratio
E	Ethanol concentration
h	Depth of the combustion chamber at time of ignition
l	Connecting rod length
MW	Molecular weight

p	pressure
Q_{LHV}	Lower heating value
S_L	Laminar flame speed
S_p	Mean piston speed
T	Temperature
t	time
V	Volume
X	Wrist pin offset
x	Mass fraction
ϕ	Equivalence ratio
γ	Ratio of specific heat
μ	Dynamic viscosity
ν	Kinematic viscosity
θ	Crank angle

Subscript

b	Burn, bulk burn period
c	Charge
d	Early development period
dil	Dilution
i	Calculated at ignition point
i,j	Species
o	Calculated at reference point
s	Stoichiometric
u	Unburn

V.   WIEBE FUNCTION PARAMETER ESTIMATION

V.1   SINGLE-WIEBE FUNCTION PARAMETER ESTIMATION

One approach commonly used in engine combustion simulation modeling is to estimate the mass fraction burned as a function of engine position using the Wiebe function [3]. Methods to determine the Wiebe function parameters have been developed by fitting the Wiebe function to the MFB profile. In this paper, a number of possible methods were used to determine the Wiebe function (single-Wiebe function) parameters, five promising methods using a combination of least square method and direct algebraic solution. It is also found that the "a" in the Wiebe function is directly related to the combustion duration ($\Delta\theta_b$) and is not an independent parameter. An "amplitude correction factor" "b" was added in the Wiebe function to incorporate the fact that the Wiebe mass fraction burn never actually reaches one. In this paper, the Wiebe function fitting method using the least squares method on the independent variables ("m", "b", $\Delta\theta$) gave the best fit to the MFB profile.

WIEBE FUNCTION PARAMETER DETERMINATION FOR MASS FRACTION BURN CALCULATION IN AN ETHANOL-GASOLINE FUELLED SI ENGINE[4]

Yeliana, C. Cooney, J. Worm, D. Michalek, J. Naber

Michigan Technological University

Mechanical Engineering-Engineering Mechanics

1400 Townsend Drive, Houghton, Michigan, USA 49931-1295

Phone: +1 906 487-2551, fax: +1 906 487-2822

E-mail: yyeliana@mtu.edu, cpcooney@mtu.edu, jjworm@mtu.edu, donna@mtu.edu, jnaber@mtu.edu

www.me.mtu.edu/reseachAreas/aice/

Abstract

The Mass Fraction Burn (MFB) and Heat Release Rate (HRR) reflect the amount of fuel burned and the rate of burning throughout the combustion process in an internal combustion engine. These parameters play a crucial role in research and development endeavors focused on engine efficiency, emissions, and overall operating performance. Analytically in a Spark-Ignition (SI) engine, these parameters are often modeled with the Wiebe function, a well known mass fraction burn formulation, which is a function of "a" (efficiency parameter), "m" (form factor), crank angle, and the duration of combustion. This function is a simple but powerful correlation model that is well suited for zero and one dimensional engine cycle simulations.

In this work, the Wiebe function parameters are determined over a range of fuel compositions and compression ratios by fitting the Wiebe function curve to the experimentally obtained MFB data from a single-zone HRR analysis. The Wiebe function parameters are determined using a curve fitting model by finding the minimum of a scalar function of several variables. This functionality has been built into the single-zone mass fraction burned model. Experiments with five ethanol-gasoline fuel blends: E0 (gasoline), E20, E40, E60, and E84 were conducted on a SI Cooperative Fuels Research (CFR) engine while holding a constant load of 330 kPa Net Indicated Mean Effective Pressure (Net IMEP). There were five methods introduced to fit the Wiebe function parameters, which utilized a combination of least square method and direct algebraic solution. This paper details the process used to determine the Wiebe function parameters, and compare the results obtained using these methods for the ethanol-gasoline mixture concentrations.

Keywords: *ethanol-gasoline blend, mass fraction burn, IC engine, Wiebe function*

Introduction

Single-Zone Model

Rassweiler and Withrow [5] developed an approximation of the mass fraction burned by calculating the ratio of the difference between the measured pressure and the polytropic pressure to the total fuel energy. This method, known also as a single-zone heat release method, utilizes the in-cylinder pressure data to calculate the total heat release from the combustion of an air-fuel mixture in the combustion chamber, as the pressure rise over a given crank angle interval is proportional to the mass of fuel burned over that same interval. Heywood et al. [7] suggests the use of this method for SI engine simulation. Gatowski et al. [8] developed a single-zone heat release model including the crevice model, and later, Chun and Heywood [40] improved upon the single-zone model by introducing an accurate way to model the ratio of the specific heats (gamma). The method averages the gamma computed from two separate zones representing the burned and unburned masses. In the same field of study, Klein and Eriksson [41] discussed several ways to predict the value of gamma. Later Cheung and Heywood [42] concluded that the single-zone heat release model is remarkably robust, and any error most likely results from measurement errors in the pressure and mass flow rate data.

Previously a single-zone model was developed for comparison with the two-zone model using ethanol-gasoline fuel blends in a CFR engine [38]. Derived from the energy balance and the ideal gas equation, the single-zone model with two unknowns (temperature and mass fraction burn) has been proven to be as accurate as the two-zone model determination of combustion phasing. In this work, the mass fraction burn is calculated from experimental data using the single-zone model.

Wiebe Function

One approach used in engine simulation modeling is to estimate the mass fraction burned as a function of engine position using the Wiebe function [3]. The Wiebe function is expressed as:

$$x_b = \left\{ 1 - \exp \left[-a \left(\frac{\theta - \theta_o}{\Delta \theta} \right)^{m+1} \right] \right\}$$

(V-1)

The Wiebe function curve has a characteristic S-shaped curve and is commonly used to characterize the combustion process. The mass fraction burned profile grows from zero, where zero mass fraction burn indicates the start of combustion, and then tends exponentially to one indicating the end of combustion. The difference between those two ends is known as the duration of combustion. Although the Wiebe function simple and robust in specifying the combustion process, there are inherent issues. These issues, along with a proposed solution, will be discussed in the remainder of this paper.

Experimental Setup

Cylinder pressure data for this research was taken from a single cylinder CFR engine manufactured by the Waukesha Motor Company. Several modifications had been made prior to this research. The modifications included relocating the sparkplug closer to the geometric center of the combustion chamber, and fabricating a custom piston which allows the compression ratio to be adjusted from 4.5:1 to 17.5:1, as opposed as the 4:1 to 10:1 with the original piston. The experiments were conducted by sweeping ethanol concentration, spark timing, and compression ratio at constant engine speed and a constant indicated load of 330 kPa Net IMEP. The cylinder pressure data was obtained with an AVL GH12D piezoelectric transducer. Data acquisition, including the measurement of cylinder pressure and various other critical pressures and temperatures, is accomplished using a combination of National Instruments (NI) hardware and software. A control system for this CFR engine had been previously developed with Mototron's

Motohawk rapid engine control development environment [39]. Mototron's Mototune was used as the calibration tool and ECU interface. The calibration tool was also used to record engine control parameters such as intake manifold pressure, air flow rate, spark timing, fuel injection pressure, injection duration, equivalence ratio, etc.

Wiebe Function Fitting Methods

In looking closely at Equation (V-1), it is possible to see that the mass fraction burned never actually reaches one, but rather approaches a value of one as the exponential term asymptotically approaches zero. At a given crank angle such that equal to burn duration, the mass fraction burn is less than one, by factor of "exponential (-a)". To account for this, the authors have introduced an "amplitude correction factor" "b" in the Wiebe function. Adding the amplitude correction factor, the modified Wiebe function is expressed as follows:

$$ x_b = b \left\{ 1 - \exp \left[-a \left(\frac{\theta - \theta_o}{\Delta \theta} \right)^{m+1} \right] \right\} \qquad \text{(V-2)} $$

The effect of the amplitude correction factor "b" will be discussed later along with the brief description of each method.

Given the formulation in Equation (V-2), the three major parameters in the Wiebe function are, the combustion duration ($\Delta \theta$), the start of combustion (θ_o), and the form factor (m). The "a" in the Wiebe function is directly related to the combustion duration and is not an independent parameter. For example, by defining the combustion duration as the 0% to 90% mass fraction burn duration (0-90 MFB), "a" has a fixed value of 2.3026. For a combustion duration corresponding to 0-99.9% MFB, "a" is 6.9078. For a combustion duration defined as the 0-90% MFB duration, the Wiebe function can then be written as:

$$x_b = b\left\{1 - \exp\left[-2.3026\left(\frac{\theta - \theta_o}{\Delta\theta_{0-90\%}}\right)^{m+1}\right]\right\}$$
(V-3)

In this study, a number of possible methods were used to determine Wiebe function parameters by fitting theWiebe function curve to the experimental data, and a summary of the five most promising methods are discuss here. The following is a brief discussion of each method.

Method 1

Using the least squares method, the Wiebe function is fitted to the mass fraction burn data with four independent variables ($\Delta\theta_{0\text{-}90\%}$, θ_o, m, and b). This method gives the best fit, as a comparison of the combustion phasing of the engine data and the Wiebe fitted curve shows a difference of less than 0.2^o crank angle for all fuel blends tested at the given operating condition. However, the start of the combustion (θ_o) is advanced by approximately 10 to 20 degrees before the actual spark timing. Figure V-1 shows the mass fraction burn curve overlaid with the Wiebe fitted curve for this method with gasoline and a spark advance of 10° BTDC. The blue line represents the MFB of the experimental data, the green line represents the Wiebe fitted curve treating the "b" as independent variable, and the red line represents the Wiebe fitted curve with "b" fixed equal to one. The two subplots at the right hand side of Figure V-1 shows the cross plots between the location of 0, 5%, 10%, 20%, 30%, 40%, 50%, 60%, 70%, 80%, 90%, 100% MFB as computed from experimental data, and the location of the same point as determined with the fitted Wiebe function. Further validation was performed by using the fitted Wiebe function to estimate the heat release, and with that information, compute the cylinder pressure during combustion. This computed cylinder pressure was then superimposed on the measured cylinder pressure, and the Net IMEP was calculated. The maximum difference in phasing, the difference in Net IMEP, and the Sum of Squared Error (SSE) of the MFB are given at the bottom of each subplot.

<u>Method 2</u>

Method 2 addresses the issue identified by method 1 (start of combustion advanced beyond the point of ignition) by fixing the start of combustion at the point of ignition. With the start of combustion fixed, the least squares method is again used to predict the remaining independent variables, in this case $\Delta\theta_{0\text{-}90\%}$, m, and b. Including "b" as an additional variable in the least square method improved the results, as shown in Figure V-2. The maximum difference in the combustion phasing (0-90%) between the model and the experimental data in this case does not exceed 1° crank angle. The Net IMEP of the modeled data was within 0.02% of the Net IMEP as determined from the experimental data.
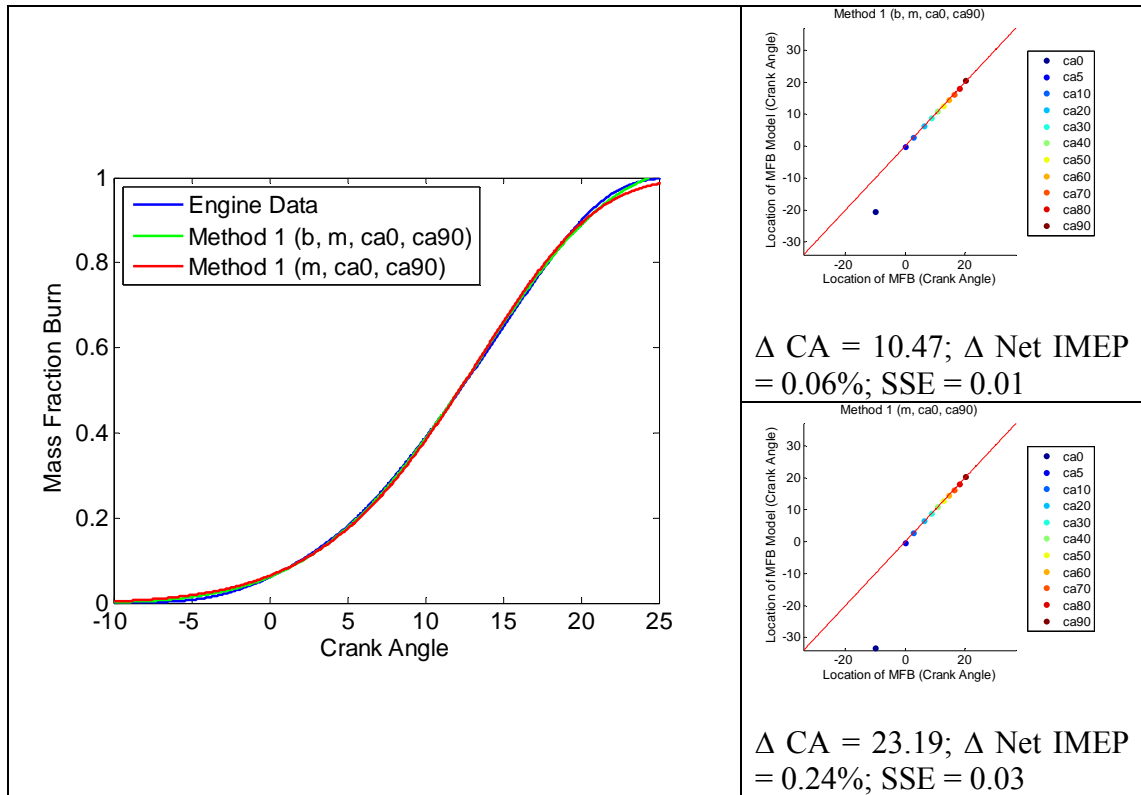
Figure V-1The mass fraction burn and the Wiebe fitted curve using Method 1 (Gasoline, CR = 8.0:1, spark advanced = 10° BTDC, speed = 900 RPM, load = 330 kPa Net IMEP).
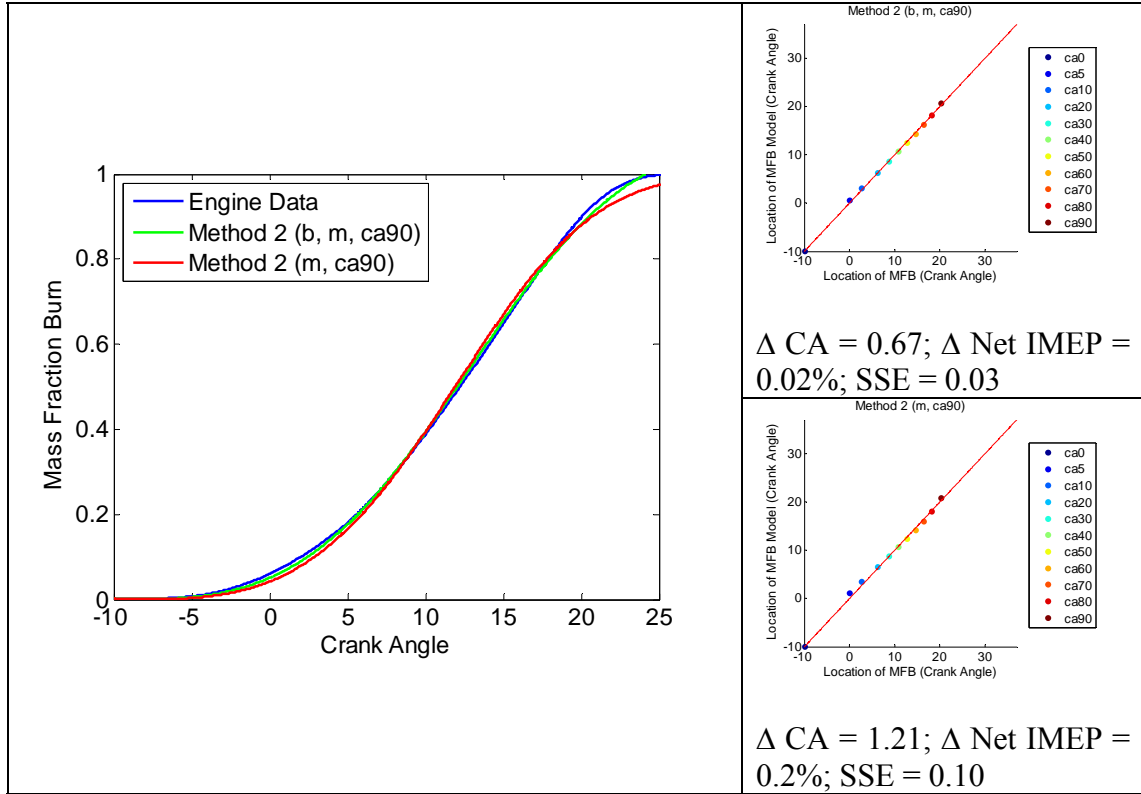
Figure V-2 The mass fraction burn and the Wiebe fitted curve using the Method 2 (Gasoline, CR = 8.0:1, spark advanced = 10° BTDC, speed = 900 RPM, load = 330 kPa Net IMEP).

Method 3

By fixing the start of combustion at the spark ignition and the duration of the combustion as the difference between the location of 90% MFB and the spark timing, the "*m*" and the "*b*" of the Wiebe function were once again determined using the least squares method. In this method, including the "*b*" term did not significantly change the results, as shown in Figure V-3. The modeled combustion phasing is slightly lower in the early phase (less than 1.5^o) and slightly higher during the second half of the combustion compared to the experimental data. Even though the modeled Net IMEP did not change significantly, SSE of this method is higher than the other methods (approximately 0.3).
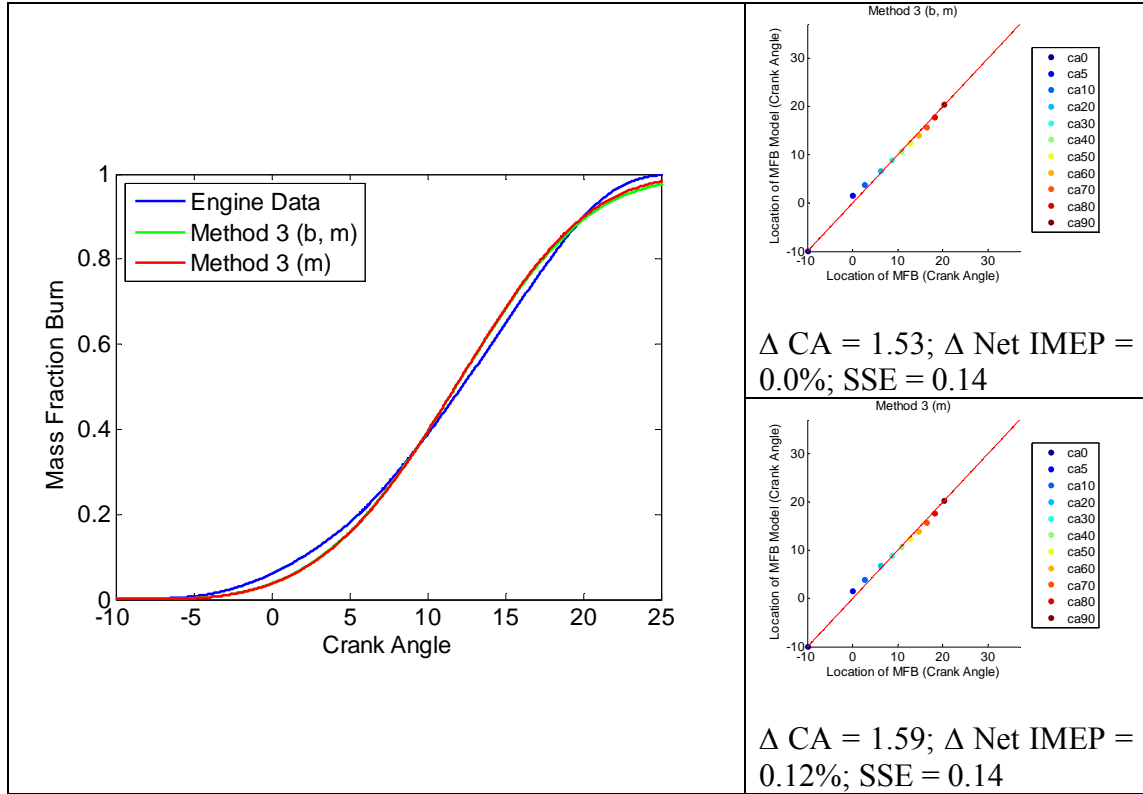
Figure V-3 The mass fraction burn and the Wiebe fitted curve using the method 3 (Gasoline, CR = 8.0:1, spark advanced = 10° BTDC, speed = 900 RPM, load = 330 kPa Net IMEP).

Method 4

This method is similar to Method 3. However, in this method, CA50 is used as a point of reference to define the duration of combustion using the analytical relation of "*m*" and "θ_o" as follows:

$$\Delta\theta_{0-90\%} = \frac{\theta_{50} - \theta_o}{\left(\dfrac{\ln(0.5)}{2.3026}\right)^{\frac{1}{m+1}}} \tag{V-4}$$

Figure V-4 shows the Method 4 results, which by adding the "*b*" parameter on the least square method, refines the Wiebe fitted curve. The difference in the combustion phasing

is approximately 0.5° crank angle. The SSE for this method is twice as much as for Method 2, but it is approximately one-third of the SSE obtained for Method 3.

Δ CA = 0.85; Δ Net IMEP = 0.03%; SSE = 0.05

Δ CA = 1.57; Δ Net IMEP = 0.52%; SSE = 0.14
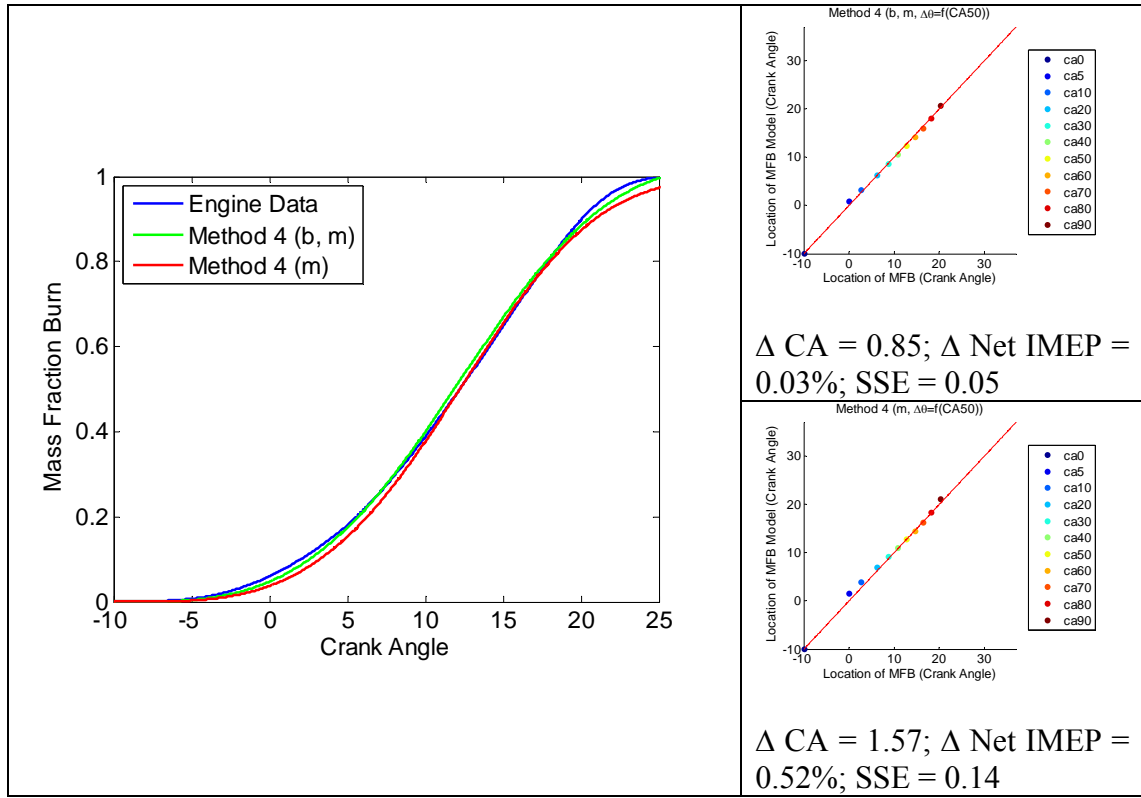
Figure V-4 The mass fraction burn and the Wiebe fitted curve using the method 4 (Gasoline, CR = 8.0:1, spark advanced = 10° BTDC, speed = 900 RPM, load = 330 kPa Net IMEP).

Method 5

This method fit the mass fraction burn to the Wiebe function by defining the "*m*" as a function of two given points of reference. The Wiebe parameter "*m*" derived based on CA10 and CA90 is written as follow:

$$m = \frac{\ln\left(\dfrac{\ln(0.1)}{\ln(0.9)}\right)}{\ln\left(\dfrac{\theta_{90} - \theta_o}{\theta_{10} - \theta_o}\right)} - 1 \qquad (V-5)$$

Figure V-5 shows the results obtained with this method by defining the "*m*" as a function of CA10 and CA90. The results obtained using this combined algebraic and least square method are not in a good agreement with the mass fraction burn engine data. The solution improves by using "*b*" as the parameter determined using the least square method and then algebraically to determine "*m*".
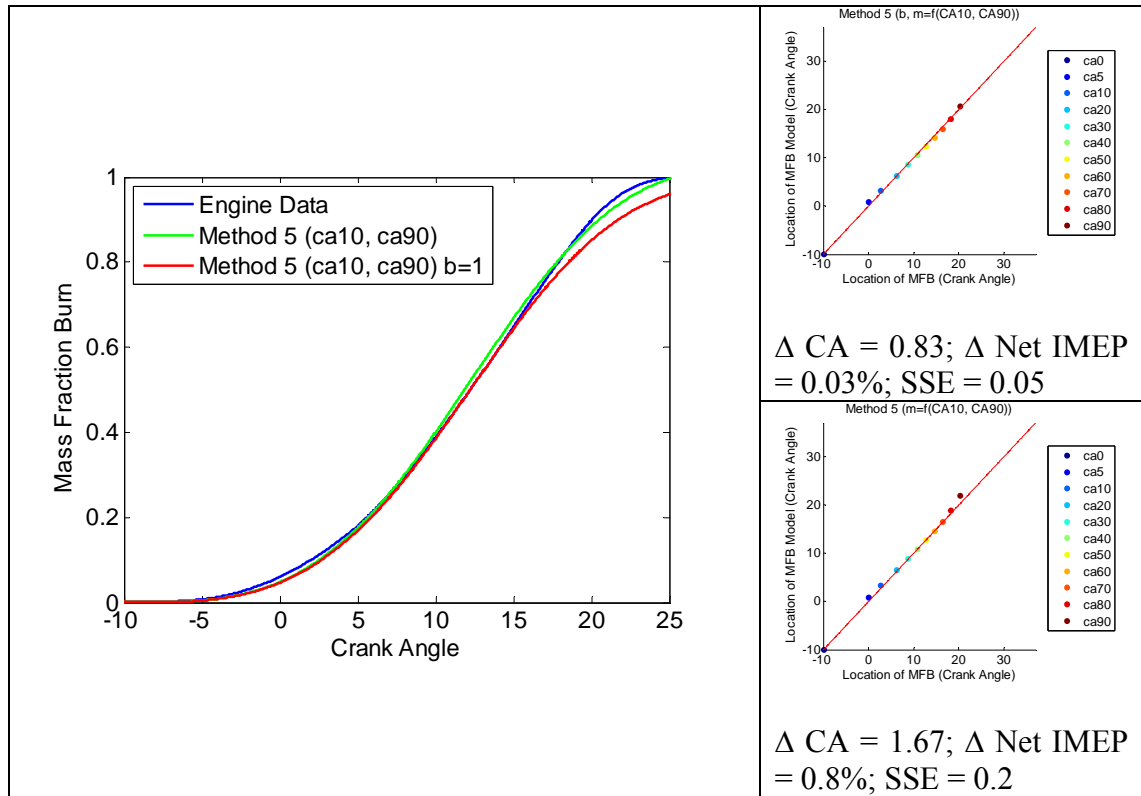
Figure V-5 The mass fraction burn and the Wiebe fitted curve using the method 5 (Gasoline, CR = 8.0:1, spark advanced = 10° BTDC, speed = 900 RPM, load = 330 kPa Net IMEP)

Conclusion

Five methods to fit the Wiebe function in the mass fraction burn profile have been discussed in this paper. Table V-1 (appendix) presents a summary of the Wiebe function parameters obtained using the five methods that are briefly explain above for all the gasoline-ethanol blend data. Excluding Method 1, Method 2 using the least square method with 3 parameters (*b*, *m*, *ca90*) produces the best fit to the original mass fraction

burn data followed by method 4 which have fixed "θ_o", and "θ_{50}", method 3 which have fixed "θ_o" and "θ_{90}", and method 5 which algebraically solves for "m" using the "θ_o" and "θ_{90}".

The conclusions from this work:

- Introducing the "b" parameter improved the fit in nearly all cases.

- The Net IMEP alone is not sufficient indicator of the fit produced by the model. The main reason for this is that the area under the mass fraction burn curve can remain the same even though the path is different. The addition of the SSE provides an addition important metric on how well the MFB curve fits the data.

- Method 2, using three parameters (b, m, $ca90$) of the Wiebe function, resulted in the best fit for this operating condition while matching the $\Delta\theta_{0-90\%}$.

Nomenclature

a the efficiency parameter of the Wiebe function
b the amplitude correction factor of the Wiebe function
m the form factor of the Wiebe function
x the mass fraction burned
θ the crank angle
$\Delta\theta$ the combustion duration
CA the location of crank angle
Subscripts
   b burned
   o start of combustion

Table V-1 The Wiebe function parameters using 5 different methods of five different ethanol concentration fuels (CR = 8.0:1, spark advanced = 10° BTDC, speed = 900 RPM, load = 330 kPa Net IMEP)

	Wiebe Fitted Params.	MFB of Engine Data	Method 1		Method 2		Method 3		Method 4		Method 5	
			LSM (b, m, ca0, ca90)	LSM (m, ca0, ca90)	LSM (b, m, ca90)	LSM (m, ca90)	LSM (b, m)	LSM (m)	LSM (b, m) & $\Delta\theta_{0\text{-}90\%}$ = f(ca50)	LSM (m) & $\Delta\theta_{0\text{-}90\%}$ = f(ca50)	m constant (ca10, ca90)	m constant (ca10, ca90) b=1
E0	a	-	2.30	2.30	2.30	2.30	2.30	2.30	2.30	2.30	2.30	2.30
	m	-	4.29	6.73	2.43	2.75	2.94	2.96	2.57	2.84	2.56	2.56
	θ_0	-10.00	-20.47	-33.19	-10.00	-10.00	-10.00	-10.00	-10.00	-10.00	-10.00	-10.00
	$\Delta\theta_{0\text{-}90\%}$	30.23	42.04	53.61	33.10	30.90	30.23	30.23	31.86	31.10	30.23	31.90
	b	-	1.04	1.00	1.08	1.00	0.99	1.00	1.04	1.00	1.04	1.00
	SSE	-	0.01	0.03	0.03	0.10	0.14	0.14	0.05	0.14	0.05	0.20
	Net IMEP (%)	-	-0.06	-0.24	0.02	-0.20	0.00	0.12	0.03	-0.52	0.03	-0.80
	Max $\Delta\theta$ Diff	-	10.47	23.19	0.67	1.21	1.53	1.59	0.85	1.57	0.83	1.67
E20	a	-	2.30	2.30	2.30	2.30	2.30	2.30	2.30	2.30	2.30	2.30
	m	-	5.41	9.00	2.57	2.95	3.15	3.19	2.74	3.05	2.70	2.70
	θ_0	-10.00	-24.80	-42.53	-10.00	-10.00	-10.00	-10.00	-10.00	-10.00	-10.00	-10.00
	$\Delta\theta_{0\text{-}90\%}$	28.82	44.79	61.51	31.77	29.47	28.82	28.82	30.41	29.67	28.82	30.51
	b	-	1.04	1.00	1.10	1.00	0.99	1.00	1.04	1.00	1.05	1.00
	SSE	-	0.01	0.02	0.03	0.11	0.15	0.15	0.05	0.15	0.06	0.22
	Net IMEP (%)	-	-0.07	-0.21	0.02	-0.18	0.00	0.13	0.03	-0.49	0.03	-0.77
	Max $\Delta\theta$ Diff	-	14.80	32.53	0.90	1.48	1.80	1.86	1.12	1.85	1.03	1.69
E40	a	-	2.30	2.30	2.30	2.30	2.30	2.30	2.30	2.30	2.30	2.30
	m	-	4.75	7.15	2.59	2.90	3.08	3.10	2.72	2.99	2.69	2.69
	θ_0	-10.00	-21.18	-32.70	-10.00	-10.00	-10.00	-10.00	-10.00	-10.00	-10.00	-10.00
	$\Delta\theta_{0\text{-}90\%}$	28.53	40.73	51.36	30.91	29.08	28.53	28.53	29.90	29.25	28.53	29.96
	b	-	1.03	1.00	1.08	1.00	0.99	1.00	1.04	1.00	1.04	1.00
	SSE	-	0.01	0.02	0.03	0.08	0.11	0.11	0.04	0.11	0.04	0.17
	Net IMEP (%)	-	-0.05	-0.18	0.02	-0.17	0.00	0.09	0.03	-0.42	0.03	-0.67
	Max $\Delta\theta$ Diff	-	11.18	22.70	0.79	1.27	1.54	1.58	0.94	1.57	0.89	1.43
E60	a	-	2.30	2.30	2.30	2.30	2.30	2.30	2.30	2.30	2.30	2.30
	m	-	4.79	7.60	2.57	2.91	3.10	3.13	2.72	3.00	2.70	2.70
	θ_0	-10.00	-21.36	-34.81	-10.00	-10.00	-10.00	-10.00	-10.00	-10.00	-10.00	-10.00
	$\Delta\theta_{0\text{-}90\%}$	28.26	40.77	53.23	30.88	28.86	28.26	28.26	29.71	29.04	28.26	29.76
	b	-	1.04	1.00	1.09	1.00	0.99	1.00	1.04	1.00	1.04	1.00
	SSE	-	0.01	0.02	0.03	0.09	0.12	0.13	0.04	0.12	0.04	0.18
	Net IMEP (%)	-	-0.05	-0.19	0.02	-0.17	0.00	0.12	0.03	-0.43	0.03	-0.68
	Max $\Delta\theta$ Diff	-	11.36	24.81	0.74	1.26	1.55	1.61	0.93	1.58	0.89	1.50
E84	a	-	2.30	2.30	2.30	2.30	2.30	2.30	2.30	2.30	2.30	2.30
	m	-	5.05	8.51	2.46	2.84	3.04	3.08	2.65	2.94	2.60	2.60
	θ_0	-10.00	-23.38	-40.20	-10.00	-10.00	-10.00	-10.00	-10.00	-10.00	-10.00	-10.00
	$\Delta\theta_{0\text{-}90\%}$	28.03	42.65	58.38	31.09	28.68	28.03	28.03	29.60	28.87	28.03	29.71
	b	-	1.04	1.00	1.10	1.00	0.99	1.00	1.04	1.00	1.04	1.00
	SSE	-	0.01	0.02	0.03	0.11	0.15	0.15	0.06	0.15	0.06	0.22
	Net IMEP (%)	-	-0.07	-0.22	0.03	-0.17	0.01	0.13	0.03	-0.45	0.04	-0.73
	Max $\Delta\theta$ Diff	-	13.38	30.20	0.93	1.51	1.82	1.89	1.16	1.86	1.07	1.68

V.2 DOUBLE-WIEBE FUNCTION PARAMETER ESTIMATION USING LEAST SQUARES METHOD

In this paper, the double-Wiebe function parameters were calculated using a least squares method by fitting MFB location as determines from analysis of measured cylinder pressure to the double-Wiebe functions. Multiple points from the experimental based MFB location were used to fit the single and double-Wiebe functions to observe the minimum number of data points required to estimate the Wiebe parameters. The conventional single-Wiebe function has two parameters, while the double-Wiebe function has five parameters including two parameters for each Wiebe function and a weighting parameter. A single-zone pressure model was developed to reconstruct the pressure trace from a given MFB profile in order to validate the estimated Wiebe parameters. This model is developed by reversing the single-zone MFB model. Once the pressure trace is recovered, the reconstructed pressure trace compared with the experimentally measured cylinder pressure trace over the range of ethanol blends from E0-E84 and combustion phasing sweeps with variable compression ratios and EGR percentages.

It is found that the double-Wiebe function model fit better to the experimental MFB profiles than the single-Wiebe function model.

ESTIMATION OF DOUBLE-WIEBE FUNCTION PARAMETERS FOR BURN DURATIONS OF ETHANOL-GASOLINE BLENDS IN A SI ENGINE OVER VARIABLE COMPRESSION RATIOS AND EGR LEVELS

Authors: Yeliana, C Cooney, J Worm, D J Michalek, J D Naber

(yyeliana@mtu.edu, cpcooney@mtu.edu, jjworm@mtu.edu, donna@mtu.edu, jnaber@mtu.edu)

Affiliations: Department of Mechanical Engineering - Engineering Mechanics, College of Engineering, 1400 Townsend Drive, Houghton, MI USA 49931-1295, Phone 906.487.2551, Fax 906.487.2822

Corresponding Author: yyeliana@mtu.edu

Abstract

Phasing and duration are two of the most important aspects of combustion in Spark Ignition (SI) engines and impacts efficiency, emissions, and overall engine performance. These aspects of combustion can be represented by the mass fraction burn (MFB) profile. Being able to accurately model the MFB profile leads to the ability to model the combustion process and, thus, properly model the overall engine in 1D engine simulation tools.

The Wiebe function is widely used in engine simulation to estimate the MFB profile as a function of crankshaft position [3]. In this work, for the purpose of validating a sub-process, the Wiebe function parameters were calculated using an analytical solution and a least squares method by fitting MFB locations as determined from analysis of measured cylinder pressure to both single and double-Wiebe functions. To determine the accuracy of the respective Wiebe function, a single-zone pressure model was applied to reconstruct the pressure trace. Once the pressure trace is recovered, the reconstructed pressure trace is then compared with the experimentally measured cylinder pressure trace. Results showed that the double-Wiebe function model fit better than the single-Wiebe function model. The root mean square error (RMSE) of reconstructed pressure trace using the double-Wiebe estimation is 7.9 kPa. In comparison, the RMSEs of reconstructed pressure traces using the single-Wiebe analytical solution and single-Wiebe least squares methods were 70.0 kPa and 75.9 kPa, respectively demonstrating a significant improvement.

Keyword: Spark Ignition Engine, Combustion Modeling, Burn Durations, Ethanol, Wiebe Function

Introduction

With computer capability continuing to increase, engine simulation has become an important part of the design and calibration phase of the development cycle for SI engines [2]. Due to its simplicity, 1D engine simulation is widely used for the design, development, calibration, and optimization of the engine. The 1D simulation tool is computationally efficient and enables dynamic modeling of the entire engine as a system including the dynamics of the flow [3]. The combustion sub-model plays a critical role in the overall engine simulation as it provides the burning rate, which represents the combustion process for a given engine geometry and set of operating conditions [2].

The Wiebe function is widely used in internal combustion engine applications to describe the fraction of mass burned in the combustion chamber during the combustion process [7, 54]. This function has a characteristic S-shaped curve, which grows from zero indicating the start of combustion and tends exponentially to one indicating the end of combustion. Due to its simplicity, this function is used instead of the complicated turbulent reacting flame front calculation to predict the rate of combustion [2, 3, 7], and is often used in SI engine modeling to describe the MFB as a function of engine position (crank-angle) during the cycle [3, 7, 27, 54, 55].

Reconstruction of the MFB by fitting a given MFB location to the Wiebe function became a critical step in the combustion model which can be used in an engine model for both design and operation optimization. In this paper, a least square method was developed to compute the double-Wiebe function parameters. A comprehensive analysis of the single-Wiebe and double-Wiebe fitted methods were performed and compared to the experimentally measured engine data over wide range of compression ratios, exhaust gas recirculation (EGR) and five different ethanol blends using a Cooperative Fuel Research engine.

Experimental Design

The engine data presented in this work was obtained from a single cylinder CFR engine that was modified to meet the criteria for this research [38, 46]. A custom piston was developed which allows engine operation over the range of compression ratios from 4.5:1 to 17.5:1. The location of the spark plug was moved to the top of the combustion chamber to improve flame propagation and to better emulate a modern SI engine combustion chamber geometry. An AVL GH12D piezoelectric pressure transducer was installed with an AVL PH01 flame arrestor to sense the in-cylinder pressure. Cylinder pressure data acquisition and on-line analysis (such as for data quality checks) was performed with a DSP ACAP system [47]. Other high speed and low speed data, including fuel and airflow rates and other critical pressures and temperatures, were measured and acquired using a combination of National Instruments hardware and software. An electronic control system for this engine was developed with Mototron's Motohawk rapid prototyping engine control development environment [39]. This enabled a full electronic control system including spark, fuel injection, and throttle. Mototron's Mototune was used as the calibration tool and engine control unit (ECU) interface. The calibration tool was also used to record engine parameters including intake manifold pressure, throttle position, air flow rate, commanded spark timing, fuel injection pressure, commanded injection duration, equivalence ratio, and exhaust gas recirculation (EGR) level.

Table V-2 lists the variables and the range associated with each that were examined in these experiments. The experiments were conducted by sweeping combustion phasing via spark timing and varying ethanol concentration, EGR rate, and compression ratio at a constant engine speed of 900 rpm and a constant load of 330 kPa NMEP[5] while maintaining a stoichiometric equivalence ratio. Combustion phasing was swept in 2° crank-angle (CA) increments from a location of 50% MFB (CA50) of approximately 30° ATDC to the point of heavy audible knock or until the combustion phasing was clearly advanced beyond maximum brake torque (MBT), whichever came first. During this

---

[5] The Net Mean Effective Pressure refers to the IMEP computed over the 720°CA operating cycle (high pressure loop, plus the pumping loop).

sweep the point of borderline audible knock, if applicable, was noted in the data. Three hundred consecutive engine cycles were recorded at each test set-point and the cycle averaged data was used to compute the MFB profile [38].

Table V-2 List of variables

Variable	Value
Fuel Blends[6]	E0, E20, E40, E60, E84
Compression Ratio	8, 10, 12, 14, 16
Spark Timing	From 4° ATDC in 2° increments (To Knock Limit)
EGR Rate (%)	0, 10, 20, 25, 30 (or COV Limit)

Wiebe Function Estimation

The Wiebe function is expressed as:

$$x_b = 1 - \exp\left[-a\left(\frac{\theta - \theta_o}{\Delta\theta}\right)^{m+1} \right] \qquad \text{(V-6)}$$

Where:

a Efficiency parameter

m Shape factor

x_b Mass fraction burn

θ Crank angle in degrees

---

[6] E84 = 84 % ethanol by volume

θ_o Start of combustion

$\Delta\theta$ Combustion duration

In this function, θ_o indicates the start of combustion; however, because of delays in flame kernel development, the location of first detectable combustion of does not always match the spark timing. However, θ_o is widely accepted as the spark discharge. Therefore the main difference observed in Wiebe function application is in determining the Wiebe parameters ("m", "a", and $\Delta\theta$) that define the burn rate characteristic [3, 7, 13]. In terms of the combustion duration, the 90% MFB is used as the end of combustion and 0, 1%, 5% or 10% MFB is used as the start of combustion. It is also widely known that "a" and "m" are adjustable parameters and the common values used for SI engine simulation are equal to 5 and 2, respectively [3, 7]. However, this set of constants results in a large estimation error especially for high dilution operating conditions and in combustion knock applications [13, 55].

Previously, several methods to determine the Wiebe function parameters have been developed by fitting the Wiebe function to the MFB profile using a combination of the least squares method and direct algebraic solution [56]. From this it is observed that the "a" is not an independent variable, but rather directly related to the combustion duration ($\Delta\theta$) [27, 56]. In this work, α is introduced as an efficiency parameter to represent both the "a" and $\Delta\theta$, thus simplifying the formulation of the Wiebe function.

$$x_b = 1 - \exp\left[-\left(\frac{\theta - \theta_o}{\alpha}\right)^{m+1}\right] \tag{V-7}$$

$$\alpha = a^{-1/m+1}\,\Delta\theta \tag{V-8}$$

A simple analytical solution of the Wiebe function parameters ("m" and $\Delta\theta$) given at least two MFB locations is obtained by rearranging terms and taking the natural log twice of Equation (V-7):

$$(m+1)\ln(\theta - \theta_o) - (m+1)\ln(\alpha) = \ln(-\ln(1-x_b))$$

(V-9)

This clearly shows that "$m+1$" is the slope of the plot of $\ln(-\ln(1-x_b))$ versus $\ln(\theta-\theta_o)$ with the intercept on the y-axis and the x-axis is $(-(m+1)\ln(\alpha))$ and $\ln(\alpha)$. Figure V-6 shows the plot of $\ln(-\ln(1-x_b))$ versus $\ln(\theta-\theta_o)$ using the experimental data using gasoline at a compression ratio of 8:1, zero EGR, and the spark swept from 4° to 12° BTDC. The circle symbols from left to right indicate the location of 5%, 10%, 25%, 50%, 75% and 90% MFB. The estimated values of $\hat{m}$ and $\hat{\alpha}$ from the linear correlation are:

$$\hat{m}_{AS} = \frac{\ln\left(\dfrac{\ln(1-x_{b1})}{\ln(1-x_{b2})}\right)}{\ln\left(\dfrac{\theta_1-\theta_o}{\theta_2-\theta_o}\right)} - 1$$

(V-10)

$$\hat{\alpha}_{AS} = \exp\left[\frac{(m+1)\ln(\theta_1-\theta_o) - \ln(-\ln(1-x_{b1}))}{\hat{m}+1}\right]$$

(V-11)

where subscripts 1 and 2 refer to the data points 1 and 2, respectively.

Alternatively, a least squares method can be used to estimate the "$\hat{m}$" and $\hat{\alpha}$ as follows:

$$\hat{m}_{LS} = \frac{n\sum_{i=1}^{n}(\ln(\theta-\theta_o))(\ln(-\ln(1-x_b))) - \sum_{i=1}^{n}(\ln(\theta-\theta_o))\sum_{i=1}^{n}(\ln(-\ln(1-x_b)))}{n\sum_{i=1}^{n}(\ln(\theta-\theta_o))^2 - \left(\sum_{i=1}^{n}(\ln(\theta-\theta_o))\right)^2} - 1 \quad \text{(V-12)}$$

$$\hat{\alpha}_{LS} = \exp\left(-\frac{\sum_{i=1}^{n}(\ln(-\ln(1-x_b))) - (\hat{m}+1)\sum_{i=1}^{n}(\ln(\theta-\theta_o))}{n(\hat{m}+1)}\right)$$

(V-13)
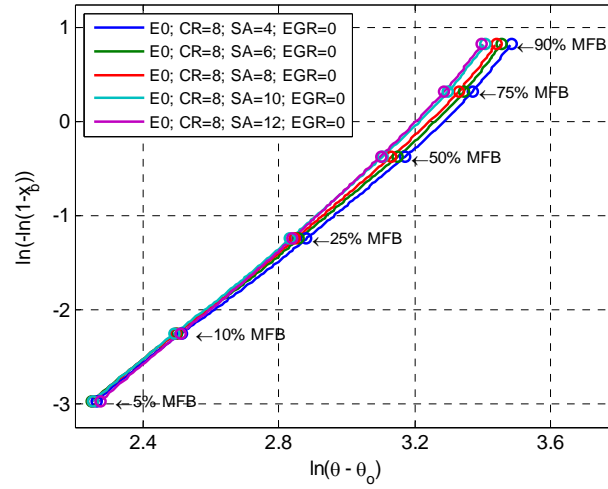
Figure V-6 Log plot of MFB profile (CFR; E0; CR=8:1; SA=5-13; EGR=0; Speed=900 RPM; Load=330kPa NMEP)

These formulas for estimating the Wiebe function parameters are simple and straightforward to apply. Another method to estimate "*a*" and "*m*" is a graphical approach, by plotting the $\ln(-\ln(1-x_b))$ against $\ln(\theta-\theta_o)$ which is essentially the same as the analytical solution method, as shown in Figure V-6. When the plot is a straight line, this means that the data set is adequately described using the single-Wiebe function. However, when the plot is not a straight line, it indicates a second Wiebe function is needed to match the engine data.

The double-Wiebe function has been used in HCCI [57, 58] and in knocking cases for SI engines [55], because the double-Wiebe function provides a better match to the experimental data compared to the standard Wiebe function for these non-symmetric combustion profiles. The double-Wiebe function parameters are estimated using a non-linear least squares method. In this work, estimation of the parameters for the double-Wiebe function is studied and developed for cases with only a limited number of data points from the MFB profile. Seven locations of MFB (0, 10%, 25%, 50%, 75%, 90%, and 99%) are used in the fitting processes. These data points are selected because they are

121

spread well across the MFB profile, are often used in combustion analysis and can be obtained from the recorded combustion analysis.

Existing literature describes several ways to combine more than one Wiebe function [59-61]. These applications are widely used in mechanical failure and reliability analysis. The double-Wiebe function has two efficiency and two shape parameters as well as a weighting factor (p) as shown in Equation (V-14). This weighting factor reflects the influence of each Wiebe function on the overall MFB profile. The least squares method is used to estimate these parameters, which were obtained by finding the minimum RMSE over a given set of data points that satisfied the double-Wiebe equation. A fixed set of initial values are given to start the estimation. Location of 10%, 25%, 50%, 75%, and 90% MFB are then calculated and compared to the location of 10%, 25%, 50%, 75%, and 90% MFB from experimental data. Figure V-7 shows the flow chart describing the process of estimating the double-Wiebe function parameters.

$$x_b = p\left(1 - \exp\left[-\left(\frac{\theta - \theta_o}{\alpha_1}\right)^{\beta_1}\right]\right) + (1-p)\left(1 - \exp\left[-\left(\frac{\theta - \theta_o}{\alpha_2}\right)^{\beta_2}\right]\right) \qquad \text{(V-14)}$$
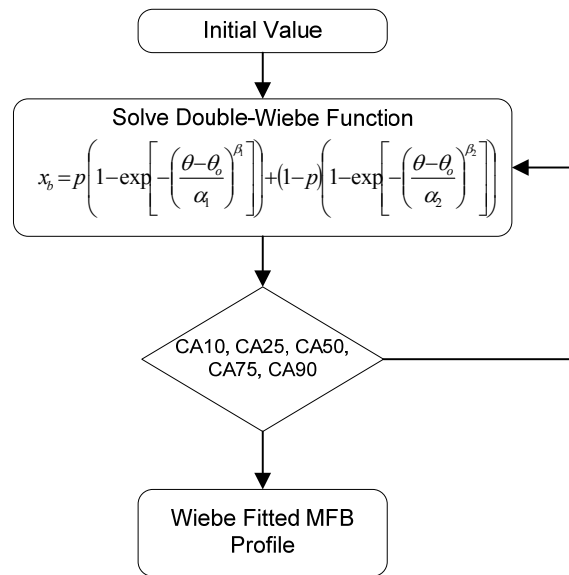

Figure V-7 Flow chart of double-Wiebe function parameters estimation

Results

The MFB which represents the percentage of fuel consumed versus crank-angle during the combustion portion of an engine cycle is obtained by analyzing the experimentally measured in-cylinder pressure, which is typically measured using a piezo-electric pressure transducer [44, 62]. This curve is commonly used to characterize the combustion process in SI engines. In this study, the MFB is compute using a single-zone MFB analysis method which is derived from the balance of energy in the combustion chamber by assuming the products and reactants behave as an ideal gas, the mass is constant, and both the products and reactants have a constant and equal molecular weight during the combustion process. A single-zone MFB model, along with a two-zone model, was developed by this research team and compared with a traditional apparent heat release model [38]. The single-zone model with two unknowns (temperature and mass fraction burn) and the two-zone model with five unknowns (burned and unburned temperature, burned and unburned volume, and mass fraction burn) is shown to correlate well with the apparent heat release model, particularly in regards to combustion phasing [38]. Due to its simplicity and good correlations, the single-zone MFB model was used to compute burn rate in this research.

Figure V-8 shows the engine MFB profile on the primary y-axis and the rate of MFB profile on the secondary y-axis for the CFR engine data at a compression ratio 8:1, spark advance at 6°BTDC, zero EGR, a constant speed of 900 RPM and a constant load of 330 kPa NMEP using an 84% ethanol blend. This MFB profile is normalized to its maximum value of 0.7. This means that 30% of the energy is lost through heat transfer, blow-by and crevice effects. The red cross symbols in Figure V-8 represent the location of 0, 10%, 25%, 50%, 75%, 90% and 100% MFB, which are used in the Wiebe function analysis.
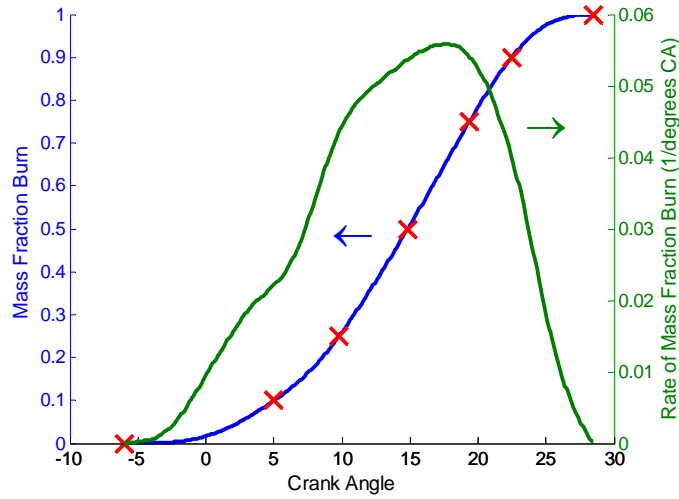
Figure V-8 MFB and rate of MFB profile (CFR; E84; CR=8:1; SA=6; EGR=0; Speed=900 RPM; Load=330kPa NMEP)

Figure V-9 shows the comparison between the engine data and the Wiebe function profile with parameters calculated using the analytical approach using the MFB value at the CA10 and CA90 locations. It is shown that the fitted Wiebe function failed to follow the engine data in the range of CA25 to CA75. This deviation impacts the rate profile causing an advance in the peak pressure and lowering the value of peak pressure.

Similarly in Figure V-10, the Wiebe function with the parameters estimated using the least squares method (LSM) for the same engine data using seven MFB values (0, 10%, 25%, 50%, 75%, 90% and 100%) in the fitting process. Compared to the analytical method, the LSM method also does not match the engine profile exactly. This is mainly due to the non-symmetrical nature of the MFB profile. Similar to the previous discussion, this deviation leads to shifting the rate of the Wiebe fitted MFB profile and furthermore shifting the reconstructed pressure trace.

Figure V-9 Single-Wiebe function with parameters estimated using analytical solution (CFR; E84; CR=8:1; SA=6; EGR=0; Speed=900 RPM; Load=330kPa NMEP)

Figure V-10 Single-Wiebe function with parameters estimated using least squares method (CFR; E84; CR=8:1; SA=6; EGR=0; Speed=900 RPM; Load=330kPa NMEP)

To improve the estimation of non-symmetrical cases, which are prevalent in the borderline knock or stability limit situations, the double-Wiebe function estimation is developed. This option is reasonable because the rate of combustion is continuously changing. For example, in the case above, due to the nature of the engine, the rate of combustion in the first half is slightly different than the rate of combustion in the second half. This difference is mainly caused by geometrical factors and the flame propagation with the small height-to-diameter ratio at high compression ratios in the CFR engine as well as the quenching effect on the flame as it travels close to the cylinder wall.

Figure V-11 shows that the double-Wiebe function model with the parameters estimated using the least squares method agrees well with the experiment MFB profile. Figure V-12 shows a similar comparison using the rate of MFB profile.
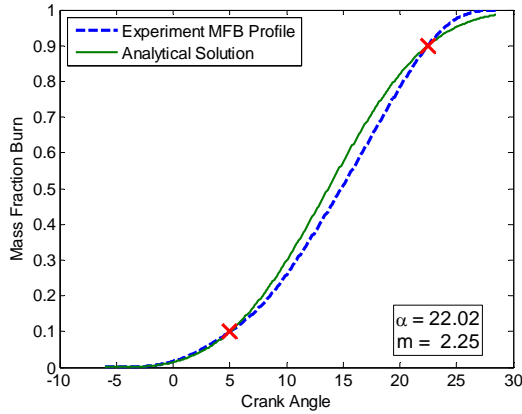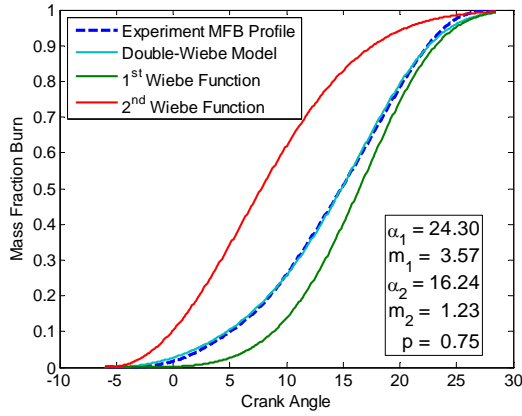
E84; CR=8; SA=6; EGR=0

Figure V-11 Double-Wiebe function with parameters estimated using least squares method (CFR; E84; CR=8:1; SA=6; EGR=0; Speed=900 RPM; Load=330kPa NMEP)
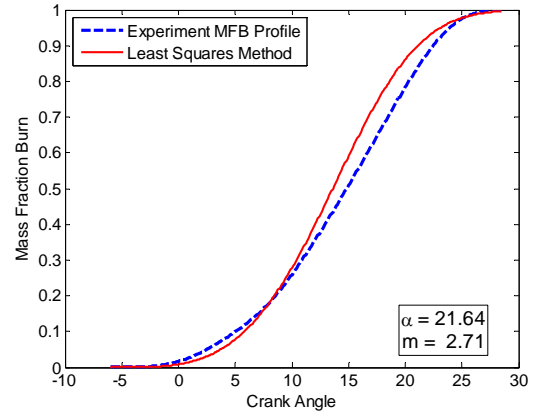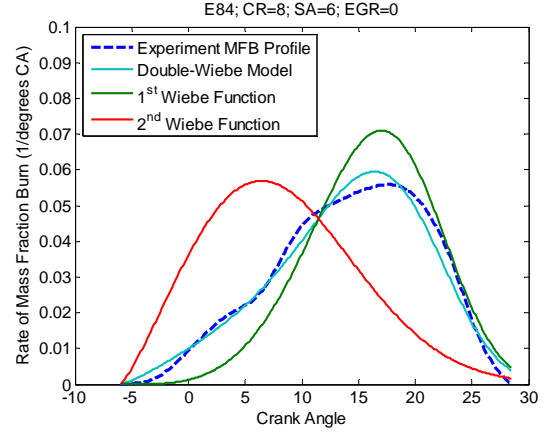
Figure V-12 Double-Wiebe function with parameters estimated using least squares method (CFR; E84; CR=8:1; SA=6; EGR=0; Speed=900 RPM; Load=330kPa NMEP)

Validation Process

Validation was performed using the fitted Wiebe function to estimate the heat release, and using that information, compute the cylinder pressure during combustion. For this purpose, a single-zone pressure model was developed by inverting the single-zone MFB analysis. Derived from the ideal gas equation and the energy balance, the single-zone pressure model is expressed in matrix form as:

$$
\begin{bmatrix} \dfrac{h\,V_{cr}}{\bar{R}/M\,T_w} & m_c\,C_v \\[2ex] V & -m_c\dfrac{\bar{R}}{M} \end{bmatrix} \begin{bmatrix} dp \\ dT \end{bmatrix} = \begin{bmatrix} \left(\dfrac{\eta_c\,Q_{LHV}\,m_c\,(1-x_{dil})}{(AFR+1)} \right) dx_b - p\,dV + A\,\bar{h}\,(T-T_w) \\[2ex] -p\,dV \end{bmatrix} \quad \text{(V-15)}
$$

Using the equation above, the unknown pressure and temperature are solved using LU matrix factorization given the MFB profile. There are number of terms estimated including heat transfer coefficient, residual fraction, combustion efficiency, wall temperature and crevice volume [38]. Once the pressure trace is recovered, the accuracy of the reconstructed pressure trace can be determined by a comparison with the measured cylinder pressure trace of the engine data. The maximum difference in phasing, the difference in NMEP, and the RMSE are used as metrics to quantify the Wiebe function fitting methods discussed in this paper.

Figure V-13 and Figure V-14 show the MFB and MFB rate respectively based on the engine data and three Wiebe functions obtained with parameters estimated using the analytical solution and least squares method for both single and double-Wiebe functions. The estimation is based on seven MFB locations (0, 10%, 25%, 50%, 75%, 90% and 99%), except for the analytical solution for the single-Wiebe function that uses only the values at 10% and 90% of MFB. It is shown that the double-Wiebe function matches the trend of the experimentally obtained MFB and MFB rate profiles better than the single-Wiebe or analytical solution.
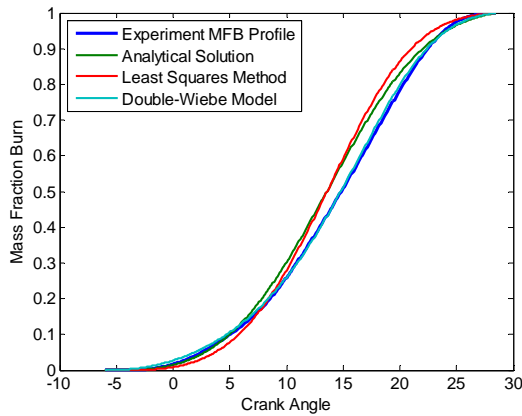

Figure V-13 Comparison of three curve fits of the engine MFB profile (CFR; E84; CR=8:1; SA=6; EGR=0; Speed=900 RPM; Load=330kPa NMEP)
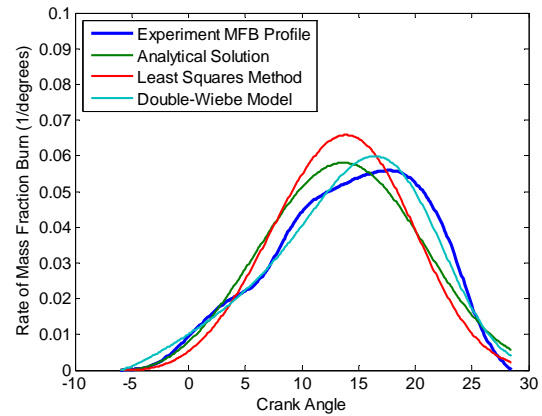
Figure V-14 Comparison of three curve fits of the engine MFB rate profile (CFR; E84; CR=8:1; SA=6; EGR=0; Speed=900 RPM; Load=330kPa NMEP)

Figure V-15 shows the reconstructed pressure trace using three different curve fits along with the inverted MFB profile obtained from the measured cylinder pressure and the actual cylinder pressure trace. The first blue line is the reconstructed pressure trace calculated using the engine MFB profile, and is thus a validation of the single-zone pressure model that is given in Equation (V-15). The second green line is reconstructed pressure trace calculated using the single-Wiebe function with the parameters estimated using the analytical solution. The parameters in the third red line are estimated using the least squares method, and the fourth turquoise line is computed using a double-Wiebe function with the parameters estimated using the least squares method. It is shown that the reconstructed pressure trace obtained using the double-Wiebe function is overlaid on top of the engine pressure trace.

Table V-3 shows the evaluation metrics for the reconstructed pressure traces for the CFR engine data using an 84% ethanol blend at a compression ratio of 8:1, spark advance of 6° BTDC, zero EGR, at a constant speed of 900 RPM and constant load of 330 kPa NMEP. The pressure model RMSE is approximately 1.6 kPa, the error in the double-Wiebe estimation is 7.9 kPa, and the error in the linear and LSM estimations are 70.0 kPa and 75.9 kPa, respectively. In terms of the Δ NMEP, the double-Wiebe is approximately 0.4 kPa lower than the experimental data, while the single-Wiebe applications estimate is about 4 kPa lower than the experimental data. As shown in the Table V-3, the maximum pressure difference between the models and the measured pressure trace shows the same trends.

Table V-4 shows the histograms of 745 CFR data points and the 5th and 95th percentile of the metrics used for the reconstructed pressure trace. These data cover different ethanol blends with sweeps of spark timing, compression ratio, and EGR rate at a constant engine speed of 900 RPM and a constant indicated load of 330 kPa NMEP. The 5th percentile error of Δ NMEP of the double-Wiebe function model approximation as compared to the engine data is less than 1 kPa, while the 5th percentile error using the single-Wiebe function is 3 kPa. The 95th percentile of RMSE for the double-Wiebe function approximation is 44 kPa, while for the single-Wiebe function approximations are greater

than 100kPa. Similarly the 5th percentile of maximum Δ pressure for the double-Wiebe approximation is half of the error obtained using the single-Wiebe function.
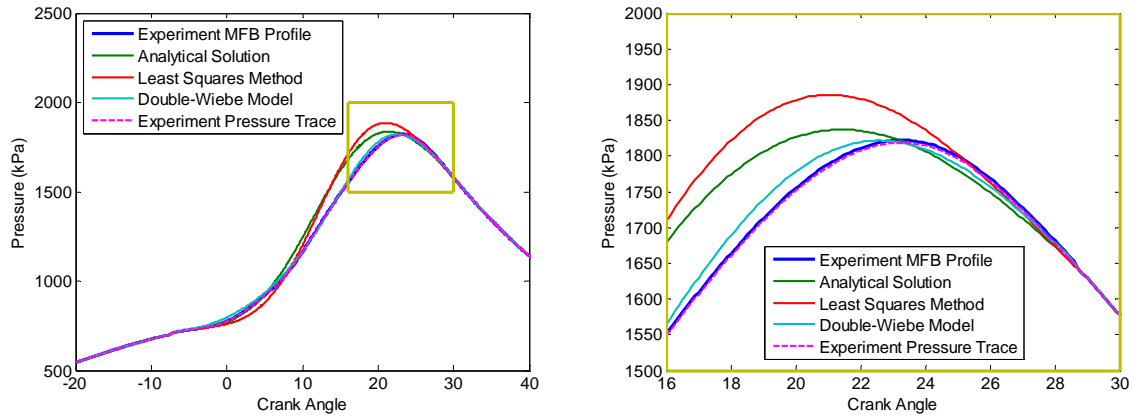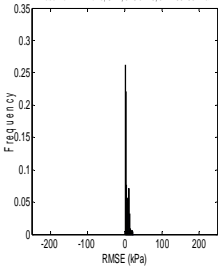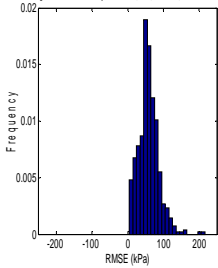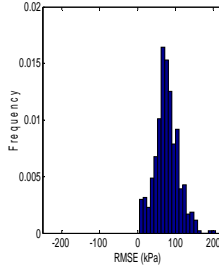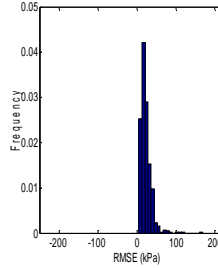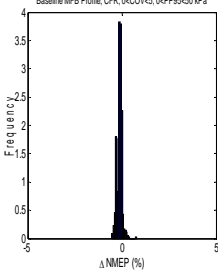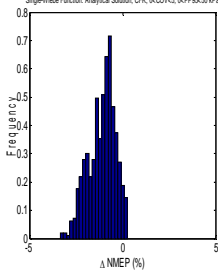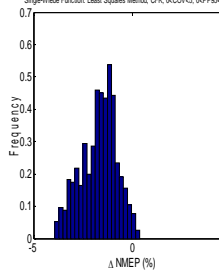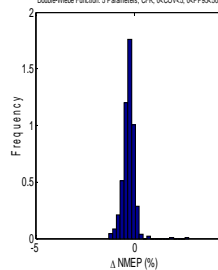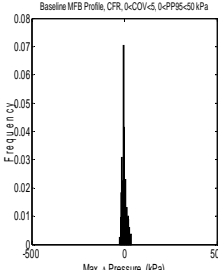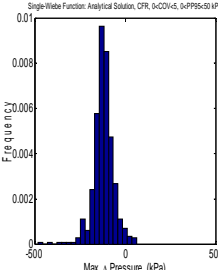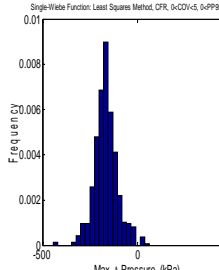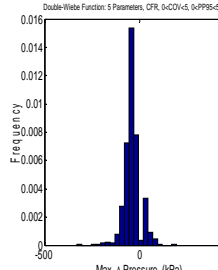
Figure V-15 Comparison of four curve fits to the engine pressure trace (CFR; E84; CR=8:1; SA=6; EGR=0; Speed=900 RPM; Load=330kPa NMEP)

Table V-3 Evaluation metrics of the reconstructed pressure traces using 4 different curve fits

	Experiment MFB Profile	Single-Wiebe Function Model with Linear Estimation	Single-Wiebe Function Model with LSM Estimation	Double-Wiebe Function Model with LSM Estimation
RMSE (kPa)	1.6	70.0	75.9	7.9
Δ NMEP (kPa)	-0.1	-4.1	-4.6	-0.4
Max Δ Pressure (kPa)	-2.7	-143.0	-164.4	-17.0

Table V-4 The 5th and 95th percentile of the metrics used for the reconstructed pressure trace using 4 different curve fits

	Experiment MFB Profile	Single-Wiebe Function Model with Linear Estimation	Single-Wiebe Function Model with LSM Estimation	Double-Wiebe Function Model with LSM Estimation
RMSE (kPa)	 5 Percentile = 1.5 95 Percentile = 14	 5 Percentile = 14.9 95 Percentile = 108	 5 Percentile = 22.3 95 Percentile = 128.9	 5 Percentile = 7.7 95 Percentile = 44
Δ NMEP (kPa)	 5 Percentile = -0.3 95 Percentile = 0	 5 Percentile = -2.4 95 Percentile = 0	 5 Percentile = -3.3 95 Percentile = -0.3	 5 Percentile = -0.8 95 Percentile = 0.1
Max Δ Pressure (kPa)	 5 Percentile = -17.5 95 Percentile = 23.2	 5 Percentile = -216.7 95 Percentile = -26.7	 5 Percentile = -267.1 95 Percentile = -57.1	 5 Percentile = -96.2 95 Percentile = 41.1

Summary and Conclusions

The single-zone pressure model to reconstruct the pressure trace from MFB profile has been developed and validated. The double-Wiebe function parameters estimation method which used a non-linear least squares method has been developed and compared with the single-Wiebe function parameters estimation method includes the analytical solution and least squares method.

The double-Wiebe function approximation, which involves five parameters, i.e. α_1, α_2, m_1, m_2, and p, the weighting parameter, fits better than any of the other approximations investigated. This method has shown similar result with proprietary dataset under a much wider conditions including engine speeds from 1000 RPM to 6000 RPM, NMEP range from 220 kPa to 1500 kPa, and equivalence ratios from 0.8 to 1.45. This double-Wiebe function parameters estimation method then can be applied in a predictive combustion model which determines the MFB profile from given set of MFB location. The double-Wiebe function parameters may also be used to characterize the combustion process by observing the weighting factor which weighs each Wiebe function with respect to overall MFB profile.

Based on this study, several recommendations for the application of the double-Wiebe function parameter estimations are:

- Use seven locations of 0, 10%, 25%, 50%, 75%, 90% and 99% of MFB
- Considering that only a limited number of data points are used, it is necessary to set the range of p, the weighting parameter, between 0.25 to 0.75 for successful implementation of the approximation
- The combination of the RMSE and the NMEP are sufficient indicators of the model fit to the engine data

Acknowledgements

Nomenclature

Wiebe Function

AS	Analytical Solution
a, α	Efficiency parameter
LS	Least Squares Method
m	Shape factor
p	Weighted factor
x_b	Mass fraction burn
θ_o	Start of combustion
$\Delta\theta$	Combustion duration
θ	Crank angle

Single-Zone Pressure Model

A	Combustion chamber surface area
AFR	Air Fuel Ratio

Cv	Specific heat at constant volume
h	Enthalpy
$\bar{h}$	Average heat transfer coefficient
M	Molecular weight
m_c	Mass of the charge
p	Pressure
Q_{LHV}	Lower heating value
$\bar{R}$	Universal gas constant
T	Temperature
V	Volume
x	Mass fraction
Subscript	
b	Burn
cr	Crevice
dil	Dilution
w	Wall

V.3   DOUBLE-WIEBE FUNCTION PARAMETER ESTIMATION USING ANALYTICAL SOLUTION

In many cases the rate of combustion changes with respect to the crank angle, and a single Wiebe function does not sufficiently represent the MFB profile. To better match the experimental MFB profile, a double-Wiebe function has been used particularly in cases that have a non-symmetric characteristic in the combustion profile. In this paper, the step-by-step estimation of the double-Wiebe parameter is studied and developed for cases with a limited number of data points to represent the MFB profile using an analytical solution. This analytical solution method is a simple, robust and straight forward method to compute the double-Wiebe parameters, thus enabling direct application in the one-dimensional engine simulation tool that normally has computational limitations.

ANALYTICAL SOLUTION OF DOUBLE-WIEBE FUNCTION PARAMETERS FOR BURN DURATIONS OF ETHANOL-GASOLINE BLENDS IN A SI ENGINE OVER VARIABLE COMPRESSION RATIOS AND EGR LEVELS

Authors: Yeliana, J Worm, D J Michalek, J D Naber

(yyeliana@mtu.edu, jjworm@mtu.edu, donna@mtu.edu, jnaber@mtu.edu)

Affiliations: Department of Mechanical Engineering - Engineering Mechanics, College of Engineering, 1400 Townsend Drive, Houghton, MI USA 49931-1295, Phone 906.487.2551, Fax 906.487.2822

Corresponding Author: yyeliana@mtu.edu

Abstract

The mass fraction burn (MFB) profile represents the fraction of mass burned in the combustion chamber as a function of crank angle. The MFB profile is the key characteristic in spark ignition engines linking combustion rates to an important indicator of efficiency, emissions and overall engine performance. The Wiebe function is a function form fits the characteristics S-curve that is used to represent the MFB profile as a function of crankshaft position and is widely used in engine simulation. In many cases as the rate of combustion changes with crank angle, a single Wiebe function does not sufficiently represent the MFB profile. To obtain better agreement with the experimental MFB profile, a double-Wiebe function can be used, particularly in cases that have a non-symmetric combustion profile.

In comparison to the single-Wiebe function that has two parameters, the double-Wiebe function has five parameters, including two sets of single-Wiebe parameters and a mixture parameter that defines the weight of each Wiebe function in the MFB profile. In this paper, the estimation of the double-Wiebe parameter is studied and developed for cases with a limited number of data points that represent the MFB profile using a unique analytical solution. This method provides a robust and computationally efficient method for application in 1D engine simulation tools.

Keyword: Double-Wiebe Function, Combustion Modeling, Burn Durations, Ethanol, Spark Ignition Engine

Introduction

A heat release analysis is performed to gain better understanding of the combustion process in a spark ignition (SI) engine. This analysis is conducted by examining the in-cylinder pressure trace that is typically measured with a piezo-electric pressure transducer in response to engine geometry, operating conditions and combustion process. The mass fraction burn (MFB) profile, a characteristic S-shaped curve, represents the cumulative heat release during the combustion process. The derivative of this curve represents the rate at which the mass burns, starts at zero and increases after the spark discharge to a maximum level approximately halfway through the burning process and then decreases to zero as the combustion process ends. The slope of the first half of this curve is not necessary the same as the slope of the second half, particularly under high dilution and knocking combustion conditions, which have a characteristic non-symmetric combustion rate.

Considering the importance of the MFB profile to the analysis and simulation of SI engines, it is critical to accurately model the MFB profile. An accurate MFB profiles enables modeling of the combustion process and effective simulation of the overall engine for design, calibration and optimization purposes.

Experimental Design

The experimental data used for this research was obtained using the Michigan Tech Port Fuel Injected Cooperative Fuel Research (CFR) engine with variable compression ratio of 8:1 to16:1 [46] and a single cylinder Direct Injection-SI Hydra engine with a modern combustion chamber including variable compression ratio of 11:1 to 18.5:1 and variable valve timing (VVT) to control the residual fraction in the combustion chamber [21]. Both of these engines have been used in the ethanol-gasoline blend research [21, 38, 46]. Each engine has an AVL GH12D piezoelectric pressure transducer installed with an AVL PH01 flame arrestor to sense the in-cylinder pressure. Cylinder pressure data acquisition was accomplished using a DSP ACAP system [63]. Three hundred consecutive engine

cycles were recorded for every test point. Other high speed and low speed data, including fuel and airflow rates and various other critical pressures and temperatures, were measured and acquired using a combination of National Instruments (NI) hardware and software. A fully electronic control system was developed with Mototron's Motohawk rapid prototyping engine control development environment [21, 39]. Mototron's Mototune was used as the calibration tool and engine control unit (ECU) interface. The calibration tool was also used to record engine control parameters including intake manifold pressure, throttle position, air flow rate, commanded spark timing, fuel injection pressure, commanded injection duration, equivalence ratio, intake and exhaust cam phasing, and exhaust gas recirculation (EGR) level.

Wiebe Function

The Wiebe function is widely used in internal combustion engine applications to describe the fraction of mass burned in the combustion chamber during the combustion process [7]. This function starts at zero, indicating the start of combustion, and tends exponentially to one, indicating the end of combustion. Due to its simplicity, this function is used instead of the complicated turbulent reacting flame front calculation to predict the rate of combustion [2, 3, 7], and is often used in SI engine modeling to describe the MFB as a function of engine position (crank-angle) during the cycle [3, 7, 27, 54, 55].

The Wiebe function is expressed as:

$$x_b = 1 - \exp\left[-a\left(\frac{\theta - \theta_o}{\Delta\theta}\right)^{m+1}\right]$$ (V-16)

Where:

a Efficiency parameter

m Shape factor

138

x_b Mass fraction burn

θ Crank angle

θ_o Start of combustion

$\Delta\theta$ Combustion duration

Previously, several methods to determine the Wiebe function parameters have been developed by fitting the Wiebe function to the MFB profile using a combination of the least squares method and direct algebraic solution [56]. It was observed that the efficiency parameter, "a" is not an independent variable, but is directly related to the combustion duration ($\Delta\theta$) [27, 56]. In this work, α is introduced as an efficiency parameter to represent both the "a" and $\Delta\theta$, thus simplifying the formulation of the Wiebe function.

$$x_b = 1 - \exp\left[-\left(\frac{\theta - \theta_o}{\alpha}\right)^{m+1}\right] \qquad \text{(V-17)}$$

$$\alpha = a^{-\frac{1}{m+1}} \Delta\theta \qquad \text{(V-18)}$$

Considering the "$m+1$" as γ, the Wiebe function has a similar form to the Weibull formula, a cumulative distribution function that has two parameters that are widely used in reliability, failure and lifetime data analysis [64]. The Weibull distribution is expressed as:

$$F(t) = 1 - \exp\left[-\left(\frac{t - \mu}{\alpha}\right)^{\gamma}\right] \qquad \text{(V-19)}$$

Where α is the scale parameter, γ is the shape factor and μ is the location parameter. The location parameter μ is known (in this case, the spark timing that indicates the start of

combustion θ_o in SI engine). Calculation of the Weibull parameters had been studied using linear and non-linear regressions [65], a graphical approach [66], and a weighted least squares method [67]. Wiebe function terms will be used toward the discussion in this paper.

A simple analytical solution of the Wiebe function parameters is obtained by rearranging terms and taking the natural log twice of Equation (V-17) twice:

$$(m+1)\ln(\theta - \theta_o) - (m+1)\ln(\alpha) = \ln(-\ln(1-x_b)) \qquad \text{(V-20)}$$

Equation (V-20) shows that "$m+1$" is the slope of the plot of $\ln(-\ln(1-x_b))$ versus $\ln(\theta-\theta_o)$ with the intercept on the y-axis and the x-axis is $(-(m+1)\ln(\alpha))$ and $\ln(\alpha)$. The analytical solution of "m" and α from the linearized-equation are:

$$m_{AS} = \frac{\ln\left(\dfrac{\ln(1-x_{b1})}{\ln(1-x_{b2})}\right)}{\ln\left(\dfrac{\theta_1-\theta_o}{\theta_2-\theta_o}\right)} - 1 \qquad \text{(V-21)}$$

$$\alpha_{AS} = \exp\left[\frac{(m+1)\ln(\theta_1-\theta_o) - \ln(-\ln(1-x_{b1}))}{m+1}\right] \qquad \text{(V-22)}$$

Where subscript 1 and 2 refer to the data points 1 and 2, respectively.

Double-Wiebe Function

The double-Wiebe function has been used in HCCI [57, 58] and in knocking cases for SI on single-Wiebe function for these non-symmetric combustion profiles. The double-Wiebe function parameters are estimated by fitting the MFB to the Wiebe function. The least squares method has been developed to compute these parameters, which were obtained by finding the minimum root mean square error (RMSE) over a given set of data points that satisfied the double-Wiebe equation [68]. However, in this work, estimation of

the parameters for the double-Wiebe function is developed using an analytical solution given a limited number of data points from the MFB profile.

Several methods to combine more than one Weibull function have been proposed [61, 69-71]. The mixture Weibull distribution parameters were obtained using a graphical approach [60, 72]. These applications are widely used in mechanical failure and reliability analysis.

In this paper, the double-Wiebe function was combined resulting two efficiency (α_1 and α_1) and two shape parameters (m_1 and m_2) and a weighting factor (p) as shown in Equation (V-23). This weighting factor reflects the influence of each Wiebe function on the overall MFB profile.

$$x_b = p\left(1 - \exp\left[-\left(\frac{\theta - \theta_o}{\alpha_1}\right)^{m_1+1}\right]\right) + (1-p)\left(1 - \exp\left[-\left(\frac{\theta - \theta_o}{\alpha_2}\right)^{m_2+1}\right]\right) \quad \text{(V-23)}$$

Analytical Solution Approach

Two general types of combustion characteristics can be identified by observing five location of MFB (10%, 25%, 50%, 75%, and 90%). The first type has a slower burn in the first half of the combustion period as compared to the second half of the combustion period, while the second type has a faster burn in the first half as compared to the second half of the combustion period. Figure V-16a shows a profile of MFB observed in the CFR engine (ethanol content of 85 %volume (E85), compression ratio (CR) = 8, spark advance (SA) = 10 °CA before top dead center (BTDC), EGR=10, intake cam center line (ICCL) = 112 °CA before gas exchange top dead center (BGETDC) and exhaust cam center line (ECCL) = 87.5 after gas exchange top dead center (AGETDC), speed at 900 RPM and net indicated mean effective pressure (NMEP) of 330 kPa). This exhibits a slower burning rate in the first half of the combustion period. Figure V-16b shows a MFB profile that has a faster burning rate in the first half as compared to the second half of the

141

combustion period. This was observed in the Hydra engine (E85, CR = 11, SA = 42.5 ^{o}CA BTDC, EGR = 0, ICCL = 110 ^{o}CA BGETDC and ECCL = 88 ^{o}CA AGETDC, speed at 1300 RPM and NMEP = 330 kPa). The red-crosses in both figures represent the locations of 10%, 25%, 50%, 75%, and 90% of MFB. These cases will be used as examples to demonstrate the analytical solution of the double-Wiebe function parameters estimation.

(a)   (b)
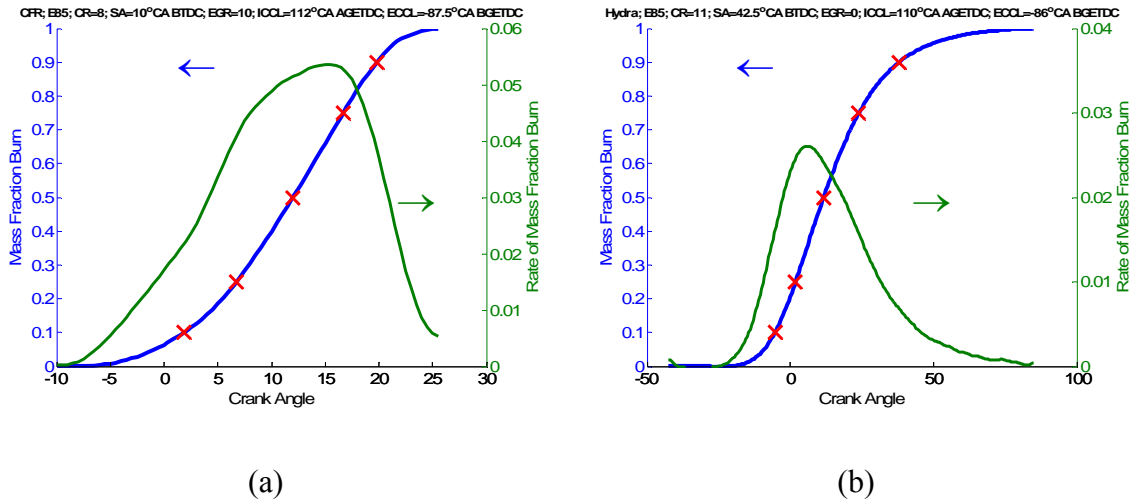
Figure V-16 Combustion characteristics of two different engines

Given these locations, which correspond to five different MFB percentages, the Wiebe parameters can be estimated using Equations (V-21) and (V-22). This method is similar to plotting the $\ln(-\ln(1-x_b))$ versus $\ln(\theta-\theta_o)$. Figure V-8a and Figure V-8b show the plots of $\ln(-\ln(1-x_b))$ versus $\ln(\theta-\theta_o)$ of the five locations of MFB profile taken from the CFR and Hydra engines, respectively. Projection to the y-axis represents the MFB, and projection to the x-axis represents the burn duration at given MFB location. The slope of the line between any two points represents the "m+1" of Wiebe parameters.
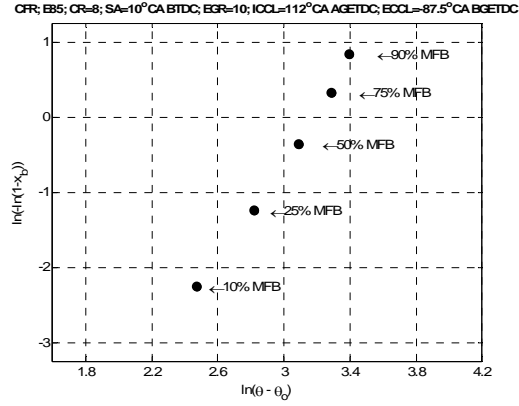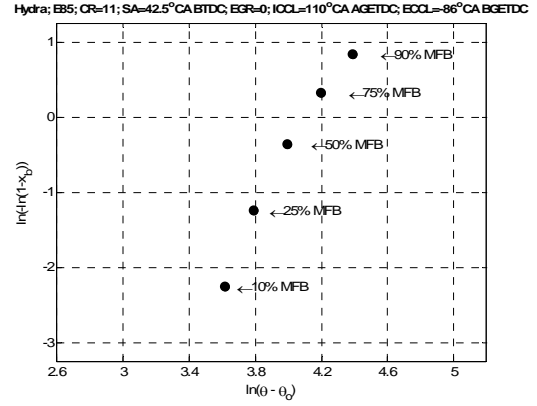
(a)   (b)

Figure V-17 Plot of ln(-ln(1-x_b)) versus ln(θ-θ_o)

The double-Wiebe parameter estimation process begins by assuming that there are two separate populations among the five MFB locations. The locations of 10% and 25% MFB describe the first population, which represents the first half of combustion period, and the location of 75% and 90% MFB describe the second population, which represents the second half of the combustion period. Figure V-9a and Figure V-9b show the same log plot for the CFR and Hydra engines, respectively. The green line represents the slope of the first population which represent the "m_1+1" of the first Wiebe function, and the red line represents the slope of the second population, which represent the "m_2+1" of the second Wiebe function. It is clearly shown that the engines have different combustion characteristics and the single-Wiebe function will not accurately represent the combustion processes. Figure V-19a and Figure V-19b show the profiles of both Wiebe functions for CFR and Hydra engines, respectively.
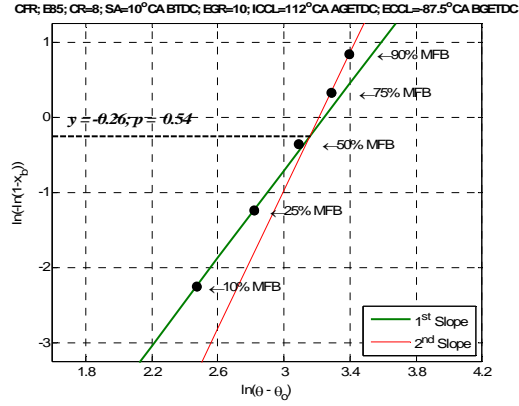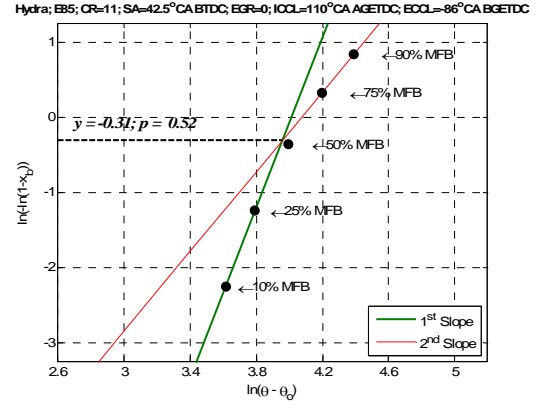
Figure V-18 Log plot of ln(-ln(1-x_b)) versus ln(θ-θ_o)
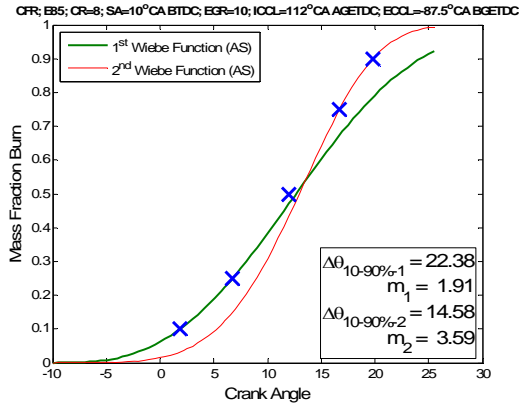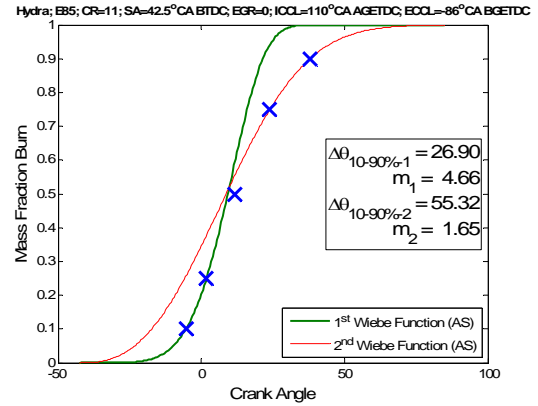
Figure V-19 Profile of both Wiebe function

Projection to the y-axis of the intersection of these two lines provides a good initial value for "p" the mixture parameter for the double-Wiebe function. From Figure V-9a and Figure V-9b, the "p" mixture parameters of the CFR and Hydra engines are 0.50 and 0.52, respectively. The estimated "p" mixture parameter can be expressed analytically as:

$$\hat{p} = 1 - \exp\left[-\exp\left(\frac{(m_1 + 1)(m_2 + 1)(\ln(\alpha_1) - \ln(\alpha_2))}{(m_1 + 1) - (m_2 + 1)}\right)\right] \quad \text{(V-24)}$$

Using the estimated "p" mixture parameter given by equation (V-24), the double-Wiebe function can be simplified as:

$$\frac{x_b - \hat{p}\left(1 - \exp\left[-\left(\frac{\theta - \theta_o}{\alpha_1}\right)^{m_1 + 1}\right]\right)}{(1 - \hat{p})} = \left(1 - \exp\left[-\left(\frac{\theta - \theta_o}{\alpha_2}\right)^{m_2 + 1}\right]\right) \quad \text{(V-25)}$$

Given a set of the first Wiebe function parameters, the second set of Wiebe function parameters can be easily determined using the following equation:

$$x_b^* = \left(1 - \exp\left[-\left(\frac{\theta - \theta_o}{\alpha_2}\right)^{m_2 + 1}\right]\right) \quad \text{(V-26)}$$

Figure V-20a and Figure V-20b show the plot of $\ln(-\ln(1-x_b))$ versus $\ln(\theta-\theta_o)$. The black line shows the double-Wiebe slope, which is a combination of the slopes of the first Wiebe function (green line) and the slope of the second Wiebe function (red line). The black line passes through the blue-dots, which represent the 10%, 25%, 50%, 75%, and 90% MFB locations.

CFR; EB5; CR=8; SA=10°CA BTDC; EGR=10; ICCL=112°CA AGETDC; ECCL=87.5°CA BGETDC

Hydra; EB5; CR=11; SA=42.5°CA BTDC; EGR=0; ICCL=110°CA AGETDC; ECCL=86°CA BGETDC
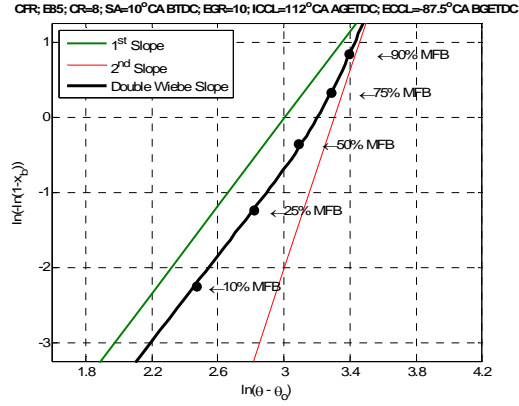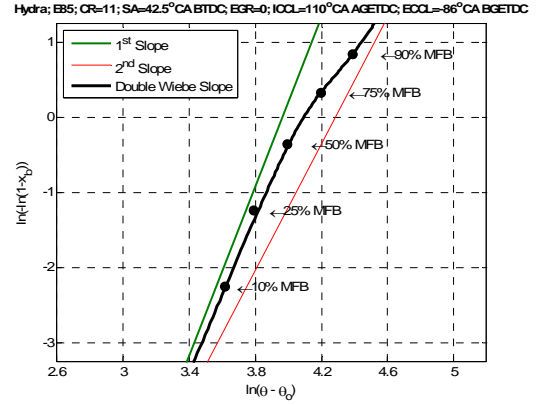
(a)   (b)

Figure V-20 Log plot of ln(-ln(1-x_b)) versus ln(θ-θ_o)

Figure V-21a and Figure V-21b show the reconstructed MFB profiles using the double-Wiebe function estimation overlaid on the calculated MFB profiles from the experimentally measured pressure trace. It is shown that the double-Wiebe function with the parameters listed on the Figure matches the experimental MFB profile.

CFR; EB5; CR=8; SA=10°CA BTDC; EGR=10; ICCL=112°CA AGETDC; ECCL=87.5°CA BGETDC

Hydra; EB5; CR=11; SA=42.5°CA BTDC; EGR=0; ICCL=110°CA AGETDC; ECCL=86°CA BGETDC
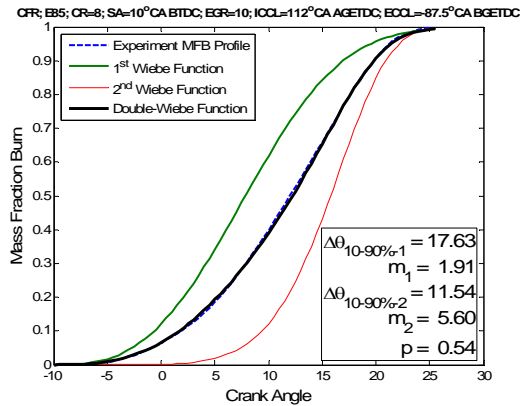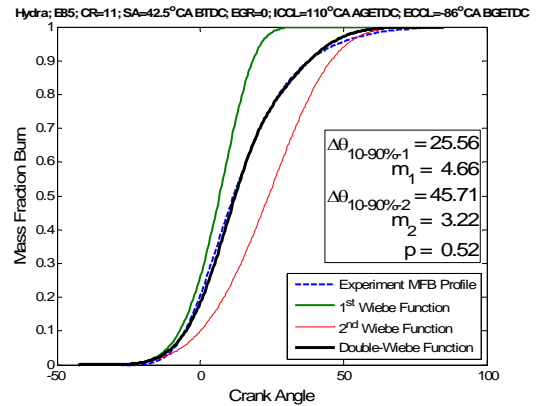
(a)   (b)

Figure V-21 Mass fraction burn profile

146

Figure V-22a and Figure V-22b show the rate of MFB calculated using the double-Wiebe function approximation with the rate of MFB calculated from the measured pressure trace.
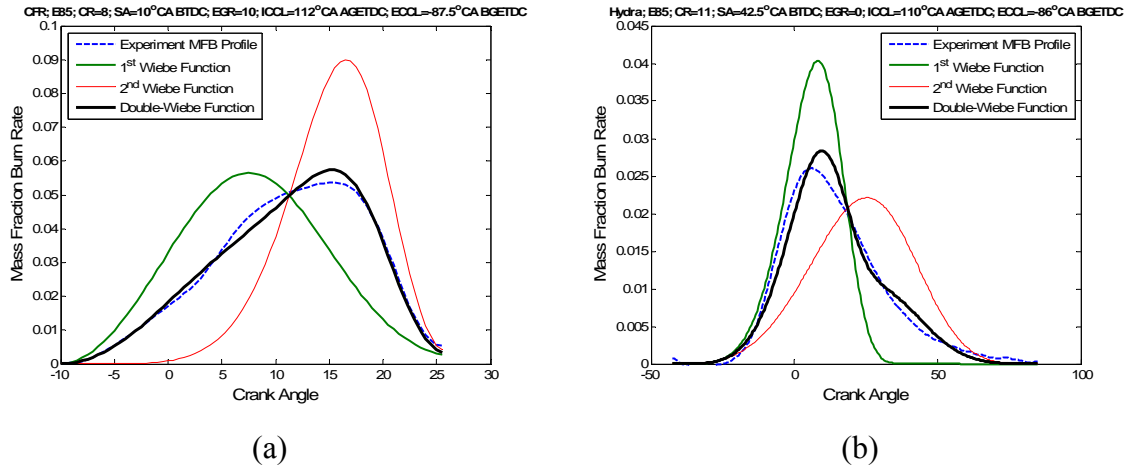
Figure V-22 Mass fraction burn rate profile

Validation of Analytical Solution for Double-Wiebe Function

Validation was performed using the fitted Wiebe function to estimate the heat release, and from that the cylinder pressure computes during combustion. For this purpose a single-zone pressure model was developed by inverting the single-zone MFB analysis, which is derived from the ideal gas equation and the energy balance [68]. A single-Wiebe function estimation using a least squares method is compared to the double-Wiebe function parameters estimation using the analytical solution described above.

Figure V-23a and Figure V-23b show the MFB profile using the single-Wiebe function and double-Wiebe function compared to the experimental MFB profile. In both cases the double-Wiebe function provides a better estimation than the single-Wiebe function. This results in a more accurate reconstructed pressure profile. Figure V-24a and Figure V-24b show the reconstructed pressure traces obtained using the single-Wiebe and double-

Wiebe function along with the experimentally measured pressure trace. Table V-5 shows the metrics calculated from the reconstructed pressure traces using the single-Wiebe and double-Wiebe functions with respect to the experimentally measured pressure trace for both cases which is chosen from two different engines. It is shown that the double-Wiebe function, which uses a simple analytical solution to estimate its parameters gives better results than the single-Wiebe function, which has parameters estimated using the least squares method.
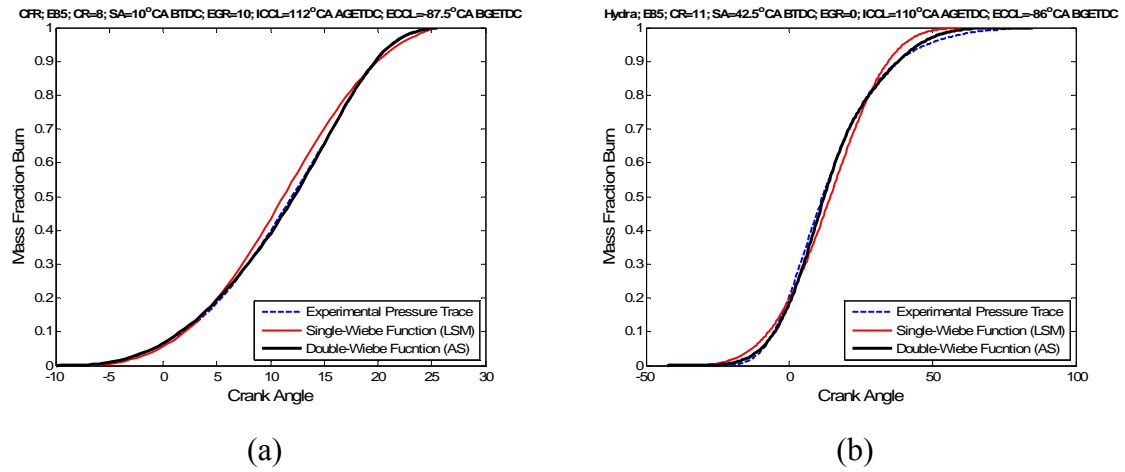
Figure V-23 Mass fraction burn profile
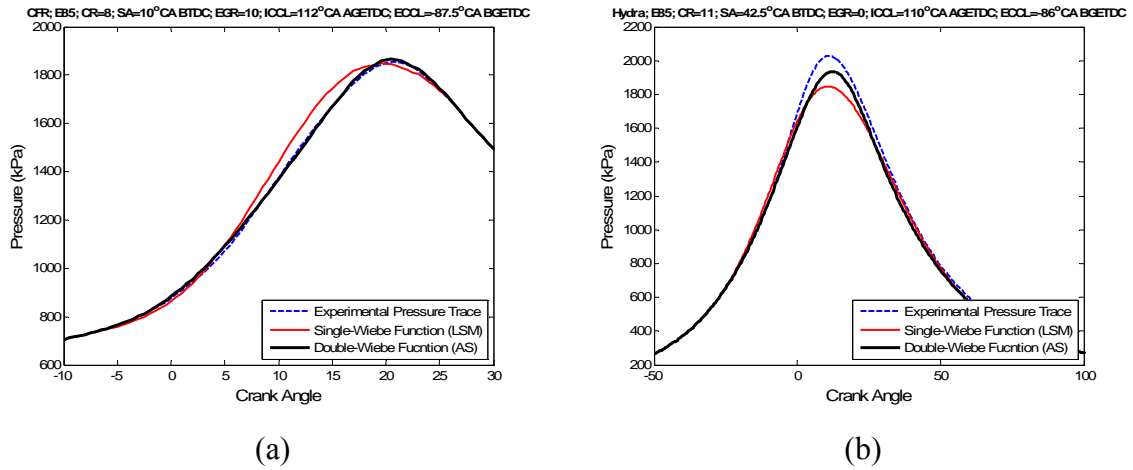
Figure V-24 Pressure trace

Table V-5 Evaluation metrics of the reconstructed pressure traces using single-Wiebe

and double-Wiebe functions

	CFR Engine		Hydra Engine	
	Single-Wiebe Function (LSM)	Double-Wiebe Function (AS)	Single-Wiebe Function (LSM)	Double-Wiebe Function (AS)
RMSE (kPa)	35.7	8.4	46.9	26.5
Δ NMEP (kPa)	-1.3	0	0	-0.4
Δ Max Pressure (kPa)	-76.8	20	134.6	87.1

Summary and Conclusions

A step-by step analytical solution to compute the five double-Wiebe function parameters has been discussed. Using the single-zone pressure model that was developed and validated by the author, the double-Wiebe function is shown to be more accurate than the single-Wiebe function which uses the least squares method to estimate two of its parameters.

The analytical approach requires carefully selected initial values of the MFB to accurately reconstruct the pressure trace. By assuming that the locations of 10% and 25% MFB to represent the first Wiebe function and the locations of 75% and 90% MFB to represent the second Wiebe function, the double-Wiebe function can be simplified to a single-Wiebe function formula, which can be solved using a simple analytical solution.

Acknowledgements

VI. COMBUSTION MODEL INTEGRATION

There are several ways to develop and integrate the combustion model in GT-Power. In this report, a user compound was developed to accommodate the parametric predictive combustion model, which contains calculation of the Wiebe function parameters as a function of engine geometry and operating conditions. An RLT-dependence was used to connect the predictive combustion compound with the multi-Wiebe combustion template in the main engine model. The RLT-dependence was chosen because there were no signal ports available in the multi-Wiebe combustion template at the time this parametric combustion compound was being developed. Even though this parametric combustion compound was built in GT-Suite V6 built-12, this parametric combustion compound was ready for the GT-Suite V7 which has open ports in the multi-Wiebe combustion template, thus enables the direct connection in and out the multi-Wiebe template. Details of the parametric combustion models, both single-Wiebe and double-Wiebe parametric combustion models and their comparison can be found in reference [73].

INTEGRATION OF PARAMETRIC COMBUSTION MODEL OF ETHANOL-GASOLINE BLENDS OVER VARIABLE COMPRESSION RATIOS AND VARIABLE CAM TIMING IN A SPARK IGNITION ENGINE MODEL

Abstract

The need to increase the performance of a spark ignition engine, include increasing efficiency and reducing the amount of toxic exhaust gas by using an environmental friendly fuel, has become a major objective in engine research and development. With computer capability continuing to increase, engine simulation has become a significant step in the design and calibration phase of engine development. The combustion process plays an important role in internal combustion engines, and thus the combustion model in the overall engine simulation, as it provides the burning rate, which represents the combustion process for a given engine geometry and set of operating condition.

A parametric combustion model has been developed, integrated and validated to the SI engine model. This model employed empirical burn duration correlations over a wide range of operating conditions, ethanol-gasoline blends, and engine geometry. This model also included the double-Wiebe function parameters calculated using a simple analytical solution. The parametric combustion model, which was built into a user-compound, was then integrated to the engine model in GT-Power through a multi-Wiebe combustion template. The double-Wiebe parameters computed in the parametric combustion model were transferred via RLT-dependent. This parametric combustion model was then validated by overlaying the pressure trace from the engine simulation result to the experimentally measured pressure trace.

Keyword: Double-Wiebe Function, Combustion Modeling, Ethanol, Spark Ignition Engine

Introduction

One-dimensional engine simulation is widely used for the design, development, calibration, and optimization of the engine. This simulation tool is computationally robust and efficient and enables dynamic modeling of the entire engine as a system including the dynamics of the flow [2, 3]. The combustion sub-model in the overall engine simulation provides the burning rate that represents the combustion process. The burning rate can be determined empirically or derived from physical and chemical kinetic correlations of the combustion process. Having a proper combustion model will enhance understanding of the physical phenomena including the effects of valve phasing, type of fuel, compression ratio, exhaust gas recirculation (EGR), etc.

GT-Power [54] was used in this research because it was widely known in industry as a simulation tool to calibrate and optimize the engine. In this paper, the development and integration of a combustion model is discussed.

Parametric Combustion Model Development

A parametric combustion model has been developed by employing the empirically determined burn durations over a wide range of engine geometries and operating conditions. The empirical burn duration correlations for this predictive combustion model were developed using experimentally measured pressure traces over a wide range of compression ratios, residual fractions, spark timings, equivalence ratios, and engine speeds and loads. Prior to developing the correlation, five physically based parameters have been selected from the literature: engine bore (B), height of the combustion chamber (h), mean piston speed (S_p), laminar flame speed (S_L), and kinematic viscosity of the unburned mixture (ν). A non-dimensional analysis using Buckingham's Pi Theorem was performed using those physically based parameters. A non-linear least squares method was then used to correlate the burn duration with the Pi groups in a product-power form. Figure VI-1 shows the development process of the parametric combustion model. The

complete procedures used to develop the empirical burn duration correlation were discussed previously by the author [74].
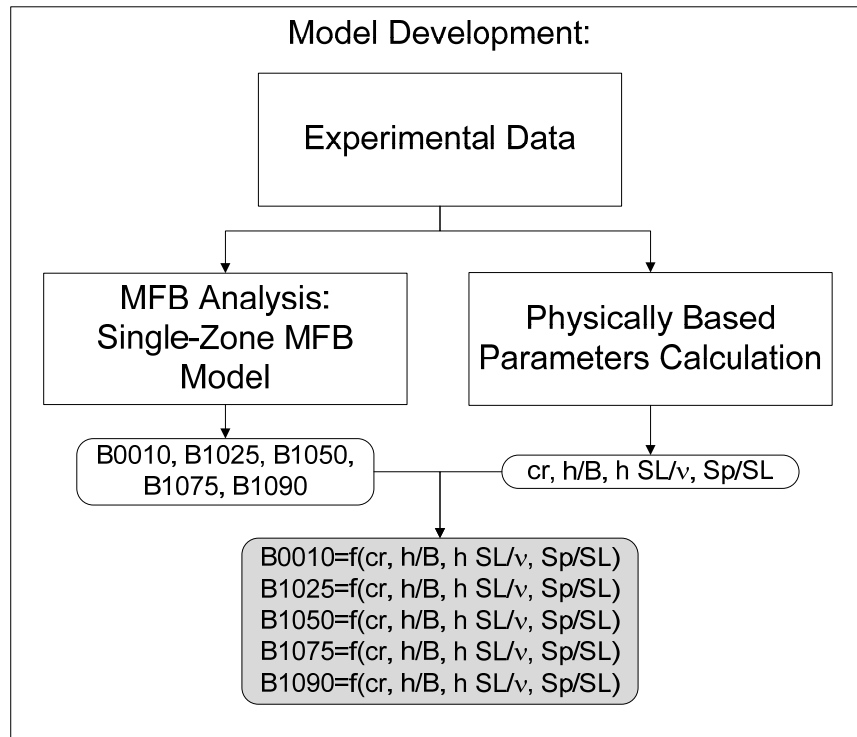
Figure VI-1 Parametric combustion model development process

The parametric combustion model was built in a user-compound within GT-Power. This model computed the double-Wiebe function parameters based on the burn durations, which computed using the burn duration correlations as a function of non-dimensional pi-groups. The double-Wiebe function was used in this parametric combustion model because it was found that the double-Wiebe function was a better representative of MFB profile, especially for profiles with non-symmetric characteristics, as compared to the conventional single-Wiebe function [68]. The double-Wiebe function consists of two single-Wiebe functions and a mixture parameter to weigh the double-Wiebe function, thus having five parameters. Several methods to estimate the double-Wiebe function parameters have been previously observed. An analytical solution was selected to be used in the predictive combustion model, due to its robustness and straight forward algebraic

calculation. Also the analytical solution can estimated the double-Wiebe function parameters using very limited data: the 0-10%, 10-25%, 10-75%, and 10-90% burn durations [75].

Figure VI-2 shows a diagram of the parametric combustion model using the double-Wiebe function. In-cylinder pressure and temperature, piston position, and crank angle were read from the main engine model. The physically based parameters for every cycle iterations were calculated based on the pressure trace, temperature at that cycle iteration. These values were then used to calculate the burn durations and compute the double-Wiebe function parameters ("p", "m_1", "m_2", "$\Delta\theta_1$", and "$\Delta\theta_2$"), which were used in the next cycle of the iteration. The location of 50% MFB (CA50), which defines the anchor of the Wiebe function, was obtained directly from the main engine model and transformed into $CA50_1$ and $CA50_2$. The $CA50_1$ and $CA50_2$ represent the anchor of the first and the second Wiebe function, respectively. The double-Wiebe parameters were estimated using the analytical method.

A routine to estimate the single-Wiebe parameters was also included in the double-Wiebe predictive combustion compound. This routine, shown by the blue dash line, was very important in calculating and balancing the CA50 transformation. The single-Wiebe parameters were estimated using the least squares method.
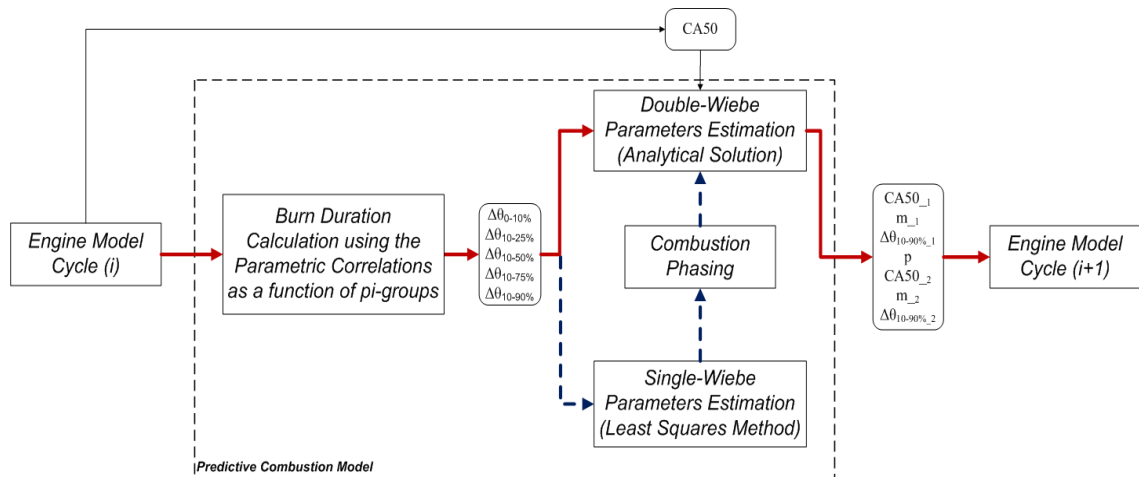
Figure VI-2 Parametric combustion model integration process

Integration Parametric Combustion Model

There are several templates that could be used to integrate the parametric combustion model to the engine model. Since the Wiebe function was used in defining the combustion profile, an SI Wiebe template or a Multi-Wiebe template might be used in the integration. The multi-Wiebe combustion template was used to accommodate the double-Wiebe parameters input in the double-Wiebe parametric combustion model. Since a direct connection was not available to the multi-Wiebe template, an RLT-dependence was set to link the parametric combustion model to the main engine model. The downside to this setup was a one iteration delay because the RLT-dependence delivered the Wiebe parameters that were computed in the previous cycle to the engine model.

Results

A full sweep of the intake cam center line (ICCL) and the exhaust cam center line (ECCL) experiments were conducted using E0, E50 and E85 fuel blends in the Ecotec Hydra engine at General Motors engine laboratory [76]. This dataset was used in the validation of the parametric combustion model by overlaying the experimental data over the GT-Power simulation result. Figure VI-3 shows the full sweep ICCL and ECCL with respect to the residual fraction that was trapped in the cylinder at 1300 RPM, 330 kPa using E85 blend. The surface plot represents the GT-Power simulation results and the black "X" represents the experimental data. The wider the valve overlap the higher fraction of residual trapped in the cylinder. The residual fraction varied from 10% to 40% at the widest valve overlap.
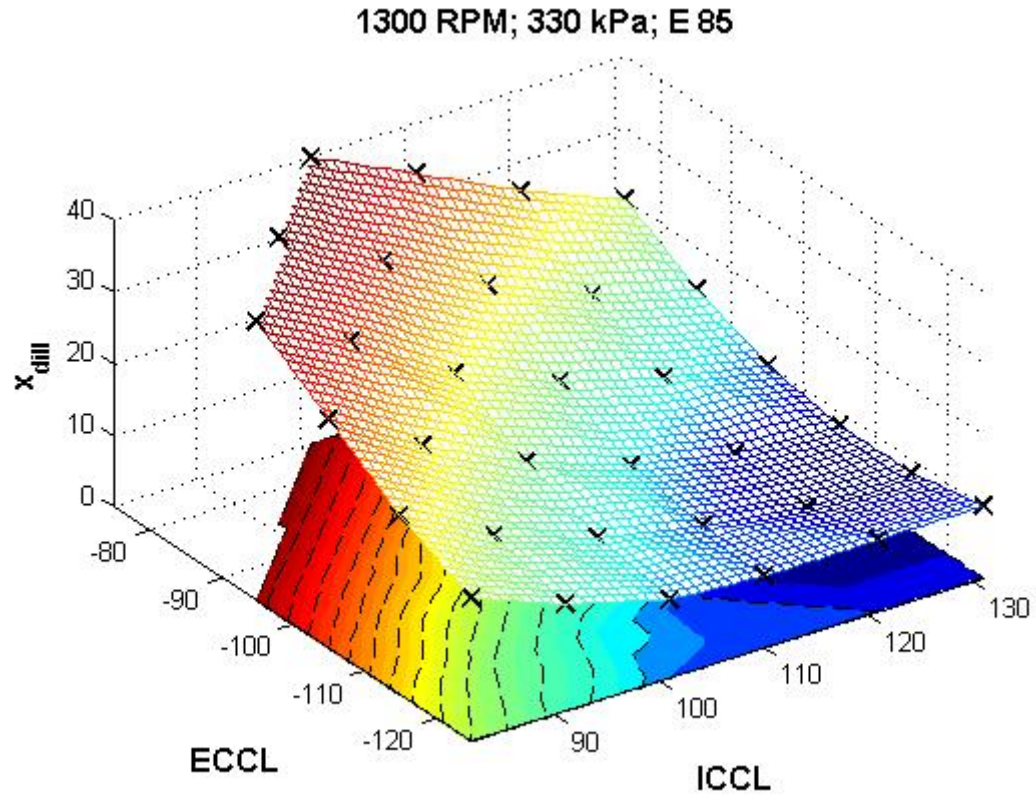
Figure VI-3 Residual fraction trapped in cylinder as function of ICCL and ECCL

Figure VI-4 shows the overlay plot of pressure trace from experimental and simulation result at 3 different ICCL and ECCL configuration in the SI engine at 1300 rpm, 330 NMEP using E85. It is shown that the double-Wiebe predictive combustion model provides the Wiebe function parameters that match the experimental data.
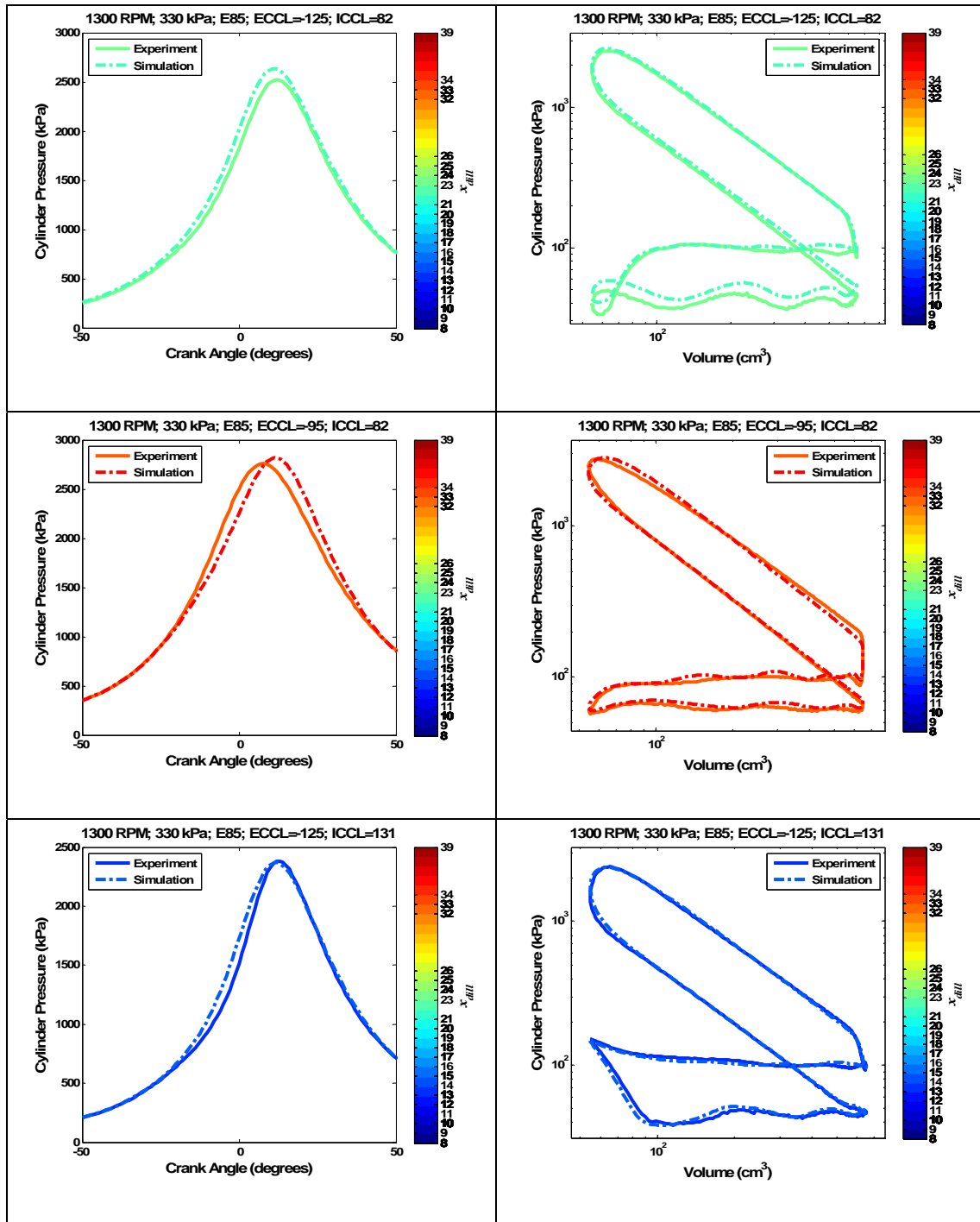
Figure VI-4 Overlay plot of experimentally measured pressure trace with simulation result

Summary and Conclusions

A mean value based double-Wiebe predictive combustion model has been developed in a user compound, integrated and validated to the SI engine model in GT-Power. It is shown that the double-Wiebe predictive combustion model is able to utilize the information from the previous cycle to compute the Wiebe function parameters that match the experimental data.

VII. CYCLE COMBUSTION VARIATION

A parametric correlation of coefficient of variance (COV) of gross indicated mean effective pressure (IMEP) has been developed using proprietary datasets. These datasets cover a wide range of engine speed and load conditions, variable compression ratios, variable valve timings, and various ethanol blends. Five correlations of COV of gross IMEP were presented in the discussion as a function of burn durations, standard deviation of burn durations, and/or non-dimensional Pi-groups. It was found that the COV of gross IMEP is highly correlated to the duration of 10%-75% mass fraction burn (B1075).

A thermodynamic engine model was developed and used to study the effect of engine operating conditions on the burn durations and COV of gross IMEP. In addition to the COV of gross IMEP correlation developed in this paper, the thermodynamic engine model also used residual fraction and burn duration correlations. While the residual fraction correlation was developed as a function of overlap factor, engine speed, map and exhaust pressure, compression ratio, and equivalence ratio, the burn duration correlations were developed as a function of physically based non-dimensional groups.

PARAMETRIC STOCHASTIC COMBUSTION MODELING FOR ETHANOL-GASOLINE FUELLED SPARK IGNITION ENGINES

Abstract

Cycle to cycle combustion variation in spark ignition (SI) engines is an important subject that has been widely studied because it limits the range of engine operation. Many studies have been done to observe the causes of cycle variation in the combustion process that leads to the cycle variation in the engine output performance. This cycle to cycle variation can be observed and characterized from the experimentally measured in-cylinder pressure traces. The cycle variation can be parametrically modeled with respect to the engine geometries and operating conditions.

Multiple correlations of COV of gross IMEP have been developed as a function of burn durations, standard deviation of burn durations, and physically based non-dimensional Pi-groups. The COV of gross IMEP is found to have a strong correlation to the duration of 10-75% mass fraction burn (B1075), and thus the COV of gross IMEP could be described solely as a function of B1075.

Introduction

Even under constant engine operating conditions, the combustion processes in the cylinder of SI engines can vary from cycle to cycle causing changes in the pressure development. This cycle to cycle combustion variation in SI engines limits the range of engine operation, especially under lean and highly diluted mixtures resulting in combustion instability, misfire and combustion knock conditions as determined by many investigators [3, 17-20, 77-79].

The main physical factors that lead to cycle to cycle variation in SI engines are incomplete mixing of fuel, air and residuals, the size of the eddy discharged from the

spark [19, 20, 77], as well as charge motion and turbulence level in the combustion chamber [3, 78].

The coefficient of variation (COV) of both indicated mean effective pressure (IMEP) and maximum pressure are commonly used to indicate the cycle variations. Although the location of maximum pressure, the maximum rate of pressure rise, the location of the maximum pressure rise, the in-cylinder pressure trace over a certain range of crank angle, and the burn durations of 0-1%, 0-10%, 0-50% and 0-90% are also found in the literature as metrics to quantify the cycle variation limits and trends [3].

Two correlations of COV of IMEP are found in the literature [22, 23]. In the first study, a linear regression of COV of IMEP was developed using three different chamber geometries and varying the total exhaust gas recirculation (EGR), air-fuel ratio, spark timing, engine speed and fueling level using a single-cylinder engine [22]. Using a wide range of engine geometries and operating conditions, it was found that the COV of IMEP has a non-linear correlation to the engine geometry and operating conditions [23].

In the second study, a non-linear regression of a polynomial form for COV of IMEP was developed as a function of engine speed and load, equivalence ratio, residual fraction, burn duration of 0-10%, burn duration of 10-90% and location of 50% mass fraction burn (MFB) using 6000 conditions collected from 13 different engines from 1.6 to 4.6 liters in displacement [23]. Although this correlation was developed using a wider range of data as compare to the first study, this regression computed negative COVs of IMEP within the range of data used in the correlation. This is mainly caused by the nature of a polynomial functional form, which has a combination of positive and negative signs in the equation.

In this work, the COV of gross IMEP is correlated using data taken from two engine families over nearly 2900 operating conditions using a product-power functional form. The cycle to cycle basis of gross IMEP were calculated by taking the integral of the in-cylinder pressure on a cycle to cycle basis per unit volume over the period from intake valve close (IVC) to exhaust valve open (EVO). The COV of gross IMEP was then

computed by taking the ratio of the standard deviation (SD) of gross IMEP to the mean value of gross IMEP, as shown in the following equations:

$$gross\ IMEP = \frac{\int_{IVC}^{EVO} p\ dV}{V_d} \qquad \text{(VII-1)}$$

$$COV\ of\ gross\ IMEP = \frac{S\ D\ of\ gross\ IMEP}{gross\ IMEP} 100\% \qquad \text{(VII-2)}$$

Where:

EVO   exhaust valve open (^{o}CA)

IVC   intake valve close (^{o}CA)

p   in-cylinder pressure trace (Pa)

V   in-cylinder volume (m^3)

V_d displacement volume (m^3)

Experimental Dataset

Two thousand test points from a multi-cylinder engine with a 2.4 liter displacement over a wide range of speeds and loads, a full sweep of cam timing, spark timing and various fuel blends were obtained from General Motors. This proprietary datasets cover engine speeds from 1200 rpm to 6600 rpm, a Net Indicated Mean Effective Pressures (NIMEP) range from 230 kPa to 1500 kPa, and equivalence ratios from 0.9 to 1.45 [76]. Additional datasets, with nearly 900 test points, were also collected using Michigan Tech's single-cylinder direct injection-spark ignition Hydra engine with a 0.5 liter displacement, variable compression ratio, and variable valve timing over a wide range of speeds and loads, and various ethanol blends [21]. This datasets covers five ethanol blends, compression ratios from 11:1 to 15.5:1, engine speeds from 1300-3400 rpm, NIMEPs from 200-900 kPa at stoichiometric mixture condition.

Physically Based Non-Dimensional Pi-Groups

A parametric non-dimensional set of burn duration correlations has been previously developed using a single cylinder Cooperative Fuel Research (CFR) engine over a wide range of compression ratios, EGR, spark timing, and ethanol-gasoline blends [74]. A similar study was also done on proprietary datasets using multiple engines over a wide range of engine speeds and loads, variable cam phaser position, multiple compression ratios, and ethanol-gasoline blends [73].

In those previous studies, six physically based parameters have been selected based on references [3, 10, 30, 31], including: engine bore (B), height of the combustion chamber (h), mean piston speed (S_p), laminar flame speed (S_L), specific internal energy ($Q^* = (m_f /m) Q_{LHV}$), and kinematic viscosity of the unburned mixture (v). These parameters were used to describe the engine parameters of: mass fraction burn, dilution, spark timing, equivalence ratio, engine speed, engine load, and valve timing [3, 11, 27, 28].

A non-dimensional analysis using Buckingham's Pi Theorem [33] was performed yielding non-dimensional groups expressed as:

$$\Delta\theta = f\left(\frac{\overline{S}_p}{S_L}, \quad \frac{S_L^{\ 2}}{Q^*}, \quad \frac{h}{B}, \quad \frac{h\,\overline{S}_p}{v}\right) \qquad \text{(VII-3)}$$

It was found that these non-dimensional Pi-groups correlate to the burn durations [73, 74].

Coefficient Correlation Analysis

A coefficient correlation matrix was usually used to observe the linear correlation between the variables. However, by taking the natural log of each variable, the coefficient correlation matrix could be used to observe a non-linear power correlation between the variables. A matrix of 2680-by-24 consists of 2680 experimental test points and twenty

four of variables including the COV of gross IMEP, standard deviation of gross IMEP, gross IMEP, Pi-groups, burn durations, and the COV of burn durations.

Figure VII-1 shows the natural log based correlation matrix. The dark red colors represent a strong positive log-based linear correlation, while the dark blue colors represent a strong negative log-based linear correlation. The white color represents no log-based linear correlation between the variables as seen in the Figure VII-1. Table VII-1 lists the correlation coefficient for COV and standard deviation of gross IMEP from the highest to the lowest correlation regardless of the sign of the correlation coefficient (+,-), which defines the direction of the correlation either positive or negative.

A strong negative non-linear correlations is observed between the COV of gross IMEP and $\dfrac{h\,\overline{S}_p}{v}$ and ϕ. A weak negative non-linear correlation is shown between the COV of gross IMEP and $\dfrac{\overline{S}_p}{S_L}$, as shown in Figure VII-1 and Table VII-1. A weak positive correlation is observed between the COV of gross IMEP and $\dfrac{S_L{}^2}{Q^*}$. A strong positive non-linear correlation is observed between COV of gross IMEP and $\dfrac{h}{B}$, $\dfrac{h_S}{B}$, the burn durations, and the COV of the burn durations. It is shown in Table VII-1 that $\dfrac{h}{B}$ has a stronger correlation to the COV of gross IMEP than $\dfrac{h_S}{B}$. This implies that the location of start of combustion has a stronger one-to-one correlation to the location of 50% MFB.

It is also observed from the Figure VII-1 that there is a strong positive correlation among the burn durations (B0010, B1025, B1050, B1075, and B1090). This strong dependency is also reflected in the COV of the burn durations, except for the COV of B0010, which has a weaker dependency to the burn duration. The correlation coefficient matrix between the burn durations and the COV of gross IMEP revealed a weaker correlation coefficient to B0010 and B1090 in comparison to the correlation coefficient to B1025, B1050, and

B1075. The B0010 in this paper was defined as a period between the location of 10% MFB and the spark timing, which is widely accepted as the location of 0% MFB.

Figure VII-1 and Table VII-1 also show the correlation coefficients between the standard deviation of gross IMEP to the Pi-groups, burn durations and the COV of burn durations. It is shown that the correlation coefficient between the standard deviation of gross IMEP to the variables were less than 0.5, which implies that there is no dominant variable, thus, it will not correlate well to the selected variables.
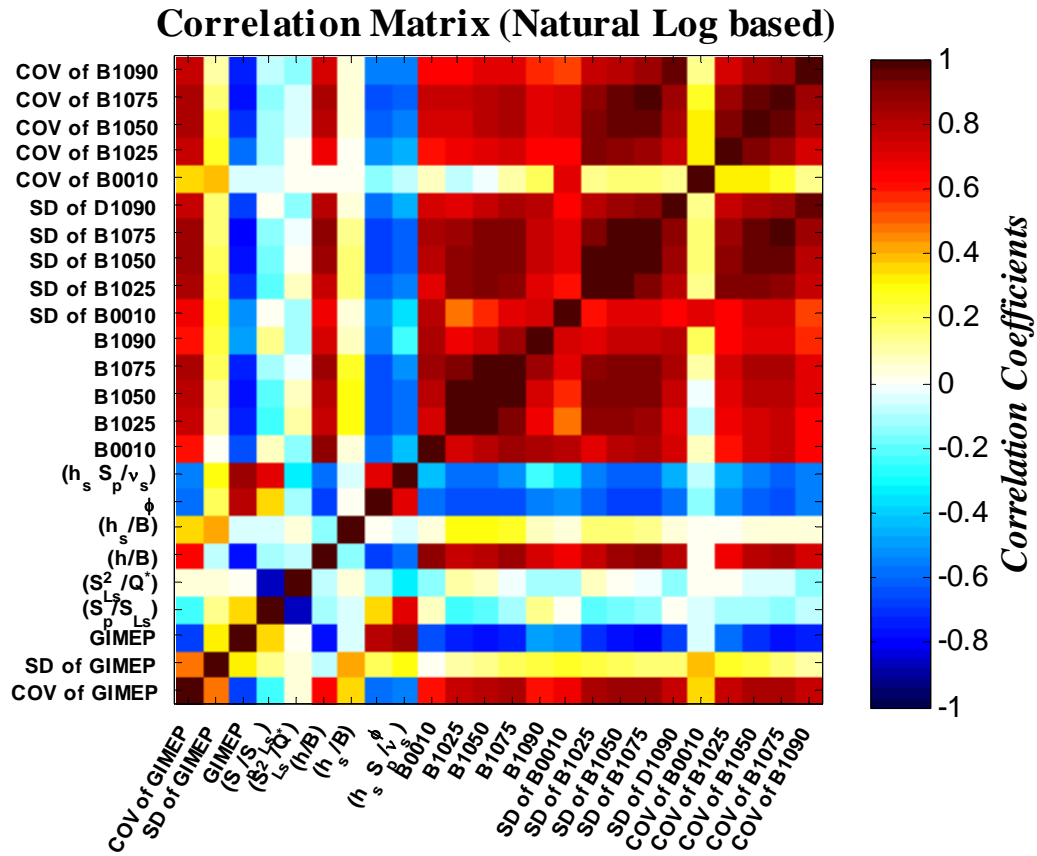
Figure VII-1 Correlation matrix of the correlation coefficient (R) between COV, standard deviation of gross IMEP, burn durations and the selected non-dimensional pi-groups (0 ≤ E ≤ 85; 11 ≤ CR ≤ 15.5; 1200 ≤ N ≤ 6600; 257 ≤ Net IMEP ≤ 1624; 0.98 ≤ ϕ ≤ 1.45)

Table VII-1 Correlation coefficient between COV and standard deviation of gross IMEP

Parameter	Correlation Coefficient to COV of GIMEP	Parameter	Correlation Coefficient to SD of GIMEP
COV of GIMEP	1.00	SD of GIMEP	1.00
SD of B1050	0.86	COV of GIMEP	0.50
SD of B1075	0.86	(h_s/B)	0.42
COV of B1075	0.84	COV of B0010	0.38
COV of B1050	0.83	GIMEP	0.32
SD of B1025	0.82	$(h_s\,S_p/\upsilon_s)$	0.30
B1075	0.81	COV of B1025	0.28
B1050	0.81	SD of B0010	0.26
B1025	0.77	COV of B1050	0.23
SD of B1090	0.75	SD of B1025	0.22
COV of B1025	0.75	B1090	0.22
COV of B1090	0.75	ϕ	0.20
SD of B0010	0.67	SD of B1050	0.20
GIMEP	-0.66	B1075	0.19
(h/B)	0.65	SD of B1075	0.17
B0010	0.62	COV of B1075	0.17
B1090	0.62	SD of B1090	0.16
ϕ	-0.57	B1050	0.15
$(h_s\,S_p/\upsilon_s)$	-0.56	(S_p/SL_s)	0.14
SD of GIMEP	0.50	B1025	0.13
(h_s/B)	0.37	COV of B1090	0.11
COV of B0010	0.35	(h/B)	-0.08
(S_p/SL_s)	-0.22	$(SL_s{}^2/Q^*)$	0.05
$(SL_s{}^2/Q^*)$	0.04	B0010	0.02

COV of Gross IMEP Correlation

A non-linear least squares method was used to correlate the cycle variation metric, COV of gross IMEP, to the burn durations. Figure VII-2(a) shows the COV of gross IMEP correlation as a function B1075. Figure VII-2(b) shows the same correlation of COV of gross IMEP as a function B1075 with an additional 235 test points in pink that were not used in the correlation because of an appearance of misfire and miss-pegging in the data. The marker symbol represents the fuel blends and the color code represents the gross IMEP in kPa. The correlation is given in the upper-left corner of the figure along with the information of the coefficient of correlation (R^2), the root mean square error (RMSE), the Akaike's information criterion (AIC) [80] and the number of experimental data points (sample) used in the correlation.

Figure VII-2(a) shows that the COV of gross IMEP increases as the B1075 increases; shown as a positive exponent (2.77) of B1075 in the equation given in Figure VII-2. Table VII-2 lists the variables and the exponent of the respective variables and the metrics to quantify the fitness of the correlation including R^2, RMSE, and AIC. The equation in Table VII-2 follows the product-power formulation as follows:

$$COV \ of \ gross \ IMEP = C \left(Variable \ 1\right)^{Exponent \ 1} \left(Variable \ 2\right)^{Exponent \ 2} ... \quad \text{(VII-4)}$$

COV of gross IMEP as a function of B1075 is expressed as:

$$COV \ of \ gross \ IMEP = 0.0006 \left(B1075\right)^{2.77} \quad \text{(VII-5)}$$

The strong correlation of B1075 to the COV of gross IMEP as observed before in the correlation matrix, shown in Figure VII-1, also reflects in the exponent of B1075. The RMSE of the fitted correlation is 0.79% from the COV of gross IMEP. The R^2, representing the fitness of the regression, is 0.70.

| (a) | (b) |
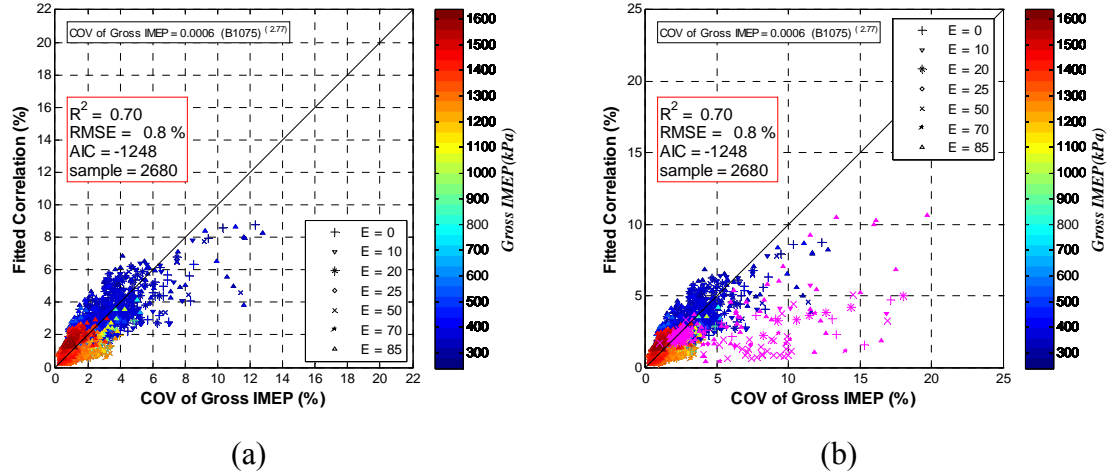
Figure VII-2 COV of gross IMEP correlation as a function of B1075 ($0 \le E \le 85$; $11 \le CR \le 15.5$; $1200 \le N \le 6600$; $257 \le Net\ IMEP \le 1624$; $0.98 \le \phi \le 1.45$)

Figure VII-3 shows the COV of gross IMEP correlation as a function of B0010. It is shown that the COV of gross IMEP correlation did not correlate well with the experimentally calculated COV of gross IMEP particularly at the low load cases, as also shown in Table VII-2 in the second column. The B0010 did not correlate to the COV of gross IMEP as well as the B1075.

The COV of gross IMEP also was correlated to burn durations (B0010, B1025, B1050, B1075, and B1090). There is no significant effect of B0010 and B1090 on the COV of gross IMEP in the presence of the B1025, B1050, and B1075 in the correlation as shown in Table VII-2 in the third column. A strong correlation of B1075 to the COV of gross IMEP is also observed as reflected in the exponent of B1075. Although the additional variables were added in the correlation, the fitness of the COV of gross IMEP correlation did not improve as much as it was expected. The RMSE is 0.78%, and the R^2 is 0.71.

Additional variables, including the standard deviation of burn durations, were also added into the correlation for COV of gross IMEP. The COV of gross IMEP correlation improves as shown in Figure VII-4 and in Table VII-3 in the first column. Figure VII-4 shows fitted correlation of COV of gross IMEP. The RMSE of the fitted correlation is 0.60% from the COV of gross IMEP, and the R^2 is 0.82. There is no significant effect of

standard deviation of B0010, standard deviation of B1025, standard deviation of B1050, and standard deviation of B1090 to the COV of gross IMEP correlation in the presence of the B1075 and standard deviation of B1075.

Figure VII-3 COV of gross IMEP correlation as a function of B0010 (0 ≤ E ≤ 85; 11 ≤ CR ≤ 15.5; 1200 ≤ N ≤ 6600; 257 ≤ Net IMEP ≤ 1624; 0.98 ≤ φ ≤ 1.45)

Figure VII-4 COV of gross IMEP correlation as a function of B1075 and SD of B1075 (0 ≤ E ≤ 85; 11 ≤ CR ≤ 15.5; 1200 ≤ N ≤ 6600; 257 ≤ Net IMEP ≤ 1624; 0.98 ≤ φ ≤ 1.45)

Table VII-2 COV of gross IMEP correlations (0 ≤ E ≤ 85; 11 ≤ CR ≤ 15.5; 1200 ≤ N ≤ 6600; 257 ≤ Net IMEP ≤ 1624; 0.98 ≤ φ ≤ 1.45; # of samples = 2680)

COV of gross IMEP = f(B1075)		COV of gross IMEP = f(B0010)		COV of gross IMEP = f(B1025, B1050, B1075)	
C = 0.0006		C = 0.03		C = 0.0006	
Variable:	Exponent	Variable:	Exponent	Variable:	Exponent
B1075	2.77	B0010	1.36	B0010	0
				B1025	0.40
				B1050	0.56
				B1075	2.04
				B1090	0
R^2	0.70	R^2	0.37	R^2	0.71
RMSE	0.79	RMSE	1.1	RMSE	0.78
AIC	-1248	AIC	695	AIC	-1359

The correlation of COV of gross IMEP solely as a function of standard deviation of B1075 is given in Figure VII-5. It is observed that the value of the COV of gross IMEP is nearly the same as the standard deviation of B1075, as shown in Table VII-3 in the second column, showing the interchangeable capability of the standard deviation of B1075 to quantify the cycle combustion variation.

The COV of gross IMEP was also fitted to the B1075 and Pi-groups, as shown in Figure VII-6. The B1075 dominated the fitted correlation of COV of gross IMEP as it was observed in Figure VII-2 and in Table VII-3 in the third column. The RMSE is 0.8% from the COV of gross IMEP, and the R^2 is 0.72.
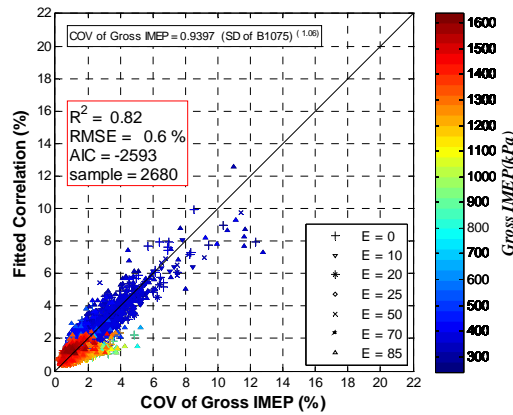
Figure VII-5 COV of gross IMEP correlation as a function of standard deviation of B1075 ($0 \leq E \leq 85$; $11 \leq CR \leq 15.5$; $1200 \leq N \leq 6600$; $257 \leq Net\ IMEP \leq 1624$; $0.98 \leq \phi \leq 1.45$)
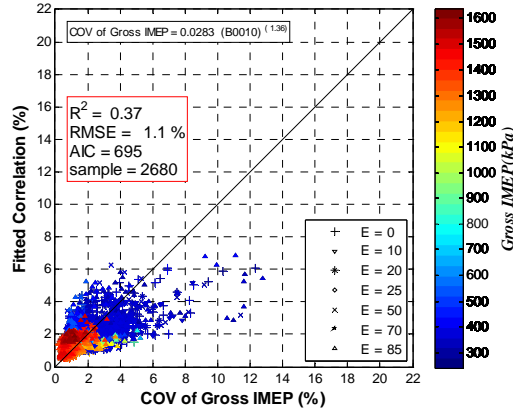
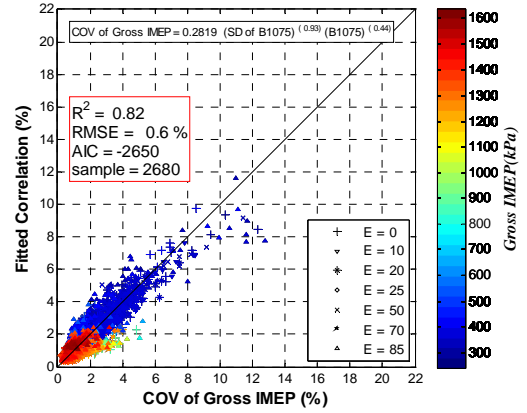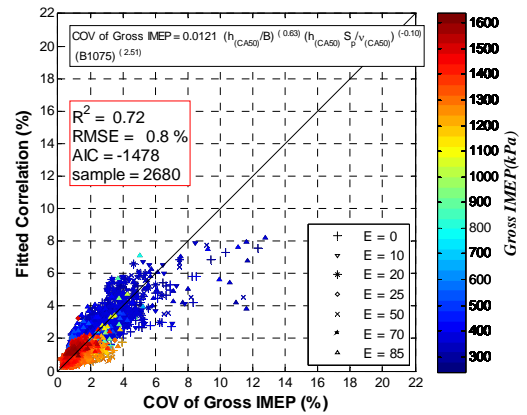*Figure VII-6 COV of gross IMEP correlation as a function of B1075 and Pi-groups ($0 \leq E \leq 85$; $11 \leq CR \leq 15.5$; $1200 \leq N \leq 6600$; $257 \leq Net\ IMEP \leq 1624$; $0.98 \leq \phi \leq 1.45$)*

Correlation of the standard deviation of B1075 as a function of Pi-groups is shown in Figure VII-7 and Table VII-4 in the first column. The RMSE of the standard deviation of the B1075 fitted correlation is 0.5 ^{o}CA, and the R^2 is 0.84. The correlation error increases as the standard deviation of B1075 increases. Figure VII-8 and Table VII-4 in the second column show the B1075 correlation as a function of the physically based non-dimensional Pi-groups. The RMSE is 1.4 ^{o}CA, and the R^2 is 0.89.

171
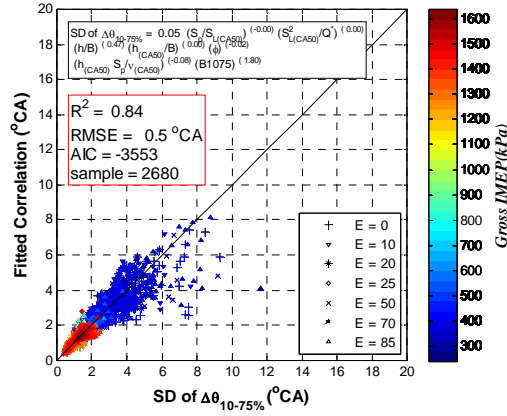
Figure VII-7 Standard deviation of B1075 correlation as a function of Pi-groups (0 ≤ E ≤ 85; 11 ≤ CR ≤ 15.5; 1200 ≤ N ≤ 6600; 257 ≤ Net IMEP ≤ 1624; 0.98 ≤ φ ≤ 1.45)
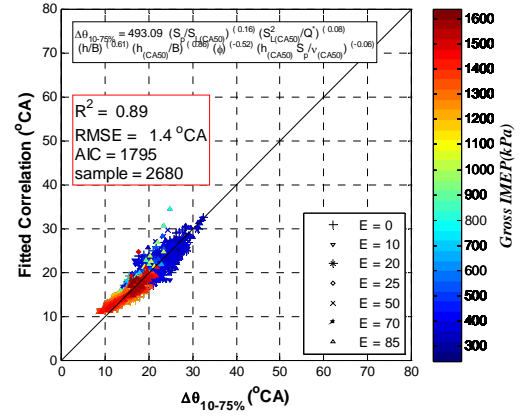
Figure VII-8 B1075 correlation as a function of Pi-groups (0 ≤ E ≤ 85; 11 ≤ CR ≤ 15.5; 1200 ≤ N ≤ 6600; 257 ≤ Net IMEP ≤ 1624; 0.98 ≤ φ ≤ 1.45)

Table VII-3 COV of gross IMEP correlations (0 ≤ E ≤ 85; 11 ≤ CR ≤ 15.5; 1200 ≤ N ≤ 6600; 257 ≤ Net IMEP ≤ 1624; 0.98 ≤ φ ≤ 1.45; # of samples = 2680)

COV of gross IMEP = f(B1075, SD of B1075)		COV of gross IMEP = f(SD of B1075)		COV of gross IMEP = f(Pi-groups, B1075)	
C = 0.28		C = 0.94		C = 0.012	
Variable:	Exponent	Variable:	Exponent	Variable:	Exponent
B1075	0.44	SD of B1075	1.06	(S_p/SL_s)	0
SD of B0010	0			(SL_s^2/Q^*)	0
SD of B1025	0			(h/B)	0
SD of B1050	0			(h_s/B)	0.63
SD of B1075	0.93			ϕ	0
SD of B1090	0			$(h_s\,S_p/\upsilon_s)$	-0.1
				B1075	2.51
R^2	0.82	R^2	0.82	R^2	0.72
RMSE	0.6	RMSE	0.6	RMSE	0.8
AIC	-2650	AIC	-2593	AIC	-1478

Standard deviation of B1075 = f(Pi-groups, B1075)		B1075 = f(Pi-groups)	
C = 0.05		C = 493.09	
Variable:	Exponent	Variable:	Exponent
(S_p/SL_s)	0	(S_p/SL_s)	0.16
(SL_s^2/Q^*)	0	(SL_s^2/Q^*)	0.08
(h/B)	0.47	(h/B)	0.61
(h_s/B)	0	(h_s/B)	0.86
ϕ	-0.02	ϕ	-0.52
$(h_s S_p/\upsilon_s)$	-0.08	$(h_s S_p/\upsilon_s)$	-0.06
B1075	1.80		
R^2	0.84	R^2	0.89
RMSE	0.5	RMSE	1.4
AIC	-3553	AIC	1795

Combustion Phasing and Cycle Variation Exercise

To study the effect of engine geometry and operating conditions on the combustion process, a thermodynamic-based engine model was developed based on ideal gas and thermodynamic laws. Figure VII-9 shows the diagram of the thermodynamic engine model. There are two sub-routines in this thermodynamics engine model. The first sub-routine applied a residual fraction correlation as a function of overlap factor, engine speed, intake pressure, exhaust pressure, compression ratio, and equivalence ratio. This residual fraction correlation has been validated to the GT-Power residual fraction calculation at operating condition of 1300 rpm and 330 kPa [73]. Assumption of zero residual fraction was chosen to start the calculation of temperature and pressure at the intake valve close (IVC), which were used to compute the residual fraction for the next iteration using the residual fraction correlation. The calculation converged when the residual fraction at iteration *"i+1"* was less than 0.5% compared to the residual fraction

at iteration "*i*". This procedure was used to determine the intake pressure (map pressure) and intake temperature to determine the motored pressure and temperature trace.

The second sub-routine applied the burn duration correlations as a function of the physically based non-dimensional Pi-groups. A set of Wiebe function parameters (m and B1090) were given for the first iteration. Once the pressure trace was reconstructed using the single-zone pressure model, the physically based Pi-groups were computed, then the burn durations as a function of Pi-groups. The Wiebe parameters for the next iteration were then computed using the calculated burn durations. The calculation converged when the Wiebe parameter "*m*" and B1090 at iteration "*i+1*" compared to the "*m*" and B1090 at iteration "*i*" were less than 0.1 and 0.5 ^{o}CA, respectively. The COV of gross IMEP correlation was also included in this routine. This routine was used to determine the firing pressure trace, the combustion profile, and the COV of gross IMEP.
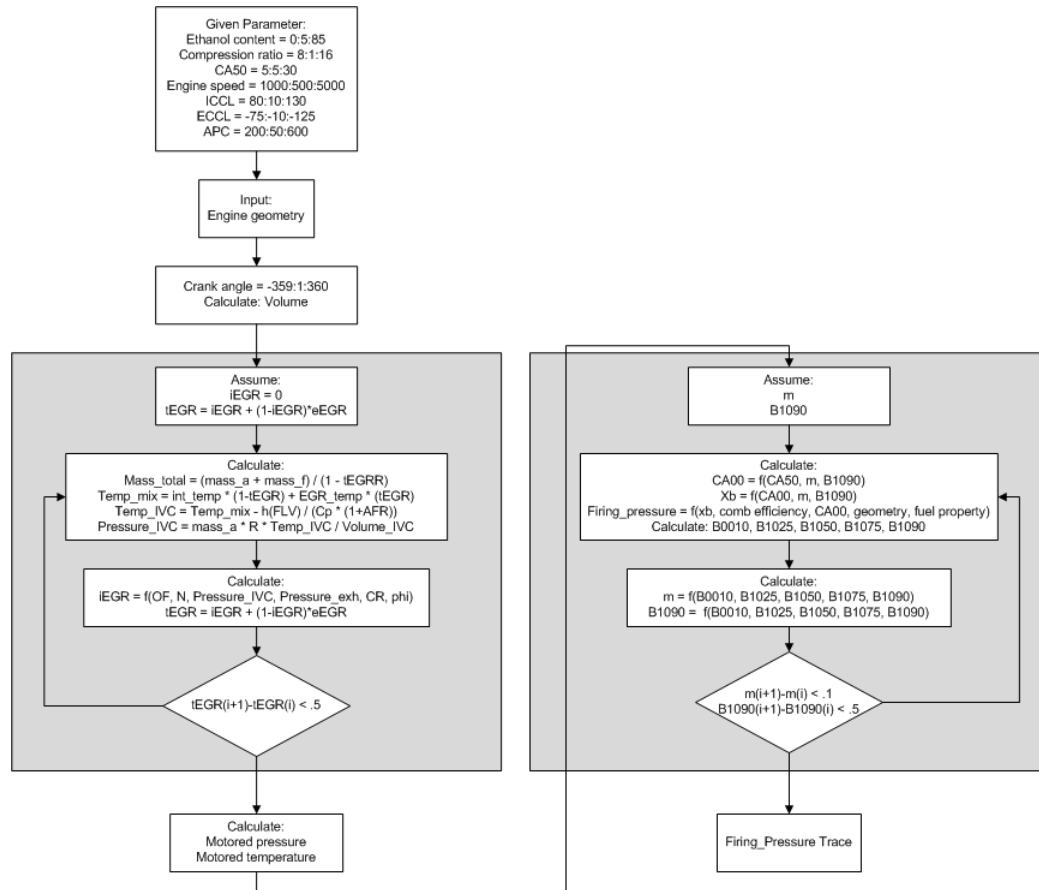

*Figure VII-9 Thermodynamic engine model routines in Matlab*

The estimated response surfaces resulting from the modeling exercise were generated over the range of ethanol concentrations from 0-85, compression ratios, a full sweep of cam timing, engine speed, and load sweeps. Figure VII-10 shows the burn duration modeling results using the thermodynamic engine model as a function of engine speed and air per cylinder (APC), which represents the engine load. At the stoichiometric fuel-air mixture condition, fixed compression ratio (CR) = 12:1, location of 50% MFB (CA50) = 10°CA after top dead center (ATDC), intake cam center line (ICCL) = 100°CA gas exchange (GE)-ATDC, exhaust cam center line (ECCL) = 95°CA GE-before top dead center (BTDC) using gasoline (E = 0), an increase in engine speed, resulting an increase in the burn durations for both B0010 and B1075. A similar trend was noted in the references [10, 27, 28, 31]. Figure VII-10 shows that the burn durations decrease as the load increases, as also found in the reference [23].

Figure VII-11 shows the modeling results of COV of gross IMEP. The COV of gross IMEP slightly increases as the engine speed increase, as found in reference [23], which showed that the COV of IMEP increased from 0.8% to 1.1% as the engine speed increased from 1000-3000 RPM at constant engine load of 400 kPa IMEP. The COV of gross IMEP increases as the engine load decreases, as found in the reference [23], which showed the COV of IMEP increased from 1-1.5% when IMEP decreased from 800 kPa to 250 kPa, and increased 5% when IMEP decreased to 200 kPa at a constant engine speed of 1500 RPM. The effect of the engine load on the COV of gross IMEP is greater than the engine speed.

Figure VII-12 shows the data range matrix as a function of engine speed and load that is used in the correlations, including COV of gross IMEP and burn duration correlations. The color code represents the number of test points in the respective operating conditions, which is also printed in the Figure VII-12. It is shown that the data covers a wide range of engine load at 1000 and 2000 RPM, but not in the rest of the modeling exercise range.
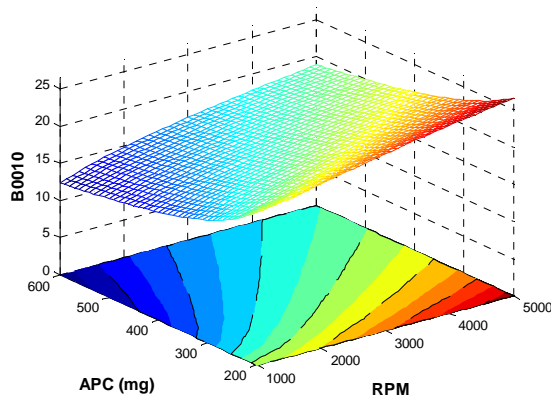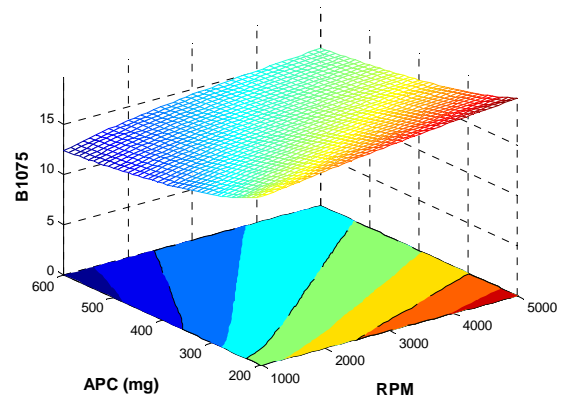
(a)   (b)

Figure VII-10 Burn duration modeling results as a function of engine speed and load (E=0; CR=12; CA50=10°CA-ATDC; ICCL=100°CA-GE-ATDC; ECCL=95°CA-GE-BTDC)
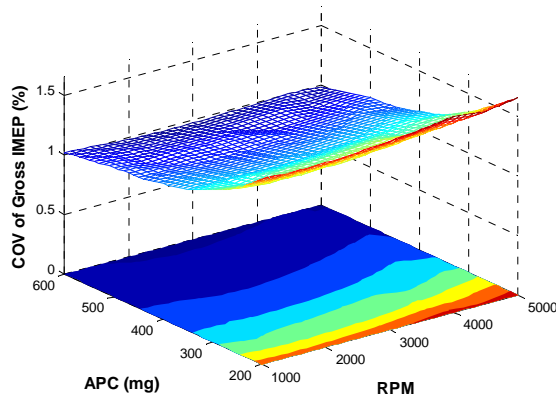
Figure VII-11 COV of gross IMEP modeling result as a function of engine speed and load (E=0; CR=12; CA50=10°CA-ATDC; ICCL=100°CA-GE-ATDC; ECCL=95°CA-GE-BTDC)
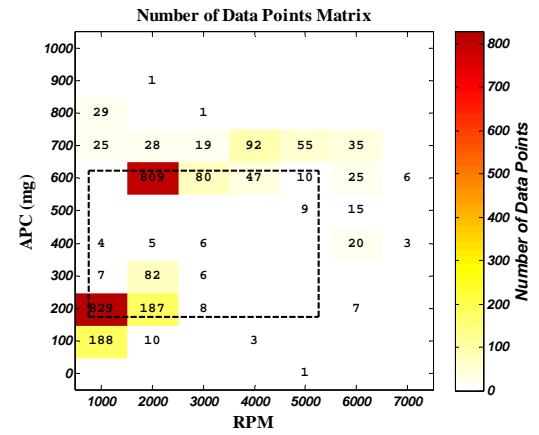
Figure VII-12 Data range matrix used in the correlation (0 ≤ E ≤ 85; 11 ≤ CR ≤ 15.5; 1200 ≤ N ≤ 6600; 257 ≤ Net IMEP ≤ 1624; 0.98 ≤ ϕ ≤ 1.45)

Figure VII-13 shows the modeling results of burn duration as a function of ethanol content and total residual fraction trapped in the cylinder at stoichiometric fuel-air mixture conditions, CR = 12:1, CA50 = 10°CA ATDC, engine speed = 2000 RPM, APC = 300 mg, which corresponds to 790 – 870 kPa of gross IMEP. The residual fraction sweep was generated by sweeping the ICCL and ECCL.

It is observed from Figure VII-13 that as the total residual fraction increases, the burn durations of both B0010 and B1075 increase, which is as expected and was also found in the references [10, 27]. As the ethanol content decreases the burn durations increase, as also found in the references [10, 28, 31, 38, 46, 74].

Figure VII-14 shows the COV of gross IMEP correlation. It is shown that the COV of gross IMEP calculated using the COV of gross IMEP correlation decreases as the ethanol content increases. It is also shown that the COV of gross IMEP increases as the residual fraction increases. A similar trend was found in the reference [23], in which the COV of IMEP increased from 1-7% as the EGR increased from 0-25% at an engine speed of 1500 RPM and load of 400 kPa IMEP.

The data range matrix as a function of ethanol blend and total dilution is shown in Figure VII-15. It is shown a well spread data of ethanol blends and ICCL and ECCL sweeps.

(a)   (b)
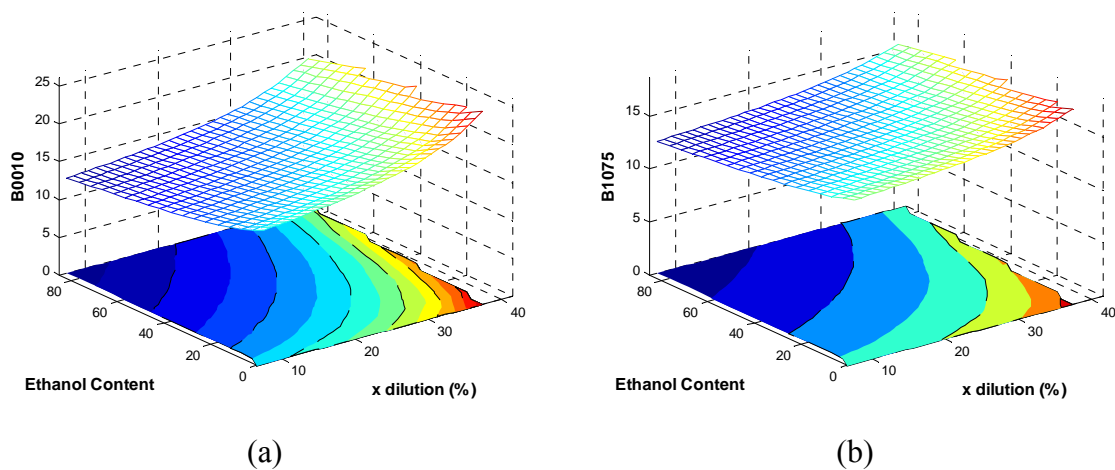
Figure VII-13 Burn duration modeling result as a function of ethanol content and total residual fraction (CR=12; CA50=10°CA-ATDC; APC =300 mg, 2000 RPM)
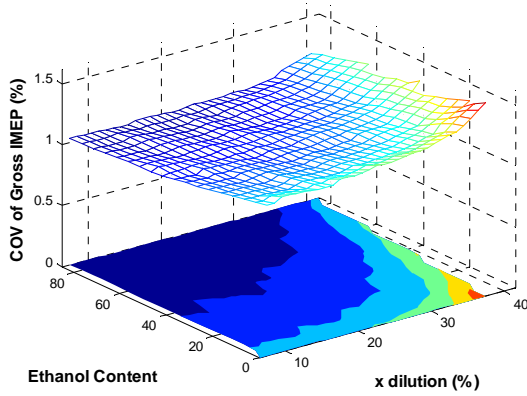
Figure VII-14 COV of gross IMEP modeling result as a function of ethanol content and total residual fraction (CR=12; CA50=10°CA-ATDC; APC =300 mg, 2000 RPM)
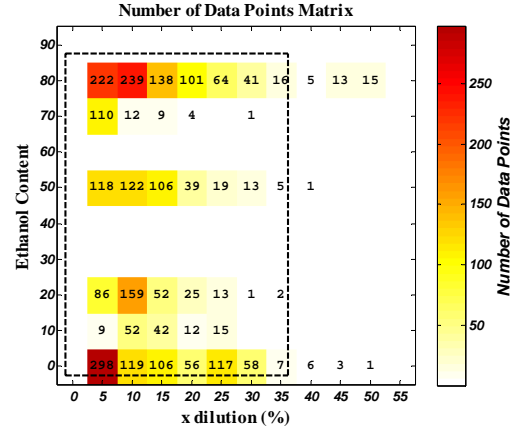
Figure VII-15 Data range matrix used in the correlation (0 ≤ E ≤ 85; 11 ≤ CR ≤ 15.5; 1200 ≤ N ≤ 6600; 257 ≤ Net IMEP ≤ 1624; 0.98 ≤ φ ≤ 1.45)

Figure VII-16 shows the modeling result of the burn duration as a function of compression ratio and location of 50% MFB at a stoichiometric fuel-air mixture condition, engine speed = 2000 RPM, APC = 300 mg, ICCL = 100°CA GE-ATDC, ECCL = 95°CA GE-BTDC using gasoline (E = 0). It is shown that the burn durations of 0-10% MFB and 10-75% MFB increase as the compression ratio decreases [28, 31, 74]. The burn durations of 0-10% and 10-75% MFB also increase as the CA50 increases.

Figure VII-17 shows the COV of gross IMEP as a function of compression ratio and CA50. The COV of gross IMEP increases as the CA50 increases. A similar trend was found from the CFR experimental data as the COV of gross IMEP increases from 0.5-1.5% when the CA50 increases from 5-25 °CA-ATDC at 300 kPa Net IMEP, 900 RPM, using E85, compression ratio 8:1, and zero EGR. Figure VII-17 also shows that the COV of gross IMEP increases as the compression ratio decreases. Although there is no significant effect of compression ratio on the COV of gross IMEP shown in the CFR experimental data, however, the Hydra experimental data shows that the COV of gross IMEP increases from 2-8% as the compression ratio decreases from 15.5:1 to 8:1 using E85, at CA50 = 5 °CA, 1300 RPM, and 330 kPa.

178

Figure VII-18 shows the data range matrix as a function of compression ratio and CA50 that are used in the correlations. A small number of high compression ratio (CR > 13) data points were found used in the correlation.

(a)   (b)

Figure VII-16 Burn duration modeling result as a function of compression ratio and location of 50% MFB (E=0; ICCL=100°CA-GE-ATDC; ECCL=95°CA-GE-BTDC; APC =300 mg, 2000 RPM)

Figure VII-17 COV of gross IMEP modeling result as a function of compression ratio and location of 50% MFB (E=0; ICCL=100°CA-GE-ATDC; ECCL=95°CA-GE-BTDC; APC =300 mg, 2000 RPM)

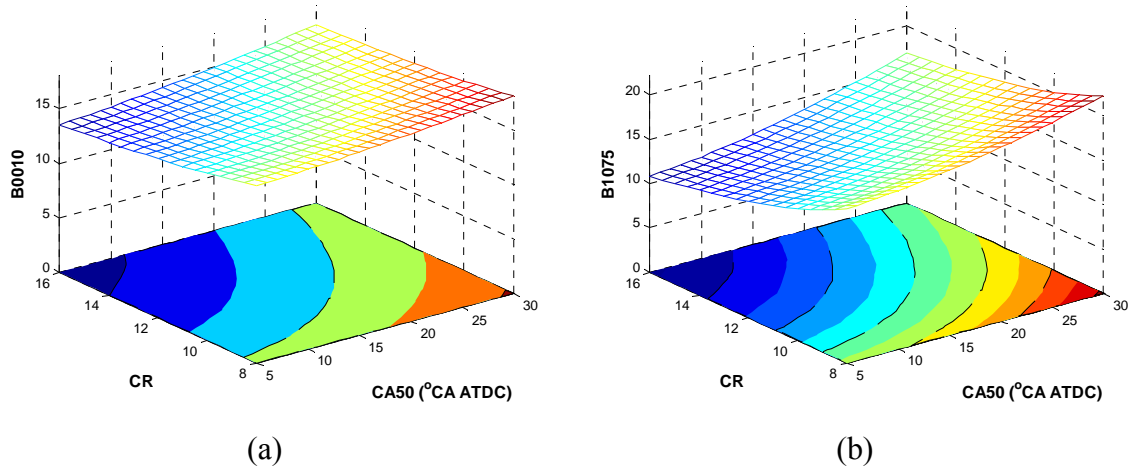*Figure VII-18 Data range matrix used in the correlation (0 ≤ E ≤ 85; 11 ≤ CR ≤ 15.5; 1200 ≤ N ≤ 6600; 257 ≤ Net IMEP ≤ 1624; 0.98 ≤ φ ≤ 1.45)*
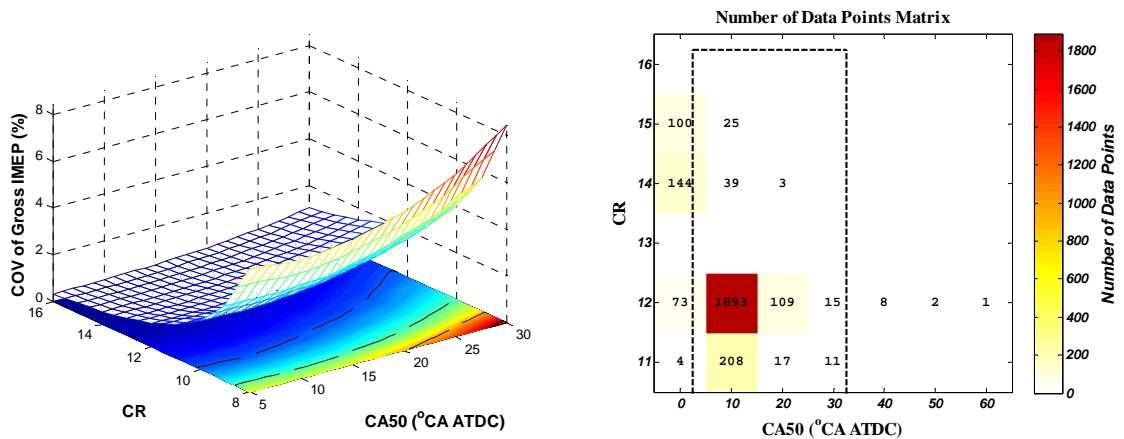
Summary and Conclusions

As compared to the gross IMEP, the standard deviation of gross IMEP has a weaker effect on the COV of gross IMEP. It was shown in Table VII-1 that the correlation coefficient between the COV of gross IMEP and gross IMEP is -0.66, while the correlation coefficient between the COV of gross IMEP and SD of gross IMEP is 0.50. In the high gross IMEP cases, the COV of gross IMEP was still considerably low even though the standard deviation of gross IMEP was considerably high.

The COV of gross IMEP was correlated to the burn durations, standard deviation of burn durations and the physically based Pi-groups using a product-power form. Six correlations of COV of gross IMEP was presented above in Table VII-2 and Table VII-3. B1075 showed a strong correlation to the COV of gross IMEP, either as the only variable in the correlation or in the presence of other variables, including burn duration, standard deviation of burn duration, and physically based non-dimensional Pi-groups. It was also found that the COV of gross IMEP is highly correlated to the standard deviation of burn duration, particularly B1075, which represents the fast burning period in the cylinder.

A thermodynamic-based engine model was developed, enabling reconstruction of the combustion phasing and cycle variation as functions of engine geometry and operating conditions using the residual fraction, burn durations, and COV of gross IMEP correlations. This model used the residual fraction, burn durations (B0010, B1025, B1050, B1075, and B1090), and the COV of gross IMEP correlations. The modeling exercise results showed the trend of the COV of gross IMEP decreased as the engine load increased, the engine speed slightly decreased, the ethanol content increased, the residual fraction decreased, the CA50 near MBT location, and the compression ratio increased.

VIII. SUMMARY

VIII.1 CONCLUSIONS

A composite fuel concept has been introduced and used to compute the properties of burned and unburned mixture of fuel-air and residual trapped in the combustion chamber. Equation II-3 showed the molar based balance in the composite fuel concepts which applicable for mixture of hydrocarbon, alcohol, and oxygenated hydrocarbon fuels. Although the Equation II-3 showed a mixture of two types of fuel, however the same concept could also applied to mixture with more than two types of fuel. This characteristic made the composite fuel concept robust in calculating the fuel blends properties including the air fuel ratio, molecular weight, specific heat, viscosity, and lower heating value [Chapter II].

Methods to analyze the mean value and cycle to cycle combustion metrics from experimentally measured pressure traces, including single-zone mass fraction burn (MFB) and two-zone MFB calculations have been developed and compared to the apparent heat release analysis. The single-zone MFB calculation was solving the first law of thermodynamic in Equation III-21 which included the heat transfer and crevice volume effects, and the ideal gas law in Equation III-11 simultaneously. The two-zone MFB calculation which assumed there was a thin boundary separating the burned and unburned mixture was solving the Equations III-22, III-23, III-24, III-25, and III-26 simultaneously. For the purpose of combustion phasing analysis, the single-zone MFB calculation with two unknowns (temperature and MFB) is found robust in the data analysis compare to the two-zone MFB calculation with five unknowns (burned and unburned temperature, burned and unburned volume and MFB). However for detailed combustion efficiency and in-cylinder temperature profile, the two-zone MFB calculation including the specific heat as a function of temperature, and the inclusion of heat transfer and crevice effects should be used because in the two-zone MFB model, the thermodynamic properties of the burned and unburned mixture was more accurately quantified [Chapter III].

Six parameters has been selected based on the literature study including: engine bore (B), height of the combustion chamber (h), mean piston speed (S_p), laminar flame speed (S_L), specific internal energy ($Q^* = (m_f /m) Q_{LHV}$), and kinematic viscosity of the unburned mixture (v). These parameters represented the engine dependent (B and h), the flow dependent (S_p and S_L), and the fuel dependent (Q^* and v). These parameters also described the engine parameters: mass fraction burn, residual fraction, spark timing, equivalence ratio, engine speed, load, and valve timing. A Buckingham's Pi theorem was performed using these physically based parameters. A non-linear least squares method to correlate the combustion phasing metrics (B0010, B1025, B1050, B1075, and B1090) to the non-dimensional Pi-groups in a product-power form has been developed. It was found that the burn duration correlations were in a good agreement with the burn durations computed from experimental data. These correlations were then used to study the effect of engine geometry and operating conditions to the burn durations [Chapter IV].

Methods to fit the combustion metrics (B0010, B1025, B1050, B1075, B1090) to the Wiebe function including single-Wiebe and double-Wiebe functions using analytical solution, least square method and combination of both methods have been developed. Section V.1 discussed several analytical solutions and a least square method to compute the single-Wiebe function parameters (m and $\Delta\theta$). It was found that the efficiency parameter of Wiebe function (a) is not an independent parameter but directly related to the combustion duration ($\Delta\theta$).

Section V.2 focused on determining the double-Wiebe function parameters using a least square method. A routine in Matlab was wrote and used to found the double-Wiebe parameters (m_1, m_2, p, $\Delta\theta_1$, and $\Delta\theta_2$) given a random value of double-Wiebe parameters to start the calculation as shown in the flow chart in Figure V-7. The double-Wiebe function matched better to the experimental MFB profile particularly for the non-symmetrical MFB profile which usually found in knocking cases for SI engines. A single-zone pressure model was also developed to reconstruct the pressure trace given the MFB profile information, thus the validation in pressure trace level could be performed in addition to the validation in the MFB level. The single-zone pressure model was derived

from the ideal gas and energy balance equation as shown in Equation V-15. Once the pressure trace reconstructed from the estimated Wiebe function, it was then compared with the experimentally measured pressure trace using metrics including the RMSE, the difference in Net IMEP, and the maximum difference in pressure trace. The double-Wiebe function fits better to the experimental MFB profile thus its reconstructed pressure trace matches better to the experimentally measured pressure trace in comparison to the single-Wiebe function.

Section V.3 discussed a step-by-step analytical solution in computing the double-Wiebe function parameters. By grouping CA10 and CA25 to compute the first Wiebe function parameters, and CA75 and CA90 to compute the second Wiebe function parameters, a good estimation of the mixture parameter (p) could be computed analytically using Equation V-24. Once the "p" was found, the double-Wiebe function can be simplified and solve as a two separated single-Wiebe function. The double-Wiebe function fitted the experimental data better than the single-Wiebe function [Chapter V].

Parametric correlation of coefficient of variance (COV) of gross indicated mean effective pressure (IMEP) has been developed using multiple engines with a wide range operating conditions. Similar method to correlate the burn duration in Chapter IV was used to correlate the cycle combustion variation to the burn durations and non-dimensional Pi-groups. It is found that the COV of gross IMEP was highly correlated to the B1075. A thermodynamic engine model has been developed to study the sensitivity of independent variables in the correlations, including burn durations and cycle combustion variation correlations. This thermodynamic engine model employed a residual fraction correlation as a function of overlap factor, engine speed, map and exhaust pressure, compression ratio, and equivalence ratio, burn duration and COV of gross IMEP correlations as a function of physically based non-dimensional groups. Figure VII-9 showed the calculation chart in the thermodynamic engine model which has two sub-routines including loop to compute the map pressure thus enable to compute the motored pressure trace, and loop to compute the MFB profile thus enable to reconstruct the firing pressure trace [Chapter VII].

Two types of parametric combustion models have been developed and integrated to GT-Power, an engine simulation tool by Gamma Technology. A single-Wiebe parametric combustion model used the single-Wiebe function which has two parameters ("m", "$\Delta\theta_{10\text{-}90\%}$"). A double-Wiebe parametric combustion model used not only single-Wiebe function but also double-Wiebe function which has five parameters ("p", "m_1", "m_2", "$\Delta\theta_{10\text{-}90\%\ (1)}$", "$\Delta\theta_{10\text{-}90\%\ (2)}$"). The single-Wiebe function was used in the double-Wiebe parametric combustion model to adjust the anchor of each Wiebe function ("$CA50_1$", "$CA50_2$") with respect to the anchor of MFB profile ("$CA50$").

A user compound was developed in GT-Power to contain the parametric combustion model. The user compound was chosen because of its flexibility in GT-Power interface, including sharing the compound with other GT-Power users and further modifications in the compound. An RLT-dependence was used to connect the predictive combustion compound with the multi-Wiebe combustion template in the main engine model. The RLT-dependence was chosen because there were no signal ports available in the multi-Wiebe combustion template at the time this parametric combustion compound being built. Even though this parametric combustion compound was built in GT-Suite V6 built-12, this parametric combustion compound was ready for the GT-Suite V7 which has open ports in the multi-Wiebe combustion template, thus enables the direct connection in and out the multi-Wiebe template [Chapter VI].

Table VIII-1 compares the single-Wiebe and the double-Wiebe parametric combustion model. Single-Wiebe parametric combustion model employed the burn duration correlations and the least square method to compute the single-Wiebe function parameters. This single-Wiebe model is robust, particularly for case which has a symmetrical burn rate profile. This single-Wiebe model also includes the B0002 correlation as a function of B0010 which enables user to anchor the Wiebe function at any location in the MFB profile including the spark timing location.

Double-Wiebe parametric combustion model application was for case which has a non-symmetrical burn rate. This double-Wiebe model employed the burn duration correlations and the analytical solution to compute the double-Wiebe function

parameters. The analytical solution was used instead of the least squares method because of the limitation of GT-Power computational capability. The analytical solution required a maximum value of weighting factor, "p", less than one, and a CA50 adjustment to synchronize the anchor location for each Wiebe function. Because of the complexity of the double-Wiebe parameters calculation, this double-Wiebe parametric combustion model could only be anchored at CA50.

Table VIII-1 Comparison between the single-Wiebe and double-Wiebe predictive combustion model

Single-Wiebe Predictive Combustion Model	Double-Wiebe Predictive Combustion Model
2 unknown parameters	5 unknown parameters
Represent the symmetrical burn rate	Represent the non-symmetrical burn rate
Parameter Estimation: Least Squares Method $$\hat{m}_{LS} = \frac{n\sum_{i=1}^{n}(\ln(\theta - \theta_o))(\ln(-\ln(1-x_b))) - \sum_{i=1}^{n}(\ln(\theta - \theta_o))\sum_{i=1}^{n}(\ln(-\ln(1-x_b)))}{n\sum_{i=1}^{n}(\ln(\theta - \theta_o))^2 - \left(\sum_{i=1}^{n}(\ln(\theta - \theta_o))\right)^2} - 1$$	Parameter Estimation: Analytical Solution $$\hat{m}_{AS} = \frac{\ln\left(\frac{\ln(1-x_{b1})}{\ln(1-x_{b2})}\right)}{\ln\left(\frac{\theta_1 - \theta_o}{\theta_2 - \theta_o}\right)} - 1$$ Problem occurs: $\theta_1 - \theta_o \cong \theta_2 - \theta_o$
	Estimation of the second Wiebe parameters: $$x_b^* = \frac{x_b - \hat{p}\left(1 - \exp\left[-\left(\frac{\theta - \theta_o}{\alpha_1}\right)^{m_1+1}\right]\right)}{(1-\hat{p})}$$ Problem occurs: $\hat{p} \cong 1$
	Need CA50 adjustment: $$x_b\big|_{CA50} = p\left(1 - \exp\left[-\left(\frac{CA50 - \theta_o}{\alpha_1}\right)^{\beta_1}\right]\right) + (1-p)\left(1 - \exp\left[-\left(\frac{CA50 - \theta_o}{\alpha_2}\right)^{\beta_2}\right]\right)$$ $\theta_{50}\big|_{xb@CA50} = \theta_o + \alpha\left(\ln(1 - xb@CA50)\right)^{1/m+1}$ $\Delta CA50 = CA50 - \theta_{50}\big|_{xb@CA50}$
Anchor at SA, CAXX (XX > 01)	Anchor at CA50

185

VIII.2 RECOMMENDATIONS

To improve the double-Wiebe parametric combustion model, the least square method could be used to compute the double-Wiebe parameters but its required additional software, Simulink, for the combustion model calculation, thus required the GT-Power and Simulink coupling.

Since the thermodynamic engine model was employed empirical correlations, it could be used not only to study the sensitivity of engine geometry and operating conditions to the engine performance, but also to generate extended engine database that could be used in the vehicle simulation and or in the virtual engine testing. Additionally, including the duration from spark timing to 2% or 10% of MFB (BSA01 or BSA10) correlations allowed the thermodynamic engine model to estimate the location of spark timing for given engine geometry and operating conditions.

IX. APPENDICES

IX.1 ENGINE SPECIFICATIONS

Table IX-1 shows the four engines specifications that have been used in this research.

Table IX-1 Engine specifications

Engine Production Name	GM-LAF	MTU-Hydra	MTU-CFR	GM-LNF
Number of Cylinder	4	1	1	4
Compression Ratio	11.9	11-18.5	4.5 – 17.5	9.3
Bore (mm)	88	86	82.6	86
Stroke (mm)	98	94.6	114.3	86
Connecting Rod Length (mm)	143.8	152.5	254	145.5
Wrist Pin Offset (mm)	0.8	0	0	0.8
Displacement Volume (cm^3)	596	550	612	500
Turbo Charged	No	No	No	Yes
Dual Independence Cam Phaser	Yes	Yes	No	Yes

IX.2 ENGINE DATABASES

Table IX-2 shows the range of engine operating conditions from the four engines that have been used in this research.

Table IX-2 Engine databases

Engine Production Name	GM-LAF	MTU-Hydra	MTU-CFR	GM-LNF
Compression Ratio	11.9	11, 12.5, 14, 15.5, 17, 18.5	8, 10, 12, 14, 16	9.3
Ethanol Blend (%)	0, 25, 50, 75, 85	0, 10, 20, 50, 85	0, 20, 40, 60, 84	0
External EGR (%)	NA	NA	0, 10, 15, 20, 25, 30	NA
Internal EGR (%)	Full Phaser Sweep	Full Phaser Sweep	NA	NA
Engine Speed (rpm)	1200-6600	1300-3400	900	1200, 2000, 4000
Spark Advance (^{o}CA)	MBT and Full Timing Sweep	MBT and Full Timing Sweep	Full Timing Sweep	MBT and Full Timing Sweep
Number of Dataset	2020	895	724	71

IX.3 BURN DURATION CORRELATIONS

Burn duration correlations were expressed as follow:

$$\Delta\theta = x0\left(\frac{\overline{S}_p}{S_L}\right)^{x1}\left(\frac{S_L^{\ 2}}{Q^*}\right)^{x2}\left(\frac{h}{B}\right)^{x3}\left(\frac{h_{@CA00}}{B}\right)^{x4}\left(\phi\right)^{x5}\left(\frac{h\,\overline{S}_p}{\nu}\right)^{x6} \qquad \text{(IX-1)}$$

Table IX-3 shows the constants for B0010 correlations and the metrics to quantify the fit.

Table IX-3 B0010 correlations

	GM-LAF	MTU-Hydra	MTU-CFR	GM-LNF	GM-LAF MTU-Hydra MTU-CFR GM-LNF	GM-LAF MTU-Hydra GM-LNF
x0	1023.56	231.62	1.3	1752.03	42.97	512.82
x1	0.18	0.02	-3.23	0.11	0.33	0.23
x2	0.09	-0.06	-1.74	-0.05	0.14	0.09
x3	1.1	1.07	0.9	0.83	1.04	1.03
x4	0.7	0.58	0.12	0.55	-0.76	0.53
x5	-0.41	0	0	0	-0.11	-0.39
x6	-0.05	0.11	0.76	-0.19	-0.1	-0.04
R^2	0.95	0.78	0.95	0.99	0.82	0.89
RMSE	1.61	2.77	0.9	0.92	3.26	2.29
AIC	1819.14	1397.21	-110.91	0.69	7477.84	4280.04
#sample	1901	681	574	71	3156	2582

Figure IX-1 shows the B0010 correlations.

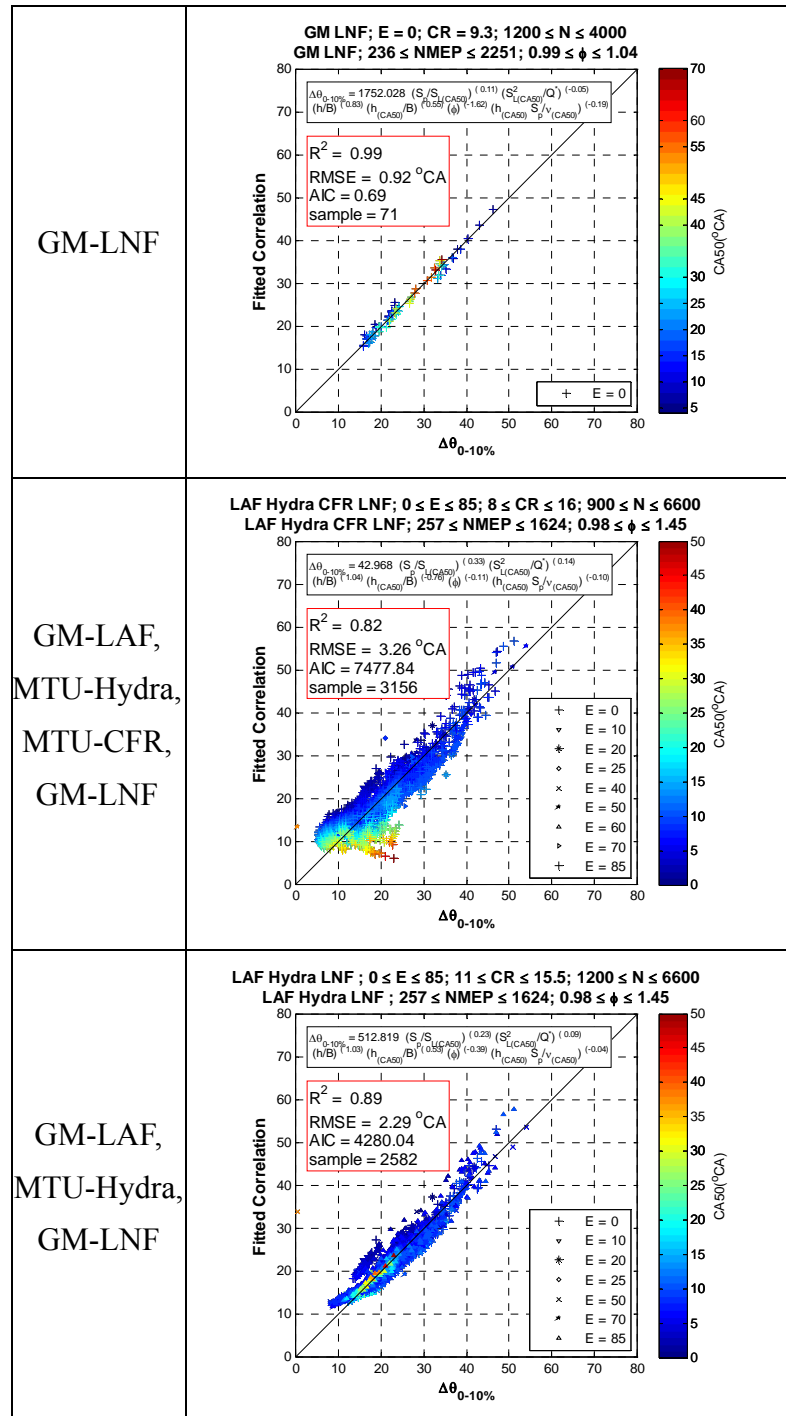|	
GM-LNF	
GM-LAF, MTU-Hydra, MTU-CFR, GM-LNF	
GM-LAF, MTU-Hydra, GM-LNF	
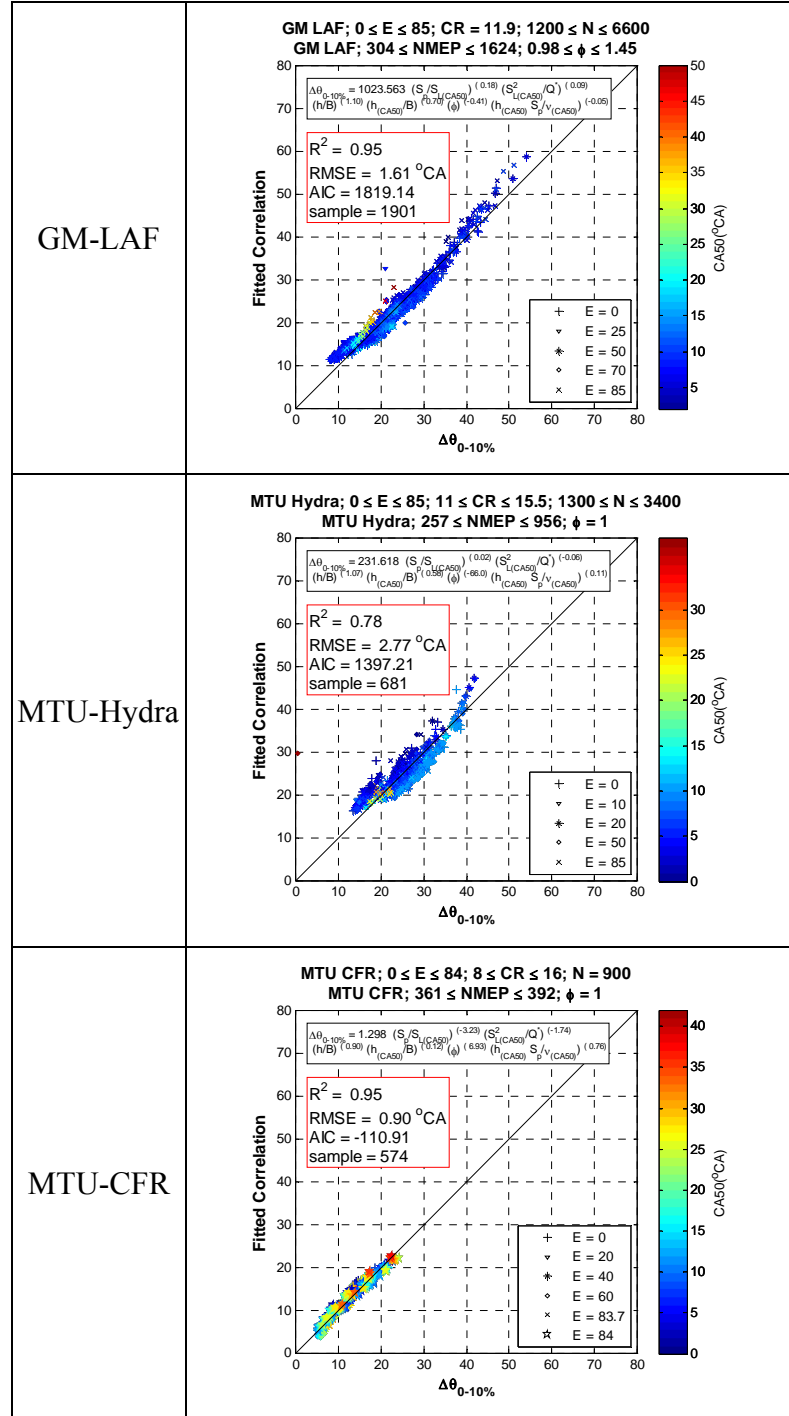
Figure IX-1 B0010 correlations

Table IX-4 shows the constants for B1025 correlations and the metrics to quantify the fit.

Table IX-4 B1025 correlations

	GM-LAF	MTU-Hydra	MTU-CFR	GM-LNF	GM-LAF MTU-Hydra MTU-CFR GM-LNF	GM-LAF MTU-Hydra GM-LNF
x0	109.97	2.97	1.2	210.21	25.56	98.8
x1	0.14	0.21	0.96	0.04	0.23	0.07
x2	0.06	0.13	0.36	-0.11	0.09	0.05
x3	0.48	0.17	-0.46	-0.03	0.23	0.5
x4	0.94	-0.65	0.39	0.67	0.04	0.78
x5	-0.4	0	0	0	-0.53	-0.41
x6	-0.03	-0.07	0.07	-0.24	-0.15	-0.04
R^2	0.85	0.24	0.89	0.97	0.5	0.73
RMSE	0.32	0.68	0.31	0.35	0.77	0.59
AIC	-4297.21	-516.07	-1342.67	-137.19	-1622.06	-2723.29
#sample	1901	681	574	71	3156	2582

Table IX-5 shows the constants for B1050 correlations and the metrics to quantify the fit.

Table IX-5 B1050 correlations

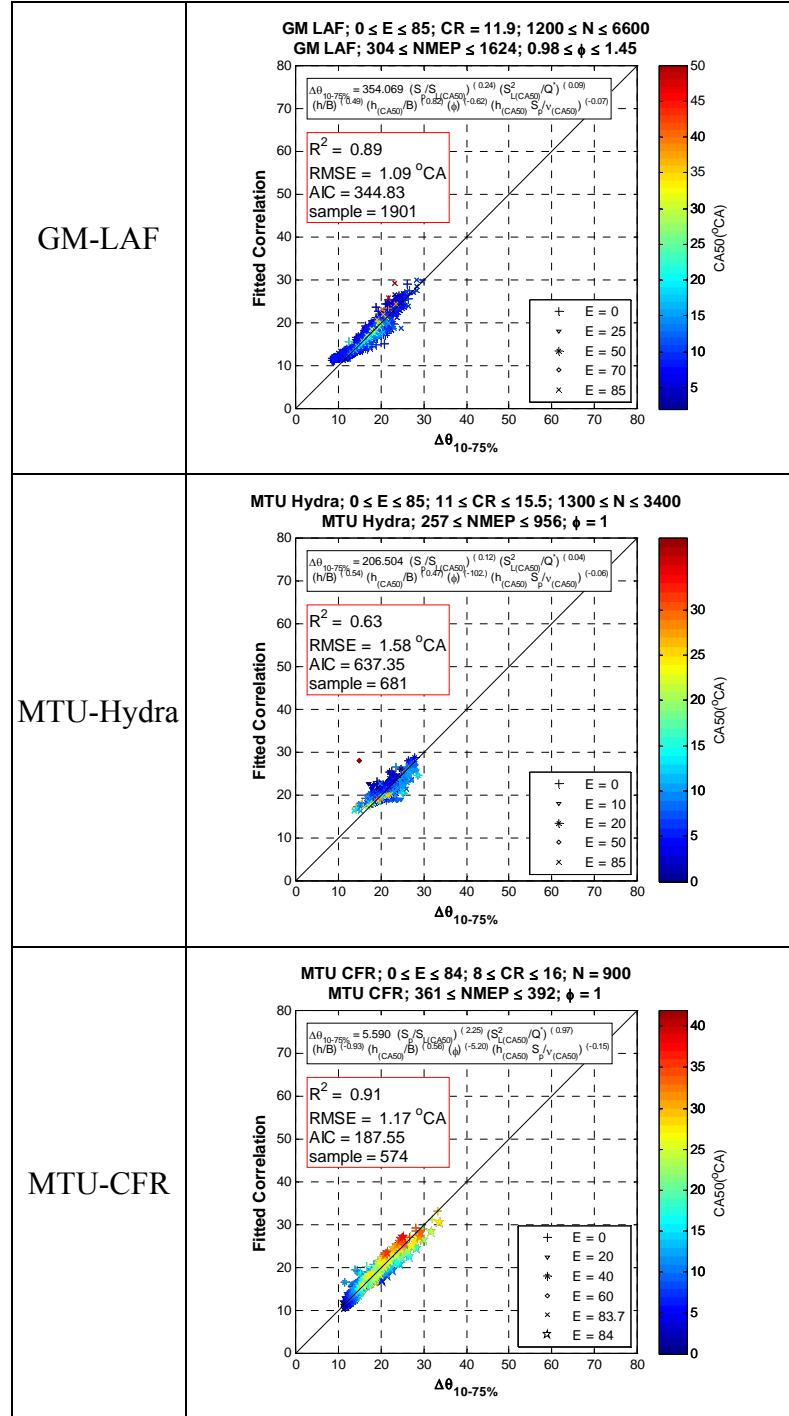|	GM-LAF	MTU-Hydra	MTU-CFR	GM-LNF	GM-LAF MTU-Hydra MTU-CFR GM-LNF	GM-LAF MTU-Hydra GM-LNF
x0	255.41	37.35	3.61	731.59	69.92	280.37
x1	0.18	0.17	1.57	0.11	0.3	0.1
x2	0.07	0.08	0.64	-0.13	0.1	0.06
x3	0.48	0.33	-0.79	-0.1	0.15	0.55
x4	0.92	-0.02	0.49	0.64	0.1	0.84
x5	-0.48	0	0	0	-0.73	-0.44
x6	-0.05	-0.08	-0.07	-0.32	-0.18	-0.05
R^2	0.89	0.32	0.92	0.96	0.54	0.82
RMSE	0.62	1.21	0.69	0.94	1.63	1.02
AIC	-1776.43	270.2	-421.11	3	3081.38	107.96
#sample	1901	681	574	71	3156	2582

Table IX-6 shows the constants for B1075 correlations and the metrics to quantify the fit.

Table IX-6 B1075 correlations

	GM-LAF	MTU-Hydra	MTU-CFR	GM-LNF	GM-LAF MTU-Hydra MTU-CFR GM-LNF	GM-LAF MTU-Hydra GM-LNF
x0	354.07	206.5	5.59	1837.18	100.16	445.99
x1	0.24	0.12	2.25	0.15	0.36	0.16
x2	0.09	0.04	0.97	-0.14	0.13	0.07
x3	0.49	0.54	-0.93	-0.12	0.19	0.61
x4	0.82	0.47	0.56	0.62	0.04	0.82
x5	-0.62	0	0	0	-0.8	-0.49
x6	-0.07	-0.06	-0.15	-0.39	-0.19	-0.05
R^2	0.89	0.63	0.91	0.94	0.57	0.87
RMSE	1.09	1.58	1.17	1.85	2.52	1.38
AIC	344.83	637.35	187.55	99.37	5843.15	1658.41
#sample	1901	681	574	71	3156	2582

Figure IX-2 shows the B1075 correlations.

GM-LNF	GM LNF; E = 0; CR = 9.3; 1200 ≤ N ≤ 4000
	GM LNF; 236 ≤ NMEP ≤ 2251; 0.99 ≤ φ ≤ 1.04

Figure IX-2 B1075 correlations

Table IX-7 shows the constants for B1090 correlations and the metrics to quantify the fit.

Table IX-7 B1090 correlations

	GM-LAF	MTU-Hydra	MTU-CFR	GM-LNF	GM-LAF MTU-Hydra MTU-CFR GM-LNF	GM-LAF MTU-Hydra GM-LNF
x0	150.65	530.25	5.57	3324.81	42.58	146.97
x1	0.23	0.11	2.19	0.18	0.38	0.2
x2	0.1	0.02	0.93	-0.14	0.15	0.09
x3	0.48	0.68	-0.99	-0.09	0.26	0.56
x4	0.44	0.75	0.62	0.58	-0.24	0.44
x5	-1.02	0	0	0	-1.02	-0.89
x6	-0.01	-0.03	-0.12	-0.42	-0.1	0.01
R^2	0.57	0.71	0.9	0.91	0.48	0.59
RMSE	4.26	2.33	1.61	3.07	4.54	3.91
AIC	5521.67	1165.27	559.14	171.16	9563.01	7053.44
#sample	1901	681	574	71	3156	2582

IX.4 COPYRIGHT PERMISSIONS

Copyright permission from SAE International for:

Yeliana, C.Cooney, J.Worm, J.Naber, *Calculation of Mass Fraction Burn Rates of Ethanol-Gasoline Blended Fuels Using Single and Two-Zone Models.* SAE 2008-01-0320, 2008.

Copyright permission from Journal of Kones for:

1. Yeliana, J. Worm, D. Michalek, J. Naber, *Property Determination for Ethanol-Gasoline Blends with Application to Mass Fraction Burn Analysis in a Spark Ignition Engine.* Journal of Kones, Powertrain & Transportation, 2008. 15, No. 2: p. 553-561.

2. Yeliana, C. Cooney, J. Worm, D. Michalek, J. Naber, *Wiebe Function Parameter Determination for Mass Fraction Burn Calculation in an Ethanol-Gasoline Fuelled SI Engine.* Journal of Kones, Powertrain & Transportation, 2008. 15, No. 3: p. 567-574.

References

1.	EPA. *http://www.epa.gov/oms/additive.htm*. 2010.
2.	Heywood, J.B., *Engine Combustion Modeling - An Overview*, in *Combustion Modeling in Reciprocating Engines*, J.N. Mattavi, C.A. Amann, Editor. 1978, Plenum Press. p. 1-35.
3.	Heywood, J.B., *Internal Combustion Engine Fundamentals*. 1988, New York: McGraw-Hill.
4.	Krieger, R., *Applications of Engine Combustion Models: An Introductory Overview.* Combustion Modeling in Reciprocating Engines, 1980: p. 485–503.
5.	Rassweiler, G.M. and L. Withrow, *Motion Pictures of Engine Flames Correlated with Pressure Cards.* SAE TRANSACTIONS, 1938. **38**: p. 185-204.
6.	Krieger, R.B. and G.L. Borman, *The Computation of Apparent Heat Release for Internal Combustion Engines.* ASME Paper, 1966.
7.	Heywood, J.B., et al., *Development and Use of a Cycle Simulation to Predict SI Engine Efficiency and NOx Emissions.* SAE 790291, 1979.
8.	Gatowski, J.A., et al., *Heat Release Analysis of Engine Pressure Data.* SAE 841359, 1984.
9.	Blizard, N.C. and J.C. Keck, *Experimental and theoretical investigation of turbulent burning model for internal combustion engines.* SAE Paper, 1974. **740191**: p. 18.
10.	Tabaczynski, R.J., C.R. Ferguson, and K. Radhakrishnan, *A Turbulent Entrainment Model for Spark-Ignition Engine Combustion.* 1977: SAE Paper 770647.
11.	Micklow, G.J., B. Murphy, and T. Abdel-Salam, *An Efficient Thermodynamic Cycle Analysis for the Performance Prediction of Fuel Inducted Spark Ignition Engines.* SAE 2008-01-0289, 2008.
12.	Annand, W.J.D., *The Estimation of Flame Propagation Rates in Routine Computer Synthesis of Spark-Ignition Engine Combustion.* Proc. IMechE, 1983. **C83**: p. 125-134.
13.	Shiao, Y. and J.J. Moskwa, *Cylinder Pressure and Combustion Heat Release Estimation for SI Engine Diagnostics Using Nonlinear Sliding Observers.* Control Systems Technology, IEEE Transactions, 1995. **3**(1): p. 70-78.
14.	Borg, J.M. and A.C. Alkidas, *Investigation of the Effects of Autoignition on the Heat Release Histories of a Knocking SI Engine Using Weibe Functions.* SAE 2008-01-1088, 2008.
15.	Van Nieuwstadt, M.J., et al., *Heat Release Regressions for GDI Engines.* SAE 2000-01-0956, 2000.
16.	Caton, J.A., *Effects of Burn Rate Parameters on Nitric Oxide Emissions for a Spark Ignition Engine: Results from a Three-Zone, Thermodynamic Simulation.* SAE 2003-01-0720, 2003.
17.	Martin, J.K., S.L. Plee, and D.J. Remboski, *Burn Models and Prior-Cycle Effects on Cyclic Variation in Lean Burn Spark Ignition Engine Combustion.* SAE 880201, 1988.
18.	Naber, J.D., et al., *Analysis of Combustion Knock Metrics in Spark-Ignition Engines.* SAE 2006-01-0400, 2006.
19.	Ozdor, N., M. Dulger, and E. Sher, *Cyclic Variability in Spark Ignition Engines--A Literature Survey.* SAE 940987, 1994.
20.	Brehob, D.D. and C.E. Newman, *Monte Carlo Simulation of Cycle-To-Cycle Variability.* SAE 922165, 1992.
21.	Rouse, B.T., *Part Load Combustion Characterization of Ethanol-Gasoline Fuel Blends in a Single Cylinder Spark Ignition Direct Injection Variable Cam Timing Variable Compression Ratio Engine.* Thesis, 2009.
22.	Young, M., *Cyclic Dispersion--Some Quantitative Cause-And-Effect Relationships.* 1980.
23.	Dai, W., N. Trigui., and Y. Lu, *Modeling of Cyclic Variation in Spark-Ignition Engines.* SAE 2000-01-2036, 2000.
24.	Minteer, S.D., *Alcoholic Fuels.* 2006: CRC Taylor & Francis.

25. Bromberg, L., D.R. Cohn, and J.B. Heywood, *Calculations of Knock Suppression in Highly Turbocharged Gasoline/Ethanol Engines Using Direct Ethanol Injection.* Massachusetts Institute of Technology, 2006.

26. Rask, E. and M. Sellnau, *Simulation-Based Engine Calibration: Tools, Techniques, and Applications.* SAE 2004-01-1264, 2004.

27. Lindstrom, F., H.E. Angstrom, G. Kalghatgi, C.E. Moller, *An Empirical SI Combustion Model Using Laminar Burning Velocity Correlations.* SAE Transactions, 2005. **144**: p. 833-846.

28. Bayraktar, H. and O. Durgun, *Development of an Empirical Correlation for Combustion Durations in Spark Ignition Engines.* Energy Conversion and Management, 2004. **45**(9-10): p. 1419-1431.

29. Vávra, J. and M. Takáts, *Heat Release Regression Model for Gas-Fuelled SI Engines.* 2004.

30. Borman, G.L., *Modeling Flame Propagation and Heat Release in Engines - An Introductory Overview*, in *Combustion Modeling in Reciprocating Engines*, J.N. Mattavi, C.A. Amann, Editor. 1978, Plenum Press. p. 1-35.

31. Hires, S.D., R.J. Tabaczynski, and J.M. Novak, *The Prediction of Ignition Delay and Combustion Intervals for a Homogeneous Charge.* Spark Ignition Engine, Society of Automotive Engineers, SAE Paper, 1978. **780232**.

32. Cesario, N., et al., *Modelling the Rate of Heat Release in Common-Rail Diesel Engines: a Soft Computing Approach.* 2004.

33. White, F.M., *Fluid Mechanics. 5th*, Boston: McGraw-Hill.

34. Croarkin, C., et al., *NIST/SEMATECH e-handbook of statistical methods*. 2003, NIST Handbook.

35. Chase, M.W., *NIST-JANAF thermochemical tables*. 1998: American Institute of Physics for the National Institute of Standards and Technology Woodbury, NY.

36. Newhall, H.K. and E.S. Starkman, *Thermodynamic Properties of Octane and Air for Engine Performance Calculations.* SAE Paper 633G, Warrendale, PA, 1963.

37. Olikara, C. and G.L. Borman, *A Computer Program for Calculating Properties of Equilibrium Combustion Products with Some Applications to IC Engines.* SAE 750468, 1975.

38. Yeliana, Y., et al., *Calculation of Mass Fraction Burn Rates of Ethanol-Gasoline Blended Fuels Using Single and Two-Zone Models.* SAE 2008-01-0320, 2008.

39. Naber, J.D., E.K. Bradley, and J.E. Szpytman, *Target-Based Rapid Prototyping Control System for Engine Research.* SAE TRANSACTIONS, 2006. **115**(7): p. 395.

40. Chun, K.M. and J.B. Heywood, *Estimating Heat-Release and Mass-of-Mixture Burned from Spark-Ignition Engine Pressure Data.* Combustion Science and Technology, 1987. **54**(1): p. 133-143.

41. Klein, M. and L. Eriksson, *A Specific Heat Ratio Model for Single-Zone Heat Release Models.* SAE TRANSACTIONS, 2004. **113**(3): p. 956.

42. Cheung, H.M. and J.B. Heywood, *Evaluation of a One-Zone Burn-Rate Analysis Procedure Using Production SI Engine Pressure Data.* 1993.

43. Guezennec, Y.G. and W. Hamama, *Two-Zone Heat Release Analysis of Combustion Data and Calibration of Heat Transfer Correlation in an IC Engine.* SAE 1999-01-0218, 1999.

44. Lancaster, D.R., R.B. Krieger, and J.H. Lienesch, *Measurement and Analysis of Engine Pressure Data.* SAE 750026, 1975.

45. Fox, J.W., W.K. Cheng, and J.B. Heywood, *A Model for Predicting Residual Gas Fraction in Spark-Ignition Engines.* SAE 931025, 1993.

46. Cooney, C.P., et al., *Combustion Characterization in an Internal Combustion Engine with Ethanol- Gasoline Blended Fuels Varying Compression Ratios and Ignition Timing.* Energy & Fuels, 2009. **23**: p. 2319-2324.

47. Manual, U., *ACAP DSP.* DSP Technology Inc., 2009.

48. Metghalchi, M. and J.C. Keck, *Laminar burning velocity of propane-air mixtures at high temperature and pressure.* Combustion and Flame, 1980. **38**: p. 143-154.

49.   Gulder, O.L., *Correlations of laminar data for alternative SI engine fuels.* SAE Paper, 1984. **841000**.

50.   Gulder, O.L., *Laminar burning velocities of methanol, ethanol and isooctane-air mixtures.* The Combustion Institute, 1982. **Nineteenth Symposium on Combustion**: p. 275-281.

51.   Bayraktar, H., *Experimental and theoretical investigation of using gasoline–ethanol blends in spark-ignition engines.* Renewable Energy, 2005. **30**(11): p. 1733-1747.

52.   Turns, S.R., *An introduction to combustion: Concepts and applications.* New York: McGraw-Hill, Inc, 1995., 1995.

53.   Borman, G.L. and K.W. Ragland, *Combustion Engineering. Number ISBN 0-07-006567-5.* 1998, McGraw-Hill.

54.   Manual, G., *GT-Suite™ Version 6.1.* Gamma Technologies, 2004.

55.   Borg, J.M. and A.C. Alkidas, *Investigation of the Effects of Autoignition on the Heat Release Histories of a Knocking SI Engine Using Wiebe Functions.* SAE 2008-01-1088, 2008.

56.   Yeliana, Y., C. Cooney, J. Worm, D. Michalek, J. Naber, *Wiebe Function Parameter Determination for Mass Fraction Burn Calculation in an Ethanol-Gasoline Fuelled SI Engine.* Journal of Kones, Powertrain & Transportation, 2008. **15, No. 3**: p. 567-574.

57.   Glewen, W.J., et al., *Analysis of Cyclic Variability in Spark-Assisted HCCI Combustion using a Double Wiebe Function.* Proceedings of the Combustion Institute, 2008.

58.   Yasar, H., et al., *Double-Wiebe Function: An Approach for Single-Zone HCCI Engine Modeling.* Applied Thermal Engineering, 2007.

59.   Croarkin, C., et al., *Engineering Statistics Handbook.* 2001: The Institute; International SEMATECH.

60.   Jiang, S., et al., *Graphical Representation of Two Mixed-Weibull Distributions.* Reliability, IEEE Transactions on, 1992. **41**(2): p. 241-247.

61.   Jiang, R. and D.N.P. Murthy, *Reliability Modeling Involving Two Weibull Distributions.* Reliability Engineering & Systems Safety, 1995. **47**(3): p. 187-198.

62.   Amann, C.A., *Cylinder-Pressure Measurement and Its Use in Engine Research.* SAE 852067, 1985.

63.   Tascillo, M.A., et al., *Implementation of a Real-Time, Multi-Processing Infrastructure for Automated Testing.* 1999-01-0952, 1999.

64.   Croarkin, C. and P. Tobias, *NIST/SEMATECH e-handbook of statistical methods.* 2002, NIST Handbook.

65.   Berger, R.W. and K. Lawrence, *Estimating Weibull Parameters by Linear and Nonlinear Regression.* Technometrics, 1974. **16**(4): p. 617-619.

66.   Jiang, R. and D.N.P. Murthy, *The Exponentiated Weibull Family: A Graphical Approach.* Reliability, IEEE Transactions on, 1999. **48**(1): p. 68-72.

67.   Pham, H., *Recent Advances in Reliability and Quality in Design.* 2008: Springer Verlag.

68.   Yeliana, Y., C. Cooney, J. Worm, D. Michalek, J. Naber, *Estimation of Double-Wiebe Function Parameters for Burn Durations of Ethanol-Gasoline Blends in a SI Engine over Variable Compression Ratios and EGR levels.* TBD, 2009.

69.   Falls, L.W., *Estimation of Parameters in Compound Weibull Distributions.* Technometrics, 1970. **12**(2): p. 399-407.

70.   Jiang, R. and D. Murthy, *Mixture of Weibull Distributions-Parametric Characterization of Failure Rate Function.* Applied Stochastic Models and Data Analysis, 1998. **14**(1): p. 47-65.

71.   Jiang, R., D. Murthy, and P. Ji, *Models Involving Two Inverse Weibull Distributions.* Reliability Engineering & System Safety, 2001. **73**(1): p. 73-81.

72.   Jiang, R. and D.N.P. Murthy, *Modeling Failure-Data by Mixture of 2 Weibull Distributions: A Graphical Approach.* Reliability, IEEE Transactions on, 1995. **44**(3): p. 477-488.

73.   Yeliana, *GM-MTU Predictive Combustion Model.* Report 2010.

74.   Yeliana, Y., D. Loveland, C. Cooney, J. Worm, D. Michalek, J. Naber, *Parametric Study of Burn Durations of Ethanol-Gasoline Blends in a SI Engine over Variable Compression Ratios and EGR Levels.* TBD, 2010.

75.   Yeliana, J.W., D. Michalek, J. Naber, *Analytical Solution of Double-Wiebe Function Parameters Estimation for SI Engines.* TBD, 2009.

76.   Marriott, C.D., et al., *Development of a naturally aspirated spark ignition direct-injection flex-fuel engine.* SAE International Journal of Engines, 2009. **1**(1): p. 267.

77.   Lee, K. and D. Foster, *Cycle-By-Cycle Variations in Combustion and Mixture Concentration in the Vicinity of Spark Plug Gap.* 1995.

78.   Aghdam, E., et al., *Study of Cyclic Variation in an SI Engine Using Quasi-Dimensional Combustion Model.* 2007.

79.   Keck, J., J. Heywood, and G. Noske, *Early Flame Development and Burning Rates in Spark Ignition Engines and their Cyclic Variability.* 1987, Society of Automotive Engineers, Warrendale, PA.

80.   Akaike, H., *Information theory and an extension of the maximum likelihood principle.* Budapest, Hungary, 1973: p. 267–281.